

**WATER VAPOR AND GAS BARRIER  
PROPERTIES OF BIODEGRADABLE POLYMER  
NANOCOMPOSITES FILMS**

**A Thesis Submitted to  
the Graduate School of Engineering and Sciences of  
İzmir Institute of Technology  
in Partial Fulfillment of the Requirements for the Degree of**

**MASTER OF SCIENCE**

**in Chemical Engineering**

**by  
Hale OGUZLU**

**July 2011  
İZMİR**

We approve the thesis of **Hale OĞUZLU**

---

**Prof. Dr. Funda TIHMINLIOĞLU**  
Supervisor

---

**Prof. Dr. Devrim BALKÖSE**  
Committee Member

---

**Prof. Dr. Metin TANOĞLU**  
Committee Member

**4 July 2011**

---

**Prof. Dr. Mehmet POLAT**  
Head of the Department of  
Chemical Engineering

---

**Prof. Dr. Durmuş Ali DEMİR**  
Dean of the Graduate School of  
Engineering and Sciences

## ACKNOWLEDGEMENTS

I would like to thank and express my gratitude to Professor Funda Tihminliođlu for her supervision, guidance and considerate patience throughout my thesis period. I am also grateful to Professor Devrim Balköse for her valuable comments and suggestions.

I am thankful to Professor Orhan Öztürk for Wide Angle X-ray analyses, to Professor Metin Tanođlu for giving access to Composites Center and to Professor Ahmet Yemeniciođlu for giving access to texture analyzer that I used for tensile tests.

The financial support of Turkish Scientific Technical Research Organization (108M335) is gratefully acknowledged. I also present my deepest thanks to Purac Company and Southern Clay Products for supplying the polymer samples and nanoclay samples.

The researchers, experts and anyone who lightened my way of research from Chemical Engineering Department of İzmir Institute of Technology are highly appreciated. Special thanks my closest friend Onur Özçalık for his contributions to my thesis and his friendship. I would like to appreciate deeply my friends Burcu Alp, Okan Akın and Alihan Karakaya, for their friendship and encouragements.

Finally, my thanks go to my family for their help, and appreciations during performing experiments and the writing of this thesis.

# ABSTRACT

## WATER VAPOR AND GAS BARRIER PROPERTIES OF BIODEGRADABLE POLYMER NANOCOMPOSITES FILMS

Poly lactide nanocomposite (PLANC) films were prepared with solution intercalation method by introducing sonication as an alternative for conventional polymers. The effect of polymer clay interaction on PLANCs was investigated with respect to molecular weight of the poly lactide, organic modifier presence and type by focusing on five major aspects: structural analysis, barrier, thermal, mechanical and rheological properties.

According to structural analyses, the best level of dispersion was obtained in PL65-10A nanocomposites due to high molecular weight poly lactide and organomodified nanoclay usage leading to better molecular interaction between the layered silicates and polymer chains. However, phase separated structure was observed in PLA composites prepared with unmodified clay as basal space between layered silicates were not sufficient enough for the penetrating of the polymer chains into the layers. Barrier and mechanical properties of the nanocomposites were improved up to critical clay content for each nanocomposite system. Thermal stability of the intercalated and exfoliated nanocomposites increased with the addition of the clay. Best improvements were obtained in PL65-10A nanocomposites in accordance with structural analyses. In dynamic mechanical analysis, glass transition temperatures and storage modulus of PLANCs increased with increasing of clay amount owing to reinforcement effect of the silicate layers. In rheological measurements, PLANCs showed solid-like behavior at lower shear rates due to the formation of a network percolating clay lamellae, besides PLANCs showed shear thinning behavior at higher shear rates leading to developments on the processability of nanocomposites. Consequently, intercalated and exfoliated PLANCs could be used as an eco-friendly promising alternative to conventional polymers for short-life applications such as food packaging and coating.

## ÖZET

### BİYOBOZUNUR POLİMER NANOKOMPOZİT FİLMLEİNİN SU BUHARI VE GAZ GEÇİRGENLİK ÖZELLİKLERİ

Polilaktid nanokompozit (PLANC) filmler geleneksel polimerlere alternatif olarak ultrasonik ses dalgası uygulanarak çözücü interkalasyon yöntemi ile hazırlandı. Polimer kil etkileşiminin etkisi polilaktidin moleküler ağırlığına, kildeki organik düzenleyici varlığına ve tipine göre yapısal analizler, bariyer, mekanik, termal ve reolojik özellikler olarak beş ana yönde odaklanarak araştırıldı.

Yapısal analizlere göre, yüksek moleküler ağırlıklı polilaktid ve organik düzenleyiciyle modifiye edilmiş kil kullanımıyla oluşan kil tabakaları ve polimer zincirleri arasındaki iyi moleküler etkileşimden dolayı PL65-10A nanokompozitlerinde en iyi derecede dağılım gözlemlendi. Fakat tabakalı silikatların arasındaki boşluk polimer zincirlerinin tabakalar arasına girmesi için yeterli olmaması nedeni ile modifiye olmayan kille hazırlanan PLA kompozitlerinde faz ayrımı yapılar gözlemlendi. Nanokompozitlerin bariyer ve mekanik özelliklerinde kritik nanokil miktarına kadar iyileştirirken, interkale ve eksfoliye yapıdaki nanokompozitlerin termal stabiliteleri kil eklenmesi ile arttı. En iyi iyileştirmeler yapısal analizlerle uyumlu olarak PL65-10A nanokompozitlerinde gözlemlendi. Dinamik mekanik analizinde silika tabakalarının güçlendirme etkisiyle PLANC'lerin camsı geçiş sıcaklığı ve depolama modülü kil miktarı arttıkça arttı. Reolojik ölçümlerde düşük frekanslarda kil tabakaları süzgeçvari ağ yapısında olmasından dolayı PLANC'leri katı-benzeri davranış gösterdi. Ayrıca yüksek frekanslarda kesmeyle incelen davranış göstermesiyle nanokompozitlerin işlenebilirliği gelişti.

Sonuç olarak, interkale ve eksfoliye yapıdaki PLANC'ler çevre dostu polimerler olarak, gıda ambalajı ve kaplama gibi kısa süreli uygulamalarda geleneksel polimerlerin yerine kullanılma potansiyeli mevcuttur.

# TABLE OF CONTENTS

LIST OF FIGURES.....	ix
LIST OF TABLES.....	xii
CHAPTER 1. INTRODUCTION.....	1
CHAPTER 2. BIODEGRADABLE POLYMERS.....	3
2.1. Classification of Biodegradable Polymers.....	4
2.2. Applications of Biodegradable Polymers.....	6
2.3. Polylactide .....	7
2.3.1. Production of Polylactide.....	7
2.3.2. Chemical Properties of Polylactide.....	8
2.3.3. Physical Properties of Polylactide.....	9
2.3.3.1. Solubility of Polylactide.....	10
2.3.3.2. Barrier Properties of Polylactide.....	13
2.3.2.3. Thermal Properties of Polylactide.....	17
2.3.2.4. Mechanical Properties of Polylactide.....	19
2.3.2. Rheological Properties of Polylactide.....	22
CHAPTER 3. POLYMER NANOCOMPOSITES.....	25
3.1. Nanoparticles.....	25
3.1.1. Nanoclays (Layered Silicates).....	26
3.2. Nature of the Polymer.....	29
3.3. Structure of Polymer-Layered Silicate Nanocomposites.....	30
3.4. Production Methods of Polymer Nanocomposite.....	32
3.4.1. Solution Intercalation Polymer/ Prepolymer Solutions.....	33
3.4.2. In Situ Intercalative Polymerization .....	34
3.4.3. Melt Intercalation.....	34
3.5. Polylactide Layered Silicate Nanocomposites (PLA-LSN).....	35
3.5.1. Barrier Properties of PLA-LSN.....	35
3.5.2. Thermal Properties of PLA-LSN.....	42
3.5.3. Mechanical Properties of PLA-LSN.....	43

3.5.4. Rheological Properties of PLA-LSN .....	44
CHAPTER 4. EXPERIMENTAL STUDY.....	46
4.1. Materials.....	46
4.2. Preparation of Polylactide (PLA) and Polylactide Nanocomposites (PLANC) Films.....	43
4.3. Determination of Thickness of PLA and PLANC Films.....	43
4.4. Structural Characterizations of PLANC Films .....	43
4.4.1. Fourier Transform Infrared (FTIR) Analysis of PLA and PLANC Films.....	43
4.4.2. X-Ray Diffraction (XRD) Analysis of PLANC Films.....	48
4.5. Permeability of Measurements.....	48
4.5.1. Determination of Relative Humidity Effect on Thickness of PLA and PLANC Films.....	48
4.5.2. Water Vapor Permeability Measurements of PLA and PLANC Films.....	49
4.5.3. Oxygen and Carbon dioxide Permeability Measurements of PLA and PLANC Films.....	55
4.6. Thermal Analysis of PLA and PLANC Films.....	51
4.7. Mechanical Property Determination of PLA and PLANC Films...	51
4.8. Rheological Measurements of PLA and PLANC Films.....	52
4.9. Contact Angle Measurements of PLA and PLANC Films.....	52
4.10. Color Measurements of PLA and PLANC Films.....	52
CHAPTER 5.RESULTS AND DICUSSIONS.....	54
5.1. Structural Characterizations.....	55
5.1.1. Fourier Transform Infrared (FTIR) Analysis.....	55
5.1.2. X-Ray Diffraction (XRD) Analysis.....	58
5.2. Transport Properties of PLANCs .....	64
5.2.1. Effect of Relative Humidity on Thickness of PLANCs.....	64
5.2.2. Water Vapor Permeability.....	64
5.2.3. Oxygen Permeability.....	67
5.2.4. Carbon dioxide Permeability.....	70
5.2.5. Permeability Models.....	72
5.3. Thermal Analysis.....	75
5.3.1. Differential Scanning Calorimetry (DSC) Analysis.....	75

5.3.2. Thermogravimetric Analysis (TGA).....	76
5.4. Mechanical Analysis.....	79
5.4.1 Tensile Test.....	80
5.4.2. Dynamic Mechanical Analysis (DMA).....	82
5.5. Rheological Analysis.....	86
5.6. Contact Angle Measurements.....	94
5.7. Color Measurement.....	95
CHAPTER 6 CONCLUSION.....	97
REFERENCES.....	99
APPENDIX A.....	106

## LIST OF FIGURES

<b><u>Figure</u></b>		<b><u>Page</u></b>
Figure 2.1.	Polymers according biodegradability and origin.....	4
Figure 2.2.	Life cycle of biodegradable polymer.....	4
Figure 2.3.	Classification of biodegradable polymers.....	5
Figure 2.4.	Relative a) energy required b) greenhouse emissions for production of various polymers.....	8
Figure 2.5.	Chemical structure of a) L and D-lactic acid b) LL-, meso- and DD-lactides and c) constitutional unit of polylactide.....	9
Figure 2.6.	Comparison of water vapor transmission rates of polymers.....	15
Figure 2.7.	Comparison of oxygen transmission rates of polymers.....	16
Figure 2.8.	Thermo analytical methods.....	18
Figure 2.9.	Sinusoidal strain and stress with phase angle $\delta$ .....	20
Figure 2.10.	Rheological behavior of matters.....	23
Figure 3.1.	Structure of MMT.....	28
Figure 3.2.	(a) Layered silicate composites structure (b) WAXD patterns and (c) TEM images of three different types of nanocomposites..	31
Figure 3.3.	Various spectra of commercial clays.....	32
Figure 3.4.	Preparation methods of layered silicate polymer nanocomposites	33
Figure 3.5.	Tortuous path in (a) conventional composite and (b) layered silicate nanocomposite.....	36
Figure 4.1.	Illustration of water vapor permeability experiment.....	49
Figure 4.2.	Illustration of gas permeability experiment.....	50
Figure 5.1.	FTIR spectra of Cloisite 10A, Cloisite 93 A and Nanofill 116.....	56
Figure 5.2.	Percent FTIR spectra of PL65-P and PL65-10A nanocomposite films in 400-600cm <sup>-1</sup> region.....	57
Figure 5.3.	Percent FTIR spectra of GF-P and GF-10A nanocomposite films in 400-600cm <sup>-1</sup> region.....	57
Figure 5.4.	Percent FTIR spectra of GF-P and GF-93A nanocomposite films in 400-600cm <sup>-1</sup> region.....	58
Figure 5.5.	Percent FTIR spectra of GF-P and GF-NF nanocomposite films in 400-600cm <sup>-1</sup> region.....	58

Figure 5.6.	XRD patterns of Cloisite 10A and Cloisite 93A.....	59
Figure 5.7.	XRD pattern of Nanofill 116.....	60
Figure 5.8.	XRD patterns of PL65-10A nanocomposites with different clay contents.....	61
Figure 5.9.	XRD patterns of GF-10A nanocomposites with different clay contents.....	61
Figure 5.10.	XRD patterns of GF-93A nanocomposites with different clay contents.....	62
Figure 5.11.	XRD patterns of GF-NF nanocomposites with different clay contents.....	63
Figure 5.12.	Water vapor permeabilities of PL65-10, GF-10A, GF-93A and GF-NF nanocomposites films with respect to clay content.....	65
Figure 5.13.	Water vapor permeabilities of PL65-10A nanocomposites films with respect to clay content.....	66
Figure 5.14.	Water vapor permeabilities of GF-10A , GF-93A and GF-93A nanocomposites films with respect to clay content.....	67
Figure 5.15.	Oxygen permeability of PL65-10A, GF-10A, GF-93A and GF-NF nanocomposites films with respect to clay content.....	68
Figure 5.16.	Oxygen permeability of PL65-10A, nanocomposites films with respect to clay content.....	69
Figure 5.17.	Oxygen permeability of GF-10A, GF-93A and GF-NF nanocomposites films with respect to clay content.....	69
Figure 5.18.	Carbon dioxide permeability of PL65-10, GF-10A, GF-93A and GF-NF nanocomposites films with respect to clay content.....	70
Figure 5.19.	Carbon dioxide permeability of PL65-10 nanocomposites films with respect to clay content.....	71
Figure 5.20.	Carbon dioxide permeability of GF-10A, GF-93A and GF-NF nanocomposites films with respect to clay content.....	71
Figure 5.21.	Permeability models fitted to experimental (a)water vapor (b) oxygen and (c) carbon dioxide permeability of PL65-10A nanocomposite films.....	73

Figure 5.22.	Permeability models fitted to experimental(a)water vapor (b) oxygen and (c) carbon dioxide permeability of GF-10A nanocomposite films.....	74
Figure 5.23.	TGA results of Cloisite 10A, Cloisite 93A and Nanofil 116.....	77
Figure 5.24.	Temperature dependence of storage modulus ( $G'$ ), loss modulus ( $G''$ ), and their ratio ( $\tan \delta$ ) for (a) PL65-10A nanocomposites (b) GF-10A nanocomposites.....	85
Figure 5.25.	Temperature dependence of storage modulus ( $G'$ ), loss modulus ( $G''$ ), and their ratio ( $\tan \delta$ ) for (a) GF-93A nanocomposites (b) GF- NF nanocomposites.....	86
Figure 5.26.	Storage modulus of GF-P and GF-10A nanocomposites as a function of %strain.....	86
Figure 5.27.	Storage modulus of GF-P and GF-10A nanocomposites as a function of a function of temperature.....	88
Figure 5.28.	Loss modulus of GF-P and GF-10A nanocomposites as a function of a function of temperature.....	88
Figure 5.29.	Complex viscosity of GF-P and GF-10A nanocomposites as a a function of temperature.....	89
Figure 5.30.	Shear Viscosity of GF-P and GF-10A as a function of shear rate.....	90
Figure 5.31.	Steady shear viscosity of GF-P as a function of time.....	91
Figure 5.32.	Steady shear viscosity of GF-10A-1 as a function of time.....	91
Figure 5.33.	Steady shear viscosity of GF-10A-2 as a function of time.....	92
Figure 5.34.	Steady shear viscosity of GF-10A-5 as a function of time.....	92
Figure 5.35.	Steady shear viscosity of GF-10A-7 as a function of time.....	93
Figure 5.36.	Steady shear viscosity of GF-10A-10as a function of time.....	93

## LIST OF TABLES

<b><u>Table</u></b>	<b><u>Page</u></b>
Table 2.1. Characteristic Infrared Spectra Bands of Polylactide.....	9
Table 2.2 Solubility parameters of polylactide and solvents at 25°C.....	12
Table 2.3. Water Vapor Permeability and diffusivity of water vapor in polylactide at different temperatures.....	16
Table 3.1. Characteristics of nanoparticles to polymers.....	26
Table 3.2. Classification of layered silicate crystals.....	27
Table 3.3. Surface energies of the different solvents and organic modifiers.	34
Table 3.4. Permeability models for nanocomposites.....	41
Table 4.1. Properties of Montmorillonite.....	46
Table 5.1. Sample codes of prepared films according to polymer and nanoclay type and nanoclay content. ....	55
Table 5.2. DSC results of PLA and PLANCs films.....	76
Table. 5.3. TGA results of PLA and PLANCs films.....	79
Table. 5.4. Tensile strength, strength at break, elongation at break and Young’s Modulus of PLA and PLANCs films.....	81
Table 5.5. Glass transition temperature values of PLA and PLANCs from DMA.....	83
Table 5.6. Terminal regions of slopes of $G'(\omega)$ and $G''(\omega)$ .....	89
Table 5.7. Contact angles measured for PLA and PLANC films.....	91
Table 5.8. The total color difference ( $\Delta E$ ) and color parameters of PLA and PLANCs.....	96

# CHAPTER 1

## INTRODUCTION

In recent years, many researches have been aimed to improve biodegradable properties of polymeric materials, thus; the use of natural polymers has grown extensively (Kolybaba et al., 2003). Polylactide is one of the promising polymers especially in food packaging application due to its economical pros of production. Polylactide is thermoplastic and aliphatic polyester which has gained enormous attention as the replacement of conventional polymers as it is biodegradable and bio-based polymer. Polylactide is mainly used in medical, coating and food packaging applications today (Shen et al., 2009; Auras et al., 2004). However, some of the other properties, such as gas barrier properties and melt-viscosity for further processing, are frequently not good enough for a wide-range of applications. To overcome this problem, biodegradable polymer nanocomposites are used with different ingredients which approve physical properties of polymers such as barrier and mechanical (Koo, 2006; Mittal, 2010).

To improve the physical properties of the polymers, several nanoparticles are used such as nanoclays, carbon fibers, carbon nanotubes, titanium oxide, etc. To acquire the improvement in barrier properties of polymer nanocomposite films, layered silicates are preferred as diffusion path in the polymer matrix increase incorporation of layered silicates into the polymer matrix. The most widely used layered silicates are montmorillonite clays having nano-scale dimensions (1-100 nm). Besides barrier properties, thermal and mechanical properties are enhanced due to the presence of layered silicate layers if the desired morphological structure is obtained. When the layered silicates are associated with a polymer, phase separated, intercalated and exfoliated structures can be obtained. and desired property is obtained if intercalated and exfoliated structures are observed. However, to achieve intercalated or exfoliated structure, clay should be dispersed very well in polymer matrix (Alexandre and Dubois, 2000; Ray and Okamoto, 2003). Morphology of the polymer layered silicate nanocomposites (PLSNCs) depends on the dispersion level of the layered silicates in the polymer matrix which can be affected by nature of the polymer (polarity,

molecular weight, etc.) and layered silicate (organomodification, etc.), preparation method and layered silicate content. Zurburtikudus and coworkers (2006) investigated effect of organomodification on the morphology and thermal properties of the polylactide nanocomposites (PLANCs). Improvements in thermal stability have been observed by Koh and coworkers (2008). They studied mechanical, thermal and carbon dioxide and oxygen barrier properties of PLANCs with respect to nanoclay content and it was seen that thermal and mechanical properties were improved up to critical clay loading while barrier properties were enhanced continuously with the addition of nanoclay. Rhim and coworkers (2009) compared commercial organomodified layered silicates (Cloisite 20A and 30B) and natural clay (Cloisite Na<sup>+</sup>) and desired structure and enhancement of the water vapor barrier properties of the PLANCs were observed due to the organomodification effect.

Although there are many studies related to PLA-layered silicate nanocomposites in literature, to our knowledge there is no study related to Cloisite 10A and Cloisite 93 layered silicates in PLA polymer. Therefore throughout this study, polylactide nanocomposite films were prepared with solution intercalation method by introducing sonication to achieve intercalated or exfoliated structure by using Cloisite 10A and 93A nanoclays. Furthermore, polymer clay interaction was investigated with respect to polymer type, organic modifier presence and type. Moreover, the barrier, mechanical, thermal and rheological properties of silicate layered polylactide nanocomposite was examined to determine the effect of the level of dispersion of layered silicates in the polymer matrix.

In conclusion, six chapters constitute this thesis report. Brief information about polymer nanocomposite and the aim of this research study were given in chapter 1. Moreover, properties of biodegradable polymers and specifically polylactide polymer were discussed in chapter 2 while polymer nanocomposites especially polylactide nanocomposites (PLANCs) concepts were covered in chapter 3. In chapter 4, experimental procedure of the PLANCs preparation method and characterization of PLANCs and measurement methods of barrier, thermal, mechanical and rheological properties were explained. The results of experiments were discussed in chapter 5. Finally, all the results and discussions were concluded in chapter 6.

## CHAPTER 2

### BIODEGRADABLE POLYMERS

Since the Second World War, polymers have been a part of human life owing to their advanced physical and chemical properties and processability. Today, global consumption of polymers is more than 200 million tones with the increase of 5% per year. However, polymer industry depends on limited fossil fuels, therefore; the increase of the price of fossil fuels affects the polymer sector. Moreover, durability of conventional polymers results in land crisis and pollution that leads to governments, scientist and industry to seek for alternatives. Thus, the idea of the use of biodegradable polymers has appeared as they are easily processable, have good performance properties and are cost competitive with conventional polymers. (Shen et al., 2009).

Not only biodegradation, but also bio-based become popular words in academic studies and industrial applications due to the environmental concern and regulations. (Figure 2.1). According to American Society for Testing and Materials (ASTM) and European Standardization Committee (CEN), degradation is defined as a reversible process leading to a significant change of the structure of a material, typically characterized by a loss of fragmentation and/or properties such as integrity, molecular weight, structure or mechanical strength and in biodegradation that structural change of material is caused by microorganisms (WEB\_1). In addition to these, an ideal polymer should be compostable which undergoes degradation by biological processes during composting to yield carbon dioxide, water, inorganic compounds and biomass at a rate consistent with other compostable materials and leaves no visible, distinguishable or toxic residue so that disposal of the polymers in the soil can be done to get rid of expensive recycling process. However, biodegradable polymers convert into biomass, water and carbon dioxide naturally (Figure 2.2). Besides, the definition of bio-based is man-made or man-processed organic macromolecules derived from biological resources. Thus, the usages of biodegradable polymers have been promising subject last two decades, especially short-life range

applications such as packaging, agriculture, etc (WEB\_1; Shen et al., 2009; Siracusa et al., 2008).

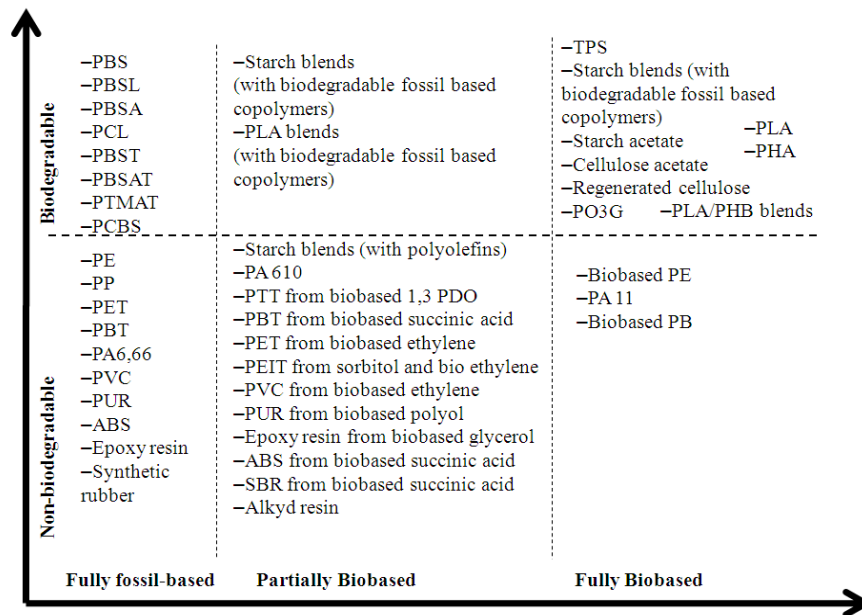


Figure 2.1. Polymers according biodegradability and origin (Source: Shen et al., 2009).

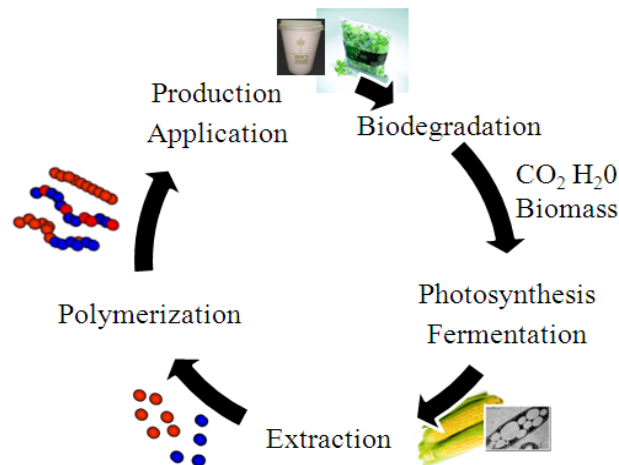


Figure 2.2. Life cycle of biodegradable polymer (Source: Siracusa et al., 2008).

## 2.1. Classification of Biodegradable Polymers

Generally, raw materials of biodegradable polymers can be both fossil-based and bio-based such as plant or animal origin. Biodegradable polymers are classified

into four groups according to their origin and production method (Figure 2.3). First group of biodegradable polymers is directly extracted or removed from biomass such as corn, exoskeleton of crustaceans, wood pulp etc. Chitosan casein, cellulose, zein are the example of that group. The second group of biodegradable polymers uses microorganisms or genetically modified bacteria to produce this type of polymers. This group consists mainly of the polyhydroxyalkanoates, but developments with bacterial cellulose are in progress. The third group of the polymers uses biotechnological methods. For instance, monomers are produced from classical chemical synthesis or fermentation, and then monomers are polymerized. A good example is polylactide polymer which is polymerized from lactic acid monomers. The monomers generally are obtained via fermentation of carbohydrate feedstock. The last group of biodegradable polymers such as polycaprolactones, polyester amides etc. is produced from the crude oil with the conventional chemical methods (Weber 2000; Chiellini and Solaro, 2003).

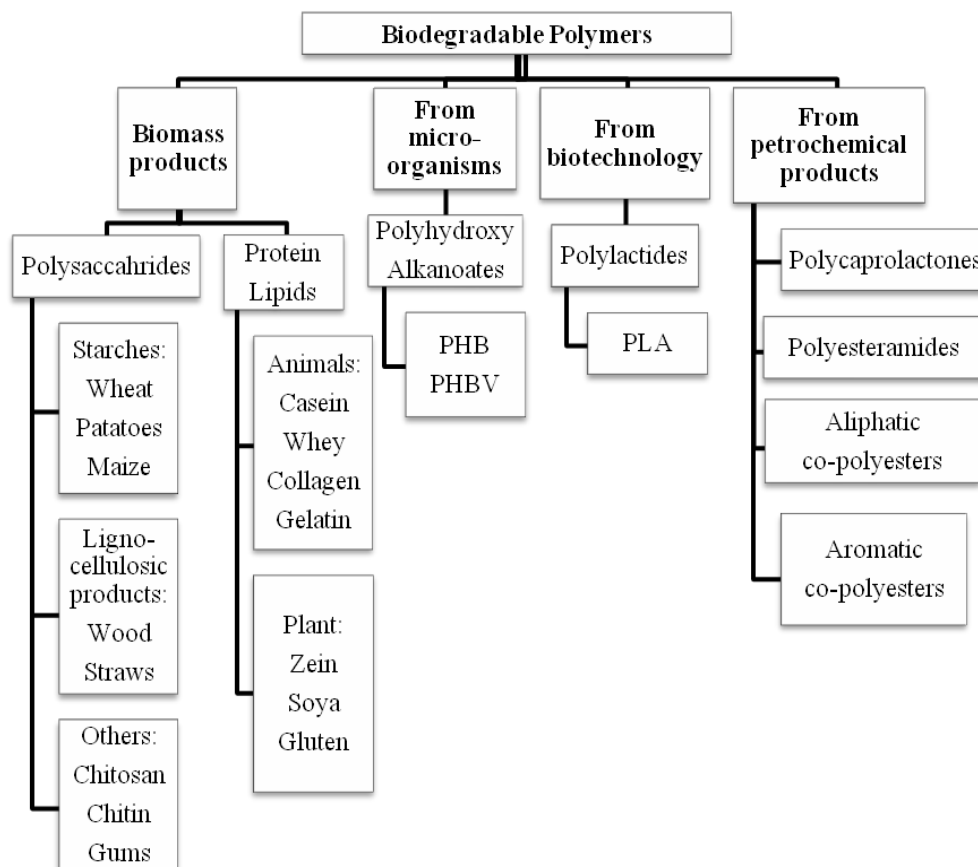


Figure 2.3. Classification of biodegradable polymers (Source:Weber, 2000; Siracusa et al., 2008)

## 2.2. Applications of Biodegradable Polymers

The biodegradable polymers are suitable for agricultural, medical uses and food packaging applications as they have certain advantages during use or recovery of the polymers. For instance, reuses of polymers are not always possible or economical because of infeasibility of process and risk of contamination.

Biodegradable polymers are applied in mulching, hydromulching, seed coating and controlled release systems in agricultural uses. For example, polymers for mulching applications are low density polyethylene (LDPE), poly(vinyl chloride) (PVC), polybutylene and copolymers of ethylene with vinyl acetate which control radiation, soil compaction, humidity, weed growth and degree of carbon dioxide retention. Despite the fact that, these films cause some problems such as harvesting, removal of the film and recycling owing to pesticide contamination. Therefore, chitosan and pectin, starch and pectin, soy protein and starch blends have been generally studied in the literature for agricultural applications as alternative to synthetic ones (Chiellini and Solaro, 2003).

Biodegradable polymers are preferred in especially short term applications such as surgical sutures, drug delivery systems and implants, besides, the absorption and degradation of biodegradable polymers are safe in the body as they do not cause inflammatory and toxic response and the degradation products can be cleared from the body (Naira and Laurencina, 2007).

Besides agricultural and medical uses, biodegradable polymers are also used in food packaging applications. Today mainly, synthetic polymers such as polypropylene (PP), polyethylene terephthalate (PET), polyamide (PA), polyethylene (PE), polystyrene (PS) and poly(vinyl chloride) (PVC) are dominating food industry sector, as they have low cost and advanced physical properties such as mechanical and barrier. However, disposal problem of the conventional synthetic polymers in food packaging have become unbearable issue for the authorities since recycling problems due to the foodstuff contamination. Polymers used in food packaging applications should maintain the food quality. To optimize the shelf-life of the foods and the production methods, barrier and both mechanical and thermal properties are effective, respectively. In addition, they should be compatible with foods; therefore, biodegradable only few polymers have been used such as polycaprolactones,

polyhydroxyalkanoates, polylactide, starch etc. Among them, polylactide polymer has gained much attention in packaging applications due to desired properties explained below in section 2.3.

## **2.3. Polylactide**

Polylactide is thermoplastic and aliphatic polyester which has gained enormous attention as the replacement of conventional polymers as it is biodegradable and bio-based polymer. Polylactide is mainly used in medical, coating and food packaging applications today. Polylactide is one of the promising polymers especially in food packaging application due to its economic pros of production and its chemical properties. Besides physical properties are nearly the same as PET and oriented PS. can be manipulated easily by changing its chemical properties (Shen et al., 2009; Auras et al., 2004).

### **2.3.1. Production of Polylactide**

Polylactide is produced via polycondensation and ring opening polymerisation of the lactide or direct polymerisation of the lactic acid. By polycondensation of lactic acid, low molecular weight polylactide are obtained and with the ring opening polymerization high molecular weight polylactide is produced. In the second method, lactic acid is converted high molecular weight polylactide directly (Shen et al., 2009).

During the production of the polylactide, less energy is required as the fossil fuel consumption is 50% less than conventional polymer. Besides, polylactide is eco-friendly polymer since the release of carbon dioxide during the biodegradation is nearly same as consumption of carbon dioxide while the production of polylactide (Figure 2.4.). Thus, the usage of polylactide has both economical and environmental benefits (Mohanty, 2005).

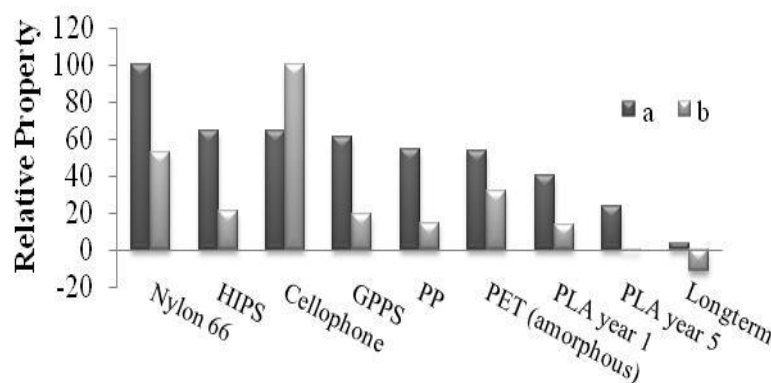


Figure 2.4. Relative a) energy required b) greenhouse emissions for production of various polymers (Source: Mohanty 2005).

### 2.3.2. Chemical Properties of Polylactide

Lactic acid- 2-hydroxypropionic acid -is water-soluble, three-carbon chiral acid, obtained from plant sources such as corn, wheat or rice or bacterial fermentation. The repeat unit of polylactide has one stereo center that can be either L or D in configuration (Figure 2.5.) Thus, molecular weight, melting point, extent of crystallization and mechanical properties of polylactide is significantly affected by the conditions of the polymerization reaction and the conformation of the lactides (Shen, 2009; Auras et al., 2004; Rasal and Janorkar, 2010).

The chemical structure of polylactide can be characterized by Fourier Transform Infrared (FT-IR) spectroscopy. Auras and coworkers (2004) summarized clearly FT-IR spectra of pure polylactide in the literature (Table 2.1). The characteristic peaks were examined in the ranges of 60 to 2995  $\text{cm}^{-1}$  absorption bands. The maximum absorbance was observed at 240 nm represented the ester group present in the backbone. Strong IR bands at 2877, 2946 and 2997  $\text{cm}^{-1}$  that were specified to the CH stretching region,  $\nu_{\text{as}}\text{CH}_3$ ,  $\nu_{\text{s}}\text{CH}_3$  and  $\nu\text{CH}$  modes were observed. At 1748  $\text{cm}^{-1}$ , a large band was seen corresponding the C=O stretching region. The region between 1500 and 1360  $\text{cm}^{-1}$  was defined as  $\text{CH}_3$  band. The peaks at 1382  $\text{cm}^{-1}$  and 1365  $\text{cm}^{-1}$  were assigned to the CH deformation and asymmetric bands, respectively. The CH bending modes resulted in the bands at 1315  $\text{cm}^{-1}$  and 1300  $\text{cm}^{-1}$ . The C–O stretching modes of the ester groups could be observed at 1225  $\text{cm}^{-1}$  and the  $\nu\text{O–C}$  asymmetric mode could appear at 1090  $\text{cm}^{-1}$ . In the region of the 1000  $\text{cm}^{-1}$  and 800  $\text{cm}^{-1}$ , it was possible to see peaks at 956  $\text{cm}^{-1}$  and 921  $\text{cm}^{-1}$  owing to the characteristic vibrations of the helical backbone with  $\text{CH}_3$  rocking modes. Amorphous and crystalline phase of

polylactide could be determined from the peaks as  $871\text{ cm}^{-1}$  and  $756\text{ cm}^{-1}$ , respectively. All peaks below  $300\text{ cm}^{-1}$  showed the  $\text{CH}_3$  torsion modes and the skeletal C–C torsions (Auras et al., 2004). Crystallinity was also supported by FTIR spectra between  $1186$  and  $1269\text{ cm}^{-1}$ .

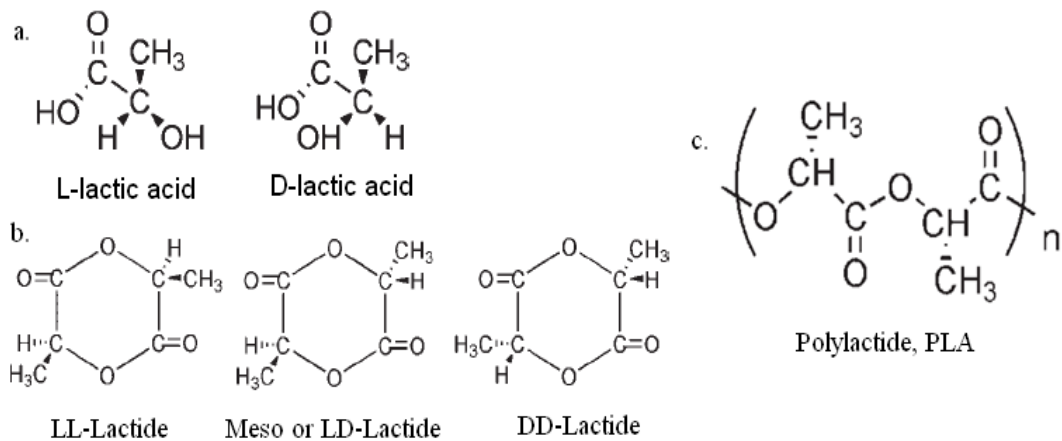


Figure 2.5. Chemical structure of a) L and D-lactic acid b) LL-, meso- and DD-lactides and c) constitutional unit of polylactide. (Source: Auras, 2009).

Table 2.1. Characteristic Infrared Spectra Bands of Polylactide  
(Source: Auras et al., 2004)

Assignment	Peak Position ( $\text{cm}^{-1}$ )
-OH stretch free	3571
-CH- stretch	2997(asym), 2946 (sym), 2877
-CO=O carbonyl stretch	1748
-CH <sub>3</sub> bend	1456
-CH- deformation including asymmetric and symmetric bend	1382 1365
-C=O bend	1225
-C-O- stretch	1194, 1130, 1093
-OH bend	1047
-CH <sub>3</sub> rocking modes	956, 921
-C-C- stretch	926

### 2.3.3. Physical Properties of Polylactide

Polylactide is one of the promising polymers in food packaging applications due to its physical properties nearly the same as PET and oriented PS. According to its

stereocomplex configuration and molecular weight; the properties of the polylactide such as solubility, barrier, thermal and mechanical properties vary. This section gives the properties of polylactide in detail.

### 2.3.3.1. Solubility of Polylactide

The relative affinity of a polymer and a solvent can be assessed using solubility parameters.

Polymer–polymer, polymer–binary-solvent, and multi-component solvent equilibria can be predicted by using solubility parameter. Hildebrand developed a relation based on cohesive energy for nonpolar systems to define the interaction between polymer and solvent, defined as (Mark, 2007):

$$\delta = c^{0.5} = -U/V \quad (2.1)$$

where  $\delta$ ,  $U$  and  $V$  are solubility parameter, the molar internal energy and molar volume, respectively.

Solubility parameter was defined as the sum of two components: nonpolar solubility and polar solubility parameter given in Equation. 2.2 (Mark, 2007).

$$\delta^2 = \delta_\lambda^2 + \delta_\tau^2 \quad (2.2)$$

where  $\delta_\lambda$  and  $\delta_\tau$  can be defined as a nonpolar solubility and a polar solubility parameter, respectively.

Hansen and co-workers proposed a practical extension of the Hildebrand parameter method to polar and hydrogen-bonding systems. In agreement with Hansen extension of the Hildebrand, dispersion, polar, and hydrogen-bonding parameters were valid simultaneously, related by this equation (Mark, 2007):

$$\delta_t^2 = \delta_d^2 + \delta_p^2 + \delta_h^2 \quad (2.3)$$

where  $\delta_t$  is Hansen's total solubility parameter,  $\delta_d$  the dispersive term,  $\delta_p$  the polar term, and  $\delta_h$  the hydrogen-bonding term.

For every system, the Hansen solubility parameters (HSP) sometimes do not show good agreement with experimental data as there has been based on a great variety of chemical and physical properties of solvents. Therefore, some solubility parameters are measures of solvent basicity, and others are obtained from direct determinations of the solubility of a representative solute in a range of liquids. Solubility parameters of solvents can be determined by using Van der Waals gas constant, surface tension, index of refraction, internal pressure, dipole moment vaporization enthalpy or boiling point. For polymers, solubility parameters can not be calculated from heat of vaporization data because of their nonvolatility. However, it can be determined by using the internal pressure, swelling data, inverse phase, gas chromatography, refractive index, intrinsic viscosity, dipole moment or group contribution methods (Mark, 2007; Agrawal, 2007). Table 2.2 gives the solubility parameters of polylactide and many different solvents predicted at 25 °C by using different solubility methods. The solubility parameters are good indicators to choose a right solvent for the polymer-solvent system. Good solubility between polymer and solvent is obtained when the difference between the solvent and polymers solubility parameters is smaller than  $2.5\text{MPa}^{0.5}$  or  $5\text{ (J/cm}^3)^{0.5}$  (Mark, 2007).

As seen in Table 2.2, acetone, acetonitrile, benzene, chloroform, m-Cresol, dimethyl formamide, dimethyl sulphoxide, 1-4 dioxane, 1-3 dioxolane, ethyl acetate, isoamyl alcohol, methylene dichloride, pyridine, toluene and xylene dissolve polylactide at 25 °C despite the fact that it is not soluble in isopropyl ether, cyclohexane, hexane, ethanol, methanol, water and diethyl ether. According to Auras and coworkers (2004), polylactides are soluble in dioxane, acetonitrile, chloroform, methylene chloride, 1,1,2-trichloroethane, dichloroacetic acid at room temperature and in ethyl benzene, toluene, acetone, tetrahydrofuran at their boiling points. However, polylactides are insoluble in water, some alcohols and alkanes (Auras et al., 2004).

Table 2.2. Solubility parameters of polylactide and solvents at 25°C  
(Source :Agrawal, 2004)

Solvents	HSP (J/cc) <sup>0.5</sup> at 25°C				Nonsolvents	HSP (J/cc) <sup>0.5</sup> at 25°C			
	$\delta_d$	$\delta_p$	$\delta_a$	$\delta_t$		$\delta_d$	$\delta_p$	$\delta_a$	$\delta_p$
Acetone	15.0	10.4	7.0	19.6	Isopropyl ether	13.7	3.9	2.3	14.4
Acetonitrile	15.3	18.0	6.1	24.4	Cyclohexane	16.5	0.0	0.2	16.5
Benzene	18.4	0.0	2.0	18.5	Hexane	14.9	0.0	0.0	14.9
Chloroform	17.8	3.1	5.5	18.9	Ethanol	15.8	8.8	19.4	26.5
m-Cresol	18	5.1	12.9	22.7	Methanol	15.1	12.3	22.3	29.6
Dimethyl formamide	17.4	13.7	11.3	24.9	Water	15.5	16.0	42.3	47.8
Dimethyl sulphoxide	18.4	16.4	10.0	26.6	Diethyl ether	14.5	2.9	5.1	15.6
1-4 Dioxane	19.0	1.8	7.4	20.5	<b>Method</b>	<b>Solubility parameters of PLA (J/cc)<sup>0.5</sup> at 25°C</b>			
1-3 Dioxolane	18.1	6.6	9.3	21.4		$\delta_d$	$\delta_p$	$\delta_h$	$\delta_t$
Ethyl acetate	15.8	5.3	7.2	18.2	Intrinsic 3D viscosity method	17.61	5.30	5.80	19.28
Isoamyl alcohol	15.8	5.2	13.3	21.3	Intrinsic 1D viscosity method	-	-	-	19.16
Methylene dichloride	18.2	6.3	6.1	20.2	Classical-3D geometric method	16.85	9.00	4.05	19.53
Pyridine	19.0	8.8	5.9	21.8	Fedors group contribution	-	-	-	21.42
Toluene	18.0	1.4	2.0	18.2	VanKrevelen group contribution	-	-	-	17.64
Xylene	17.6	1.0	3.1	17.9	Optimization method	18.50	9.70	6.00	21.73

### 2.3.3.2. Barrier Properties of Polylactide

Gas or vapor permeate through polymer films owing to pressure differences between the opposite membrane interfaces. Permeation of gases or vapor through polymer matrix consists of three main processes:

1. Solution of the gas into the polymer matrix
2. Molecular diffusion of the gas in and through polymer matrix
3. Release from the polymer matrix

Permeability of gases and vapors in polymer depends on the solubility of gas or vapor on the polymer matrix and diffusion through the polymer matrix related with the equation:

$$P = D \times S \quad (2.4)$$

where P, D and S show permeability, diffusion coefficient and solubility coefficient respectively.

Solubility coefficient depends on the difference between solubility parameters of polymer and gas/vapor ( $\Delta\delta$ ), molar volume of gas/vapor ( $V_g$ ), temperature (T) and constant characteristic of polymer property ( $\gamma$ ) which is shown in the Eqn. (2.5):

$$S = S_0 \exp \gamma \left( \frac{V_g \delta^2}{RT} \right) \quad (2.5)$$

The diffusion process for the steady state is defined by the general Fick's law (Crank, 1956; Letcher, 2007):

$$F = D \times \frac{\partial C}{\partial t} \quad (2.6)$$

where C is concentration and x is diffusion direction. The unsteady-state three-dimensional diffusion process is described by Fick's second law (Crank, 1956):

$$\frac{\partial C}{\partial t} = \frac{\partial C}{\partial x} \left( D \times \frac{\partial C}{\partial x} \right) + \frac{\partial C}{\partial y} \left( D \times \frac{\partial C}{\partial y} \right) + \frac{\partial C}{\partial z} \left( D \times \frac{\partial C}{\partial z} \right) \quad (2.7)$$

where  $t$  is time. In the case of a membrane, and if the diffusion coefficient  $D$  is independent of the concentration the one-dimensional form of relation is equal to (Crank, 1956):

$$\frac{\partial C}{\partial t} = D \times \frac{\partial^2 C}{\partial x^2} \quad (2.8)$$

Besides, if diffusing species flow at steady state is measured, rate of transfer of molecules ( $F$ ) can be assumed to be the same across all the polymers membrane with thickness of  $l$ .  $F$  can be determined with the following relation:

$$F = D \times \frac{\partial C}{\partial t} = D \frac{C_1 - C_2}{l} \quad (2.9)$$

where  $C_1$  and  $C_2$  are surface concentrations of polymer membrane, However, in practical systems surface concentrations can not be determined but only gas or vapor pressures  $P_1$  and  $P_2$  on the two side of the membrane, Therefore, permeability constant ( $P$ ) can be defined with respect to thickness and the pressure difference and diffusion rate with the following equation:

$$F = P \times \frac{(\Delta p)}{l} \quad (2.10)$$

where  $l$ ,  $A$  and  $\Delta P$  indicate thickness, pressure gradient of the across the polymer matrix, respectively(Crank, 1956).

Temperature, relative humidity, pH of the environment; molecular size, functional group and chemical potential of the diffusing species; morphology, orientation, free volume and cohesion and adhesion forces of the polymer affects the mass transfer through the polymer matrix (Letcher, 2007).

To control the mass transfer between the food and air, barrier films need to be produced since presence amount of water vapor, oxygen or carbon dioxide affects the

food quality. Water vapor leads to microbial growth, undesirable textural changes, and deteriorative chemical and enzymatic reactions. Therefore, controlling barrier properties of polymer films is necessary to extend shelf-life of food (Janjarasskul, and Krochta, 2010; Auras et al., 2005; Gontard, 1996; Weber, 2000).

Auras and coworkers (2005) studied the water vapor permeability of polylactide (PLA) and compared the permeability results with commercial synthetic polymer of polyethylene tetrathalate (PET) and oriented polystyrene (PS). It was found that permeability values of PLA were nearly the same as these conventional polymers. Weber and coworkers (2000) have compared the biopolymers and conventional polymers with respect to their water vapor transmission rates (WVTR) as low to high range (Figure 2.6.). WVTR of PLA was found to be in between PS and PHA. Moreover, Auras and coworkers (2005) have stated that permeability of polylactide changes with the relative humidity of the environment and temperature. Table 2.3 lists the permeability and diffusivity of water vapor in polylactide polymer at various temperatures.

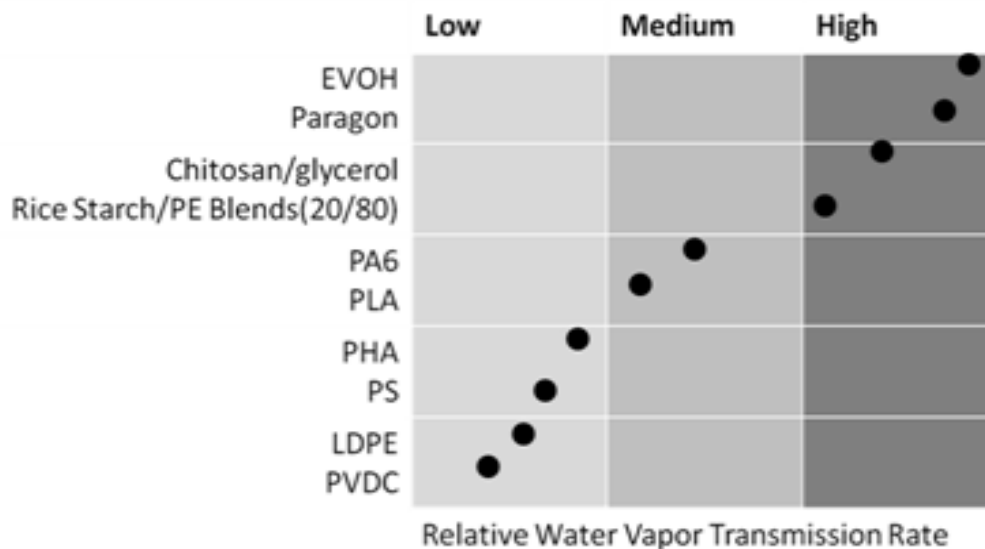


Figure 2.6. Comparison of water vapor transmission rates of polymers (Source: Weber 2000).

Table 2.3. Water Vapor Permeability and diffusivity of water vapor in polylactide at different temperatures.

Polymer Type	Reference	Water Vapor Permeability (g/m <sup>2</sup> day mmHg)mm	Diffusion coefficient (m <sup>2</sup> /s)	ΔRH (%)	Temperature (°C)
PLLA	Auras 2004	0.15	NA	100	37.8
OPLA	Auras 2005	1.48	4x10 <sup>-12</sup>	NA	20
PLA	Siparsky 1997	2.19	5-0.9x10 <sup>-11</sup>	90	40

Oxygen permeation value of polylactide was found to be the same as polyethylene, polystyrene and polyethylene tetrathalate and it permeates moderate amount of oxygen with respect to other biopolymers (Figure 2.7) (Weber , 2000 and Auras et al.,2005). Moreover, degree of crystallinity in polylactide polymers affects the permeability value. The higher the crystallinity degree in the polymer was the lower permeability values were obtained for polylactide as more tortuous path is generated for the oxygen molecule permeation. Oxygen permeability of polylactide was reported between the 3.5 and 2.0x10<sup>7</sup> ml mm/m<sup>2</sup> day atm (Maiti et al., 2002; Auras et al.,2005; Drieskens, 2009,).

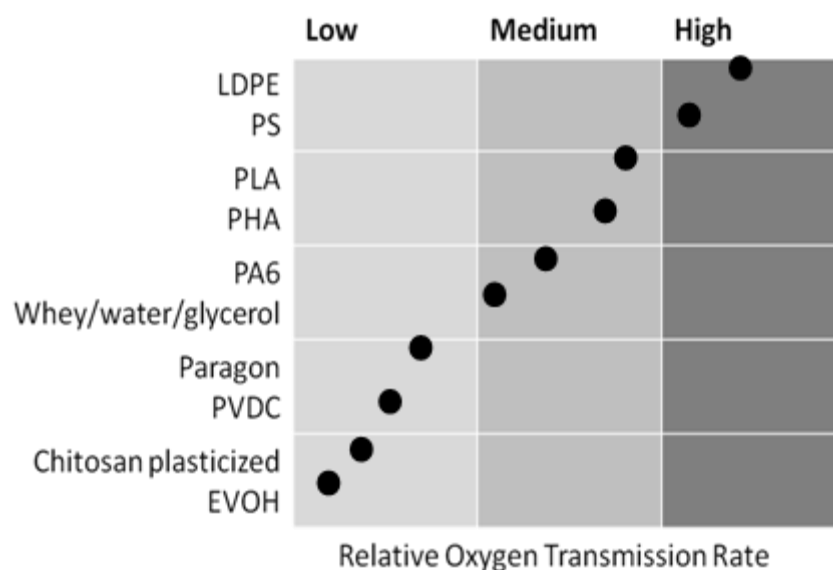


Figure 2.7. Comparison of oxygen transmission rates of polymers ( Source: Weber 2000)

Carbon dioxide permeability of PLA ( $1.7610^{-17}$ kgm/m<sup>2</sup>sPa) was found to lower than polystyrene but higher than polyethylene tetrphthalate.(Auras and coworkers, 2004).

### **2.3.2.3. Thermal Properties of Polylactide**

Nomenclature Committee of the International Confederation for Thermal Analysis (ICTA) defines thermal analysis as a group of analytical methods by which change of the physical property such as mass, dimension, enthalpy etc. of a substance is measured as a function of time; therefore, thermal analyses are not said to be chemical analysis. Differential scanning calorimetry (DSC), differential thermal analysis (DTA), thermogravimetric analysis (TGA), thermal mechanical analysis (TMA, DMTA), thermal optical analysis (TOA) and dielectric thermal analysis (DETA) are the methods of measuring specific property shown in Figure 2.8. By using these methods, melting and crystallization of flexible-chain polylactide phase transitions in liquid–crystalline polymers and chemical reactions including degradation of polylactide can be investigated. One of the important thermal properties of polymer is glass transition which determines the lower use limit of rubber and upper use limit of thermoplastics, defines the transition temperature between the glassy and rubbery state of the amorphous polymers. Besides this, melting temperature defines transition temperature between the solid state and liquid state of the crystalline polymers, therefore, semicrystalline polymers have both glass transition and melting temperature, moreover, degradation of polymers are important property and dissociation of the weakest bond of the polymer can be defined as thermal degradation which can be characterized by measuring initial decomposition temperature, half decomposition temperature, maximum rate of decomposition temperature and amount of char. By determining these quantities, mechanism of decomposition of polymer and process conditions of the polymer sample can be specified. Moreover, structural characterization of polymer composites can be done with respect to temperature (Gedde, 1996; Krevelen and Nijenhuis, 2009).

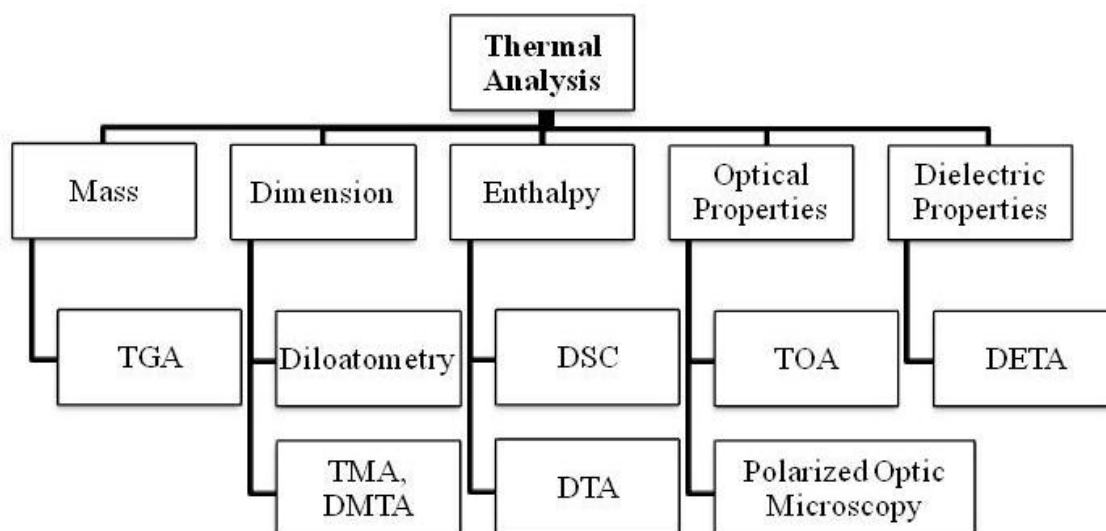


Figure 2.8. Thermo analytical methods  
(Source: Gedde, 1996).

Ahmed and coworkers (2009) studied thermal properties of polylactides with respect to microstructure, number average molecular weight and stereocomplex configuration of the polylactide. Effect of molecular weight on the glass transition temperature, melting temperature and crystallization temperatures of polylactide was also studied. It was found that the glass transition temperature of semicrystalline poly(L-lactide) increased from  $-3.8\text{ }^{\circ}\text{C}$  to  $66.8\text{ }^{\circ}\text{C}$  while the number average molecular weight increased from 550 to 2750. However, glass transition temperature started to decrease at higher molecular weight. Besides, stereocomplex structure of the polymer changed the glass transition temperature of polylactide. L-lactide polymer was found to be higher than D-lactide polymer structure. Melting temperatures and crystallization temperatures of polylactides were also increased with molecular weight increase from  $88\text{ }^{\circ}\text{C}$  to  $180\text{ }^{\circ}\text{C}$  and  $98\text{ }^{\circ}\text{C}$  to  $106\text{ }^{\circ}\text{C}$ , respectively. Degree of crystallinity was calculated by taking crystallization enthalpy of 100% crystalline polylactide as  $93\text{ J/g}$  (Ahmed, 2009). Tsuji and Fukui (2003) studied the thermal degradation behavior of poly(L-lactide), poly(D-lactide) and poly(L/D-lactide) films by thermogravimetric analysis under nitrogen flow with heating rate of  $10\text{ }^{\circ}\text{C min}^{-1}$  up to  $400\text{ }^{\circ}\text{C}$ . Onset and endset degradation temperatures of poly(L-lactide), poly(D-lactide) and poly(L/D-lactide) for non-isothermal degradation conditions were reported (Ahmed, 2009). Yang and coworkers (2008) found the glass transition temperature as  $61.2\text{ }^{\circ}\text{C}$  and melting temperature as  $170\text{ }^{\circ}\text{C}$  for pure polylactide polymer from DSC measurements.

From TGA measurements, onset degradation temperature of polylactide started at 280 °C and degradation temperatures at 10% and 50% mass loss values were reported as 292°C and 325 °C, respectively.

#### **2.3.2.4. Mechanical Properties of Polylactide**

To get an idea about long-term performance of the polylactide, mechanical properties are generally investigated by the help of short-term tests such as tensile testing, dynamic mechanical analysis etc. To characterize mechanical strength of polylactide generally tensile testing is used. With certain geometry and stretching speed, relationship between the stress and tensile strain are determined which is called Hooke law based on elasticity of the materials like a spring. Stress ( $\sigma$ ) is defined as the measurement of the average forces (F) per unit area of a surface ( $A_o$ ) shown by relation below (Mark, 2007):

$$\sigma = F/A_o \quad (2.11)$$

Tensile strain ( $\epsilon$ ) is the ratio of total deformation to the initial dimension of the material body in which the forces are being applied seen clearly by the relation:

$$\epsilon = \frac{(l-l_o)}{l_o} \quad (2.12)$$

where  $l$  and  $l_o$  are the current and original length of the material (Mark 2007) .

Tensile strength, elongation at break and modulus of elasticity (Young's modulus) give the information about polylactide mechanical behavior. Tensile strength shows the maximum load tolerance of the material per unit area. Percent elongation shows how much stress is needed to break polymer and modulus of elasticity (E). It tells us the resistance of polymer to deformation related by the Hooke's law (Mark, 2007):

$$\sigma = G\epsilon \quad (2.13)$$

Auras and coworkers (2004) studied the mechanical properties of polylactide. Tensile strength of polylactide was found to be between 44 and 66 MPa and percent elongation at break between 5% to 11%. Moreover, molecular weight and configuration of molecules also affect the mechanical properties. Mechanical properties of the polylactide show similar behavior with polystyrene. Yang and coworkers reported tensile strength, tensile modulus and elongation at break of polylactide as  $65.78 \pm 0.39$  MPa,  $1.68 \pm 0.07$  GPa, and  $8.91 \pm 0.44$ , respectively. Moreover, Lopez-Rodriguez and coworkers (2006) tabulated yield strength and stress at break as 56.8 MPa and 54.4 MPa while yield strain and strain at break were obtained as 0.4 and 0.5 respectively. Young's modulus was reported as 5.2 GPa much higher than Yang's study (Mark, 2007).

Dynamic mechanical analysis (DMA) is another mechanical analysis which investigates elastic (‘) and viscous flow (“) behavior of the polymers as a function of an oscillatory deformation (strain or stress) and temperature. The response of the polymer sample is determined as periodic strain stress. Dynamic mechanical properties can be determined by measuring the phase angle or phase shift ( $\delta$ ) between the oscillatory deformation and the response. For ideal elastic materials  $\delta$  is 0 whereas for purely viscous fluids  $\delta$  is determined as  $\pi/2$ . The sample can be loaded in a sinusoidal fashion in shear, tension, flexion, or torsion mode (Figure 2.9).

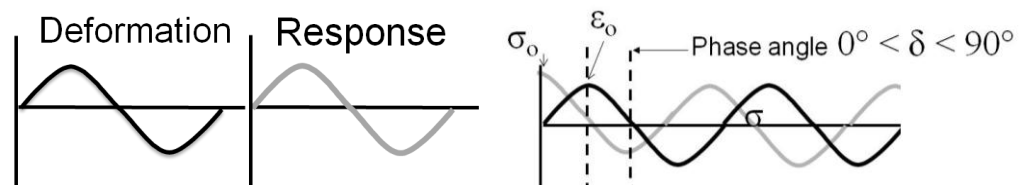


Figure 2.9. Sinusoidal strain and stress with phase angle  $\delta$   
(Source: Krevel en and Nihenjuis, 2009)

If the deformation is sinusoidal tensile strain and tensile stress can be related equations below:

$$\varepsilon = \varepsilon_0 \sin(\omega t) \quad (2.14)$$

$$\sigma = \sigma_0 \cos(\omega t) \quad (2.15)$$

where

$\varepsilon_0$ = the amplitude of the sinusoidal tensile deformation (-)

$\sigma_0$ = the amplitude of the sinusoidal tensile stress (N/m)

$\omega$ = the angular frequency (rad/sec)= $2\pi\nu$ ;  $\nu$ =frequency(Hz)

Generally investigation of polymers films are performed in tension, one determines the elastic tensile modulus  $E'$  called storage modulus and the corresponding viscous flow quantity  $E''$  called the loss modulus also glass transition temperature can be determined by the ratio of  $G''/G'$  known as  $\tan\delta$ . These three main properties in DMA related with the equations below:

$$G' = \frac{\sigma_0}{\varepsilon_0} \cos(\delta) \quad (2.13)$$

$$G'' = \frac{\sigma_0}{\varepsilon_0} \sin(\delta) \quad (2.14)$$

$$\frac{G''}{G'} = \tan(\delta) \quad (2.15)$$

where  $\delta_0$  and  $\varepsilon_0$  represent the amplitudes of stress and strain, respectively.  $\delta$  denotes the phase shift between stress and strain.

Clearly DMA data are of importance in designing products to be used in, for instance, vibration isolation, where the mechanical damping properties are used to convert mechanical vibrations into heat. DMA is also highly useful in studies of phase separation in multicomponent systems, and investigation of effects of fillers and other additives, different processing variables, degree of crystallinity, molecular orientation, internal stresses, etc on mechanical response. Dynamic mechanical behavior of polylactide was studied by Lopez-Rodriguez and coworkers (2006) and Tg value of polylactide was measured as 61.2 °C. Furthermore, at room temperature storage modulus of PLLA was found as 3000 MPa and decreased to 300 MPa above glass transition temperature, Moreover, Sarazin and coworkers (2008) studied dynamic mechanical behavior of the pure polylactide and its blends, Tg of pure PLA was found as 62.8 and storage modulus was decreased significantly above the Tg.

### 2.3.2. Rheological Properties of Polylactide

The study of rheology is the deformation of matter resulting from the application of a force. The type of deformation depends on the state of matter. Matter can have elastic or viscous behavior. Elastic behavior of the matter is defined clearly in section 2.3.2.4 which gives theoretically information about Hooke's law. Basically elastic materials store the energy as a spring also called as ideal solid. However viscous materials dissipate the energy such as water also called as ideal liquid. Ideal liquid is defined clearly Newton's law:

$$\tau = \eta \frac{\partial \gamma}{\partial t} = \eta \dot{\gamma} \quad (2.16)$$

where  $\tau$  is the shear stress and  $\dot{\gamma}$  is the applied shear rate and  $\eta$  is viscosity and the derivative of the strain with respect to time is, shear rate.

It is obviously seen that there is a linear relationship between shear rate and stress as seen in the Figure 2.10 and the equation 2.16. However, generally fluids can not behave ideally at all are called non-Newtonian fluids. At lower shear rates, some matters behaves like Newtonian liquids despite the fact that at higher shear rates, viscosity of the matter can show decreasing (shear-thinning) or increasing (shear thickening) behavior as a function of a shear rate. These materials are called as pseudoplastic and dilatant fluids, respectively. If there is a linear relationship between shear stress and strain with yield stress, this material is called as Bingham plastics and shear thinning behavior with yield stress is seen at Herschel-Bulkey fluid. ( Goodwin and Hughes, 2000; Smith, 2011)

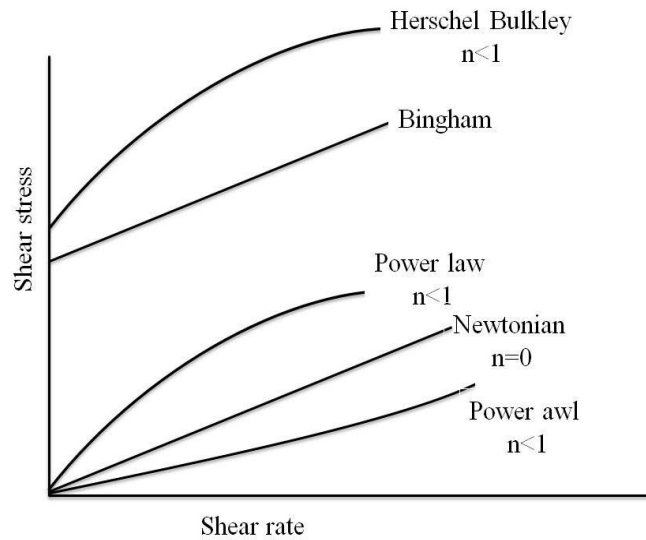


Figure 2.10. Rheological behavior of matters  
(Source: Smith, 2011)

Polymer melts can store and dissipate the energy therefore; they are viscoelastics materials and generally show; moreover, shear thinning behavior is generally observed in polymer melts can be related by Power Law model:

$$\tau = K \dot{\gamma}^n \quad (2.17)$$

where K is the flow consistency index and n is the flow behavior index . Based on flow behavior index, the fluid type can be classified, (Goodwin and Hughes,2000; Smith, 2011):

if  $n < 1$  pseudoplastic

$n = 1$  Newtonian

$n > 1$  Dilatant

Besides Herschel-Bulkey model can also be applied for polymers:

$$\tau = K \dot{\gamma}^n + \tau_0 \quad (2.18)$$

where  $\tau_0$  is yield stress

It is very essential to control the rheological properties of polymer melts during processing and applications such as mixing, dispensing, settling and flow control.

Polymer type, additive amount and type, temperature and shear affect the rheological behavior of the polymer (Smith, 2011).

Thermal processes such as injection molding, extrusion, film blowing, fiber spinning sheet forming and thermoforming are affected from the rheological properties of polymers especially shear viscosity. Polystyrene and polylactide have the same melt behavior. Melt viscosities of high molecular weight polylactide are reported as 500 to 1000 Pas at 50 to 10 s<sup>-1</sup>. From the rheological measurements, polylactide is viscoelastic fluid. (Auras et al., 2004). Sarazin and coworkers (2008) measured shear viscosities of pure polylactide and its blends and shear thinning behaviour was observed and viscosity changed between the range of a 40 to 2000 Pas at 1000 to 10 s<sup>-1</sup>.

## CHAPTER 3

### POLYMER NANOCOMPOSITES

Industrial uses of polymers are generally in the form of composites which can be defined as a combination of two or more materials (reinforcing elements, fillers and composite matrix binder) differing in form or composition on a macro or micro scale as they have better physical properties than pure polymers (WEB\_2). However, length scale of conventional fillers in micrometers at least which leads to more filler usage to enhance the physical property. Therefore, authorities turn toward new concept, nanocomposite which results in the development of materials with properties that are far superior to conventional composites. With low filler loadings, typically 1-10 wt%, physical properties of the polymer can be improved significantly so the overall cost can remain low as less filler is required to increase the performance of the polymer matrix (Koo, 2006).

Polymer nanocomposites consist of polymeric material (thermoplastics, thermosets or elastomers) and nanoparticles. In case of nanocomposites, the filler particles have at least one dimension on the nanometer length scale (1-100 nm) results in ultra large interfacial area to volume ratio, and the distance between the polymer and filler are extremely short. Therefore, with the increase the molecular interaction between polymer matrix and nanoparticles, mechanical, barrier properties dimensional stability, chemical resistance etc are improved, despite the fact that; dispersion difficulties, viscosity increase, optical issues occur (Table 3.1.). Properties of polymer nanocomposites are affected by:

- Nature of the nanoparticles (aspect ratio, size, geometry, cation exchange capacity etc.)
- Nature of the polymer (polar or apolar, crystallinity, molecular weight, polymer chemistry etc.)
- Morphology of polymer nanocomposites
- Synthesis methods
- The amount of the nanoparticles (Koo, 2006; Mittal 2010)

Table 3.1.Characteristics of nanoparticles to polymers.  
(Source: Koo, 2006).

Improved properties	Disadvantages
Mechanical Properties ( tensile strength, stiffness, toughness)	Viscosity increase ( limits processability)
Barrier	Dispersion difficulties
Dimensional stability	Optical Issues
Thermal stability	Sedimentation
Chemical resistance	
Reinforcement	

### 3.1. Nanoparticles

With the incorporation of different types of nanoparticles into polymer matrix, different improved properties can be obtained in polymer nanocomposites so nanoparticles selection should be done according to application area of the material. In the literature most common used nanoparticles are:

- Nanoclays (Montmorillonite(MMT), bentonite)
- Nanosilica (N-silica)
- Carbon nanofibers (CNF)
- Carbon nanotubes (multiwall (MWNTs), smaller-diameter (SDNTs) and single-wall (SWNTs))
- Polyhedral oligomeric silsesquioxane (POSS)
- Nanoaluminum oxide ( $Al_2O_3$ )
- Nanotitanium oxide ( $TiO_2$ )
- Others (Koo, 2006).

Among all nanoparticles, nanoclays are the most extensively researched group of nanoparticles. They belong to the layered silicate family.

#### 3.1.1. Nanoclays (Layered Silicates)

Nanoclays or layered silicates (LS) have been more widely investigated in the literature as it is easy to access o layered silicate nanocomposites exhibit markedly

improved barrier, mechanical, thermal properties with respect to the pure polymer or conventional composites (Alexandre and Dubois, 2000; Ray, 2003). Layered silicates are briefly classified according to the types and the relative content of the unit crystal lamellae (Table 3.2) (Ke, 2005).

Table 3.2. Classification of layered silicate crystals  
(Source: Ke, 2005)

Unit crystal lamellae type	Family of clay	Examples of Clay
1:1	Family of kaolinite Family of illite	Kaolinite, perlite clay, etc. Illite, etc.
2:1	Family of saponite Family of hydromica	Montmorillonite, saponite, vermiculite Illite, glauconite
2:2	Chlorite family and others	Chlorite
Mixed layer chain structure	Family of saponite	Sepiolite, palygorskite, etc.

According to the relative ratio of two unit crystal, the layered silicates are divided into three types:

- 1:1 type: Its unit lamellar crystal is composed of one crystal sheet of silica tetrahedron combined with one-crystal lamellae of alumina octahedron.
- 2:1 type: Its unit lamellar crystal is composed of two crystal sheets of silica tetrahedron combined with one crystal sheet of alumina octahedron between them.
- 2:2 type: Four crystal sheets form its unit lamellar crystal, in which crystal sheets of silica tetrahedron and alumina or magnesium octahedron are alternately arranged.

In mixed lamellar and chain-like structure, the lamellar hexagon rings composed of silica tetrahedron sheets are arranged opposite to one another in a right direction from the top down (Ke, 2005).

Montmorillonite (MMT) is the most common used clay mineral to prepare layered silicate nanocomposites; has a low content of alumina and a high content of silica. The chemical formula of the montmorillonite clay is  $\text{Na}_{1/3}(\text{Al}_{5/3}\text{Mg}_{1/3})\text{Si}_4\text{O}_{10}(\text{OH})_2$ . MMT is plate-like particles and belong to the family of 2:1 phyllosilicates. Silica is the dominant constituent of the montmorillonite clay with alumina being essential. The chemical structure of montmorillonite clays are seen in Figure 3.1. The 2:1 layer consists of two tetrahedral silica sheets that consist of  $\text{SiO}_4$  groups linked together to form a hexagonal network of repeating units of composition  $\text{Si}_4\text{O}_{20}$  and sandwiches an alumina octahedral sheet. The physical dimensions of one such layer may be 100 nm in diameter and 1nm in thickness. Owing to isomorphic substitutions in octahedral and tetrahedral sheets, the layers have negative charges. The negative charges are counterbalanced by the interlayer alkali or alkaline earth metal cations such as  $\text{Na}^+$  etc. and as a result of this the 2:1 layers are held together in stacks by electrostatic and van der Waals forces (Alexandre and Dubois, 2000; Ke, 2005; Koo, 2006; Mittal, 2010).

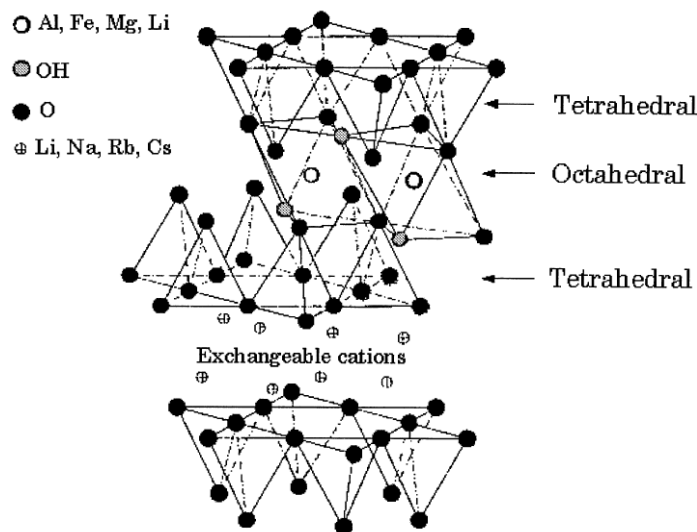


Figure 3.1. Structure of MMT  
(Source: Alexandre and Dubois 2000)

Most of alkali or alkaline earth metal cations have high energetic hydrophilic surfaces which make them incompatible with hydrophobic polymer matrix. Therefore, agglomeration of layered silicates in polymer matrix prevents to achieve maximum properties of nanocomposites. Dispersion of layered silicates in polymer matrix is typically accomplished via ion exchange between inorganic alkali cations on the clay

surface with the desired organic cation so interlayer distance between the layers and molecular interaction between layered silicates (LS) and polymer matrix increase. The several surface treatments are (Koo, 2006; Mittal, 2010):

- Quaternary ammonium salts based on textile antistatic agents
- Alkyl imidazoles which provides improved thermal stability
- Coupling and tethering agents
- Other kind of cations containing phosphorous ionic cations.

Since degree of dispersion of layered silicates depends on both interlayer charge (cation) of the clay and polymer character. Next section will briefly mention how the nature of polymer effects the dispersion of LS.

### **3.2. Nature of the Polymer**

Achieving impressive property improvements in polymer-clay composites depends on the dispersion of the clay in polymer matrix. Polarity and molecular weight of the polymers affect the mode of filler delamination (Koo, 2006; Mittal, 2010).

Polar polymers are observed to have better filler dispersion as compared to nonpolar polymers owing to the better match of polarity of polar polymers with partially polar surface of the clay. Thus, in the case of polar polymers, it is more likely the interfacial interactions between the organic and inorganic phases which lead to the delamination of the filler. To avoid delamination problem in nonpolar polymer systems organomodified clays are introduced therefore, electrostatic forces between the layers are reduced by increasing the basal spaces between the layers (Koo, 2006; Mittal, 2010).

The molecular weight ( $M_w$ ) of polymers affects the dispersion of fillers in polymer matrix owing to their viscosities. When the molecular weight of a polymer is low, it will easily penetrate into the basal spaces of the silicate layers as wetting of the silicate layer are enough to prepare the nanocomposites. In contrast to this, when the molecular weight and viscosity of the polymer is high, then the incorporation of the

fillers may be difficult as the fillers break easily due to strong shear and elongational forces during mixing leading to good dispersion (Mittal, 2010). However, Fornes and coworkers (2001) studied nylon6 nanocomposites by using three different molecular weight (low, medium and high) of nylon. In this study, it was found that a mixed structure for the low Mw based nanocomposites, having regions of intercalated and exfoliated clay platelets, while the medium molecular weight and high molecular weight composites revealed well exfoliated structures were observed. The physical property improvement was obtained at the high molecular weight based nanocomposites (Fornes, 2001).

### **3.3. Structure of Polymer-Layered Silicate Nanocomposites**

The physical mixture of a polymer and layered silicate may form four different types of nanocomposite depending on the strength of interfacial interactions between the polymer matrix and layered silicate. (Figure 3.3-a):

- Phase-separated composites
- Intercalated nanocomposites
- Flocculated nanocomposites
- Exfoliated nanocomposites

Owing to the poor molecular interaction between layered silicates and polymer matrix, phase separated structure is obtained and the property of that composite is the same as the conventional composites. In intercalated nanocomposites, the insertion of a polymer matrix into the layered silicate structure occurs in a crystallographically regular fashion, regardless of the clay to polymer ratio. Intercalated nanocomposites are normally interlayer by a few molecular layers of polymer. Flocculated nanocomposites are conceptually same as intercalated nanocomposites. However, silicate layers are sometimes flocculated due to hydroxylated edge-edge interaction of the silicate layers. In an exfoliated nanocomposite, the individual clay layers are separated in a continuous polymer matrix by an average distances that depends on clay loading. Usually, the clay content of an exfoliated nanocomposite is much lower than that of an intercalated nanocomposite (Koo, 2006).

Characterization of nanocomposites has been primarily done by wide-angle X-ray diffraction (WAXD) and transmission electron microscopy techniques (TEM) (Figure 3.2-b&c). In WAXD measurements, characteristic peaks of layered silicates give the information about the structure of the PLSNCs as  $2\theta$  denotes the basal spaces between the LSs. If the XRD peaks of the nanocomposite is same as the clay characteristic peaks, phase separated structures are obtained. In XRD measurements smaller and broaden is attribute to intercalated structure. Intercalateation with flocculation is identified by observing new lower angles peaks. Disappearance of peaks is caused by large gallery height indicates exfoliation structure of the nanocomposite.

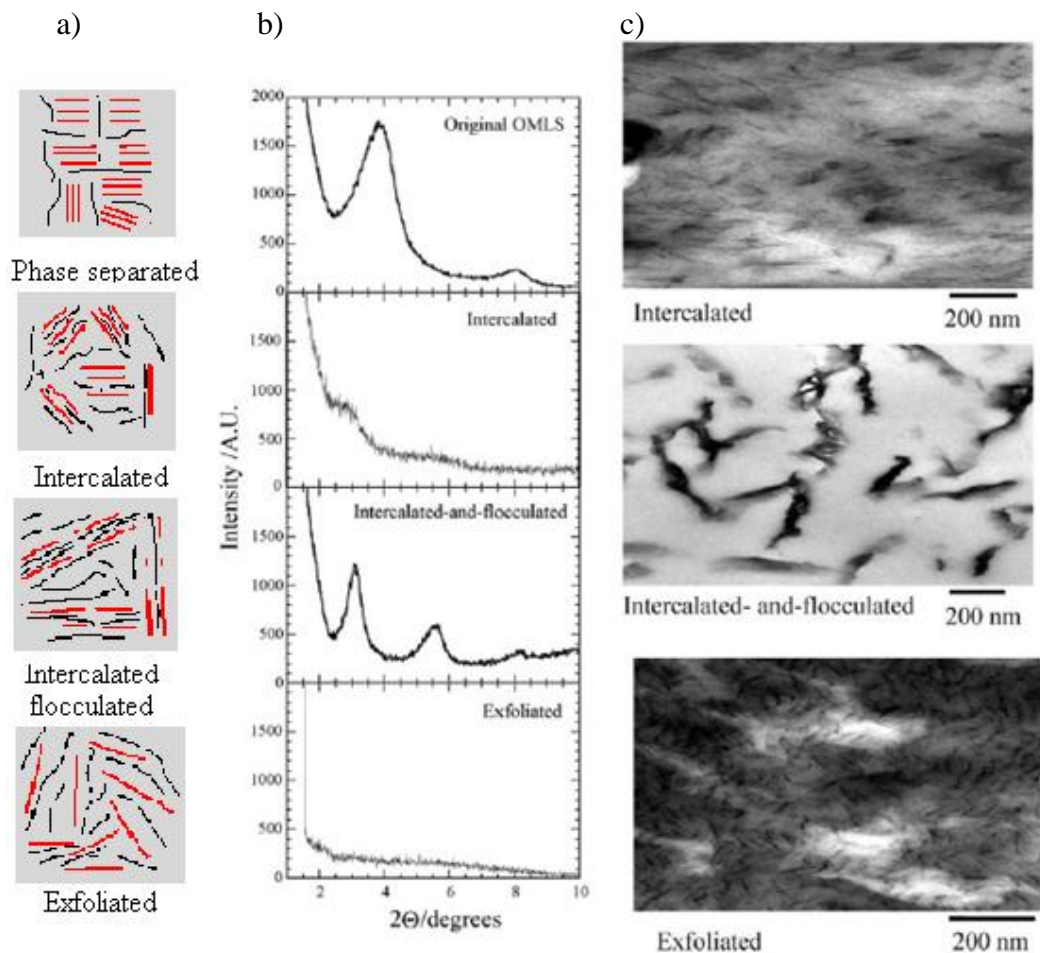


Figure 3.2. (a) Layered silicate composites structure (b) WAXD patterns and (c) TEM images of three different types of nanocomposites (Source: Okomato, 2005).

Besides, other techniques such as FTIR and NMR can also be used to support XRD technique. Natural and organomodified montmorillonites were characterized by FTIR analysis in the literature. By this method, characteristics bands of all layered

silicate types were obtained at  $3636$  and  $3395\text{ cm}^{-1}$  attributed to O–H stretching for the silicate and water,  $1639\text{ cm}^{-1}$  (related to O–H bending),  $1040\text{ cm}^{-1}$  (owing to stretching vibration of Si–O–Si from silicate) and  $917\text{ cm}^{-1}$  (from Al–OH–Al deformation of aluminates), respectively (Figure 3.3). There are also unique bands due to tetrahedral  $\text{SiO}_4$  near  $200$  and  $700\text{ cm}^{-1}$  in layer silicates that can be used for specific mineral identification. However, there are some bands in organomodified layered silicates spectra which are not exhibited by the natural montmorillonite; these bands were located at  $2924$ ,  $2842$  and  $1475\text{ cm}^{-1}$  and were assigned to C–H vibrations of methylene groups (asymmetric stretching, symmetric stretching and bending, respectively) from chemical structure of the surfactant (Cervantes-Uc, 2007).

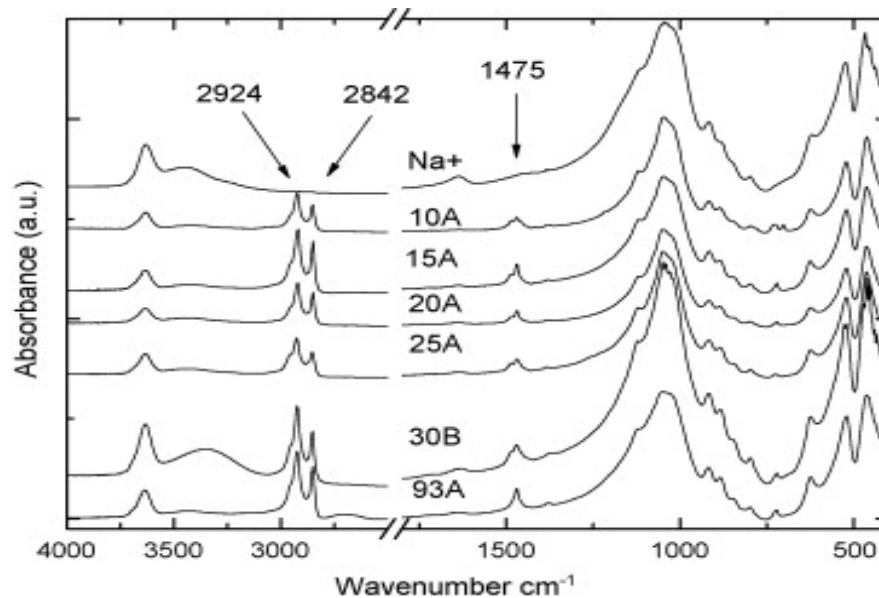


Figure 3.3. Various spectra of commercial clays  
(Source: Cervantes-Uc, 2007)

### 3.4. Production Methods of Polymer Nanocomposites

To create desired polymer nanocomposite, a proper nanocomposite preparation method should be applied. There are three main preparation methods used to prepare polymer-layered silicate nanocomposites (Koo 2006) (Figure 3.4.):

- Solution intercalation polymer/ prepolymer solutions
- Melt Intercalation
- In situ intercalative polymerization

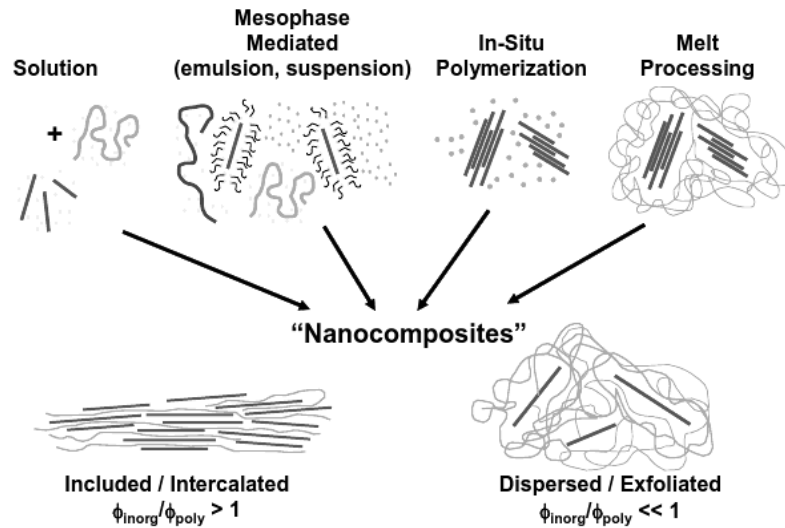


Figure 3.4. Preparation methods of layered silicate polymer nanocomposites (Source: Koo, 2006)

### 3.4.1. Solution Intercalation Polymer/ Prepolymer Solutions

Solution intercalation is the simplest method to prepare layered silicate polymer nanocomposite. The silicate layers are transformed into single layers using a solvent in which the polymer (or a prepolymer in case of insoluble polymers) is soluble. There are several different steps carried out in literature. It is well known that layered silicates can be easily dispersed and swollen in an adequate solvent, due to the weak forces that stack the layers together as clay type and solvent surface energy are important factors in the swelling process of layered silicates. Besides, basal spacing of the layered silicates increases by applying shear stress such as mixing or ultrasound. Then, polymer chains can adsorb onto the delaminated sheets when the solvent is evaporated (or the mixture precipitated) and finally exfoliated and intercalated structure can be obtained (Alexandre and Dubois, 2000; Koo, 2006; Mittal, 2010).

For the selection of the adequate solvent, interaction between the clay and solvent should be investigated. Swelling degree and increase in the basal spacing is related with the difference between the surface energies of the silicate layers and solvent. Table 3.3 lists the surface energies of solvents and organic modifiers. It was seen that among many solvents studied surface energy of benzyl alcohol is larger than organic modifiers which means basal spacing of the layered silicates in benzyl alcohol is larger than others (Burgentzlé, 2004).

Table 3.3. Surface energies of the different solvents and organic modifiers  
(Source: Burgentzlé, 2004)

Solvent/ Organic Modifiers	Surface Energy (mNm <sup>-1</sup> )	Solvent/ Organic Modifiers	Surface Energy (mNm <sup>-1</sup> )
Ethyl alcohol	22.8	Ethyl Benzene	29.2
Acetone	23.7	Xylene	30.1
Ethyl acetate	23.9	Dimethylformamide	35.8
Butane 1-ol	24.6	Benzyl alcohol	39.0
Methyl Ethyl Ketone	24.6	Na+	44.0
Cyclohexane	25.5	2MBHT	30.0
Chloroform	27.1	2H2HT	25.4
Toluene	28.5	MT2EtOH	34.5

### 3.4.2. In situ Intercalative Polymerization

In this technique, the layered silicate is swollen within the liquid monomer (or a monomer solution) so as the polymer formation can occur in between the intercalated sheets. Polymerization can be initiated either by heat or radiation, by the diffusion of suitable initiator or by an organic initiator or catalyst fixed through cationic exchange inside the interlayer before the swelling step by the monomer (Alexandre and Dubois, 2000).

### 3.4.3. Melt Intercalation

Most commonly used and industrially promising method is melt intercalation method for nanocomposite preparation. High molecular weight polymers are melted after which clay powder is added to the molten polymer in the extruder. Under these conditions and if the layer surfaces are sufficiently compatible with the chosen polymer, the polymer can crawl into the interlayer space and form either an intercalated or an exfoliated nanocomposite structure. Since shear is applied during preparation method, intercalation of silicates followed by exfoliation becomes more effective compared to other methods. In this technique, no solvent is required. However, onset degradation temperatures of organic modifiers which are

approximately at 200 °C limit the process temperature of the nanocomposite preparation (Alexandre and Dubois 2000, Mittal 2010).

### **3.5. Polylactide Layered Silicate Nanocomposites (PLA-LSN)**

As mentioned in section 2.3, to date, polylactide is the front runner and the most promising polymer among alternatives to petroleum based plastics for biodegradable film applications and disposable items because of some similarities with PS and PET synthetic polymers. However, some properties still need to be improved such as thermal stability, barrier improvements for shelf life of the foods and mechanical properties. However, improvements can be done by several approaches such as blending, copolymerization or nanofillers addition. Of particular interest is a nanocomposite technology consists of polylactide and layered silicates. Last two decades, many investigations have been done in polylactide layered silicate nanocomposites to develop their barrier, thermal, mechanical and rheological properties with respect to their morphology.

#### **3.5.1. Barrier Properties of PLA-LSN**

Permeation through PLA-LSNs is based on the same processes as pure polylactide which is explained in detail in chapter 2. The basic theory -Fick's law- is related with permeability of PLA-LSNs as that the polylactide matrix maintains the same properties and characteristics as the pure polylactide. However, the PLA-LSNs consist of a permeable phase (polylactide matrix) in which non-permeable layered silicates are dispersed. Basically, improvements in barrier properties by the introduction of fillers in the polymer matrix are primarily attributed to the tortuous path formed for the permeating molecules.

There are three main factors that influence the permeability of a nanocomposite(Choudalakis, 2009):

- the volume fraction of the layered silicate
- their orientation relative to the diffusion direction

- their aspect ratio (L/W ratio)

Incorporation of the silicate layers, a decrease of the solubility is expected in the nanocomposite due to the reduced polymer matrix volume, as well as a decrease in diffusion due to a more tortuous path for the diffusing molecules. But, volume fractions of the layered silicates are low results in small reduction of polylactide matrix. Therefore, decrease in the permeability of PLA-LSNs is more affected from change of diffusion coefficient than solubility. The tortuosity is the main factor, related to the shape and the degree of dispersion of the layered silicates.(Figure 3.5.) Dispersion degree of the layered silicates is also determined by the degree of exfoliation. The fully exfoliated nanocomposite presents much higher values for the tortuosity factor and the aspect ratio in comparison with the intercalated nanocomposite leads to improved barrier properties.(Ray, 2003; Lu, 2007; Choudalakis, 2009).

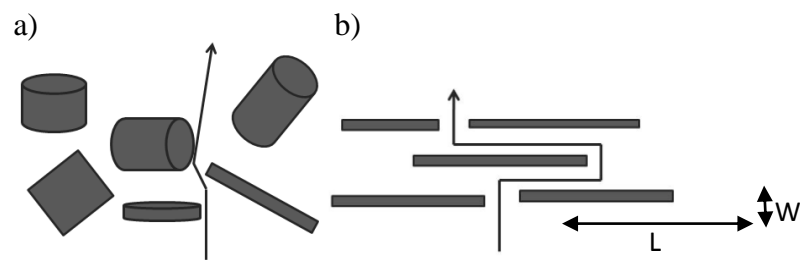


Figure 3.5. Tortuous path in (a) conventional composite and (b) layered silicate nanocomposite.

The principle of mass transfer through the nanocomposites films same as pure polymer and like pure polymers diffusion and solubility coefficient control the permeation through the films (Equation 2.4.). However, these parameters are modified owing to the presence of silicate layers:

$$S = S_0(1 - \phi) \quad (3.1)$$

$$D = D_0/\tau \quad (3.2)$$

where

$\phi$  =volume fraction of nanoparticles in the matrix

$\tau$  =the tortuosity factor

$D_0$ =diffusion of pure polymer

$S_0$ =solubility coefficient of pure polymer.

The ratio between the length (L) and width (W) (aspect ratio) and shape and orientation of the layer in the polymer matrix affect the tortuosity can be defined as:

$$\tau = l'/l \quad (3.3)$$

where

$l$  = membrane (film) thickness

$l'$  = the distance a solute must travel in the presence of silicate layers

With the presence of silicate layers the diffusion length increases. To standardize that effect of silicates layers on the theory, solute travelling distance is calculated by the relation:

$$l' = l + N(L/2) \quad (3.4)$$

where  $N$  denotes the number of silicate layers on the path which is related with thickness of the film, volume fraction and width of the layers:

$$N = \frac{l\phi}{W} \quad (3.5)$$

so the distance a solute must travel in the presence of silicate layers becomes as:

$$l' = l + \frac{l\phi}{W} \quad (3.6)$$

and tortuosity ( $\tau$ ) can be determined with the following relation:

$$\tau = 1 + \frac{l\phi}{2W} \quad (3.6)$$

Then with incorporation of silicate layers into polymer matrix diffusion coefficient and permeability of nanocomposites are determined with the following relations:

$$D = \frac{D_o}{1 + \frac{l\phi}{2W}} \quad (3.8)$$

Consequently, permeability of the nanocomposites is obtained with the following relation by using Eqns (3.8) and (3.1):

$$P = \frac{D_o}{1 + \frac{l\phi}{2W}} S_o (1 - \phi) \quad (3.9)$$

Several empirical models were developed based on the tortusity effect to determine the aspect ratio and give the idea about amount the structure of the nanocomposites. Most of the permeability models ignored any possible structure change occurred. Among these models, the first model was the Nielsen Model assuming regular arrangement of 2 dimensional rectangular platelets which are aligned perpendicular to diffusion direction. Nielsen model was obtained by dividing the nanocomposite permeability equation (Equation 3.9) by permeability of pure polymer. (Nielsen, 1967)

Relative theoretical permeability can be calculated as:

$$\frac{P}{P_o} = \frac{1 - \phi}{1 + (\alpha/2)\phi} \quad (3.10)$$

where

P=permeability of pure polymer

P<sub>o</sub>= permeability of nanocomposites

$\alpha$  = aspect ratio (L/W)

Volume fraction of nanofillers in composites can be calculated by using relation given below:

$$\phi = \frac{1}{1 + \left( \rho_c \frac{(1 - M_c)}{\rho_p M_c} \right)} \quad (3.11)$$

where

$\rho_c$  = density of clays

$\rho_p$  = density of polymer

$M_c$  = mass fraction of clay.

Besides Nielsen, Cussler and coworkers also developed mathematical model for gaseous diffusion in polymer matrix containing impermeable flakes, based on the idealization of the geometries that includes pores, slits and random shapers flakes. Layers are positioning regularly and align normal to the diffusion direction. According to their assumptions, the derived relation is:

$$\frac{P}{P_o} = \frac{1 - \phi}{1 + \left(\frac{\alpha}{2}\phi\right)^2} \quad (3.12)$$

Moreover, with the assumption of random positioning of layers Cussler model was developed as:

$$\frac{P}{P_o} = \frac{1 - \phi}{\left(1 + \frac{\alpha}{3}\phi\right)^2} \quad (3.13)$$

By including the orientation of layers, Nielsen model is extended by Bharadwaj:

$$\frac{P}{P_o} = \frac{1 - \phi}{1 + \frac{\alpha}{3}\phi(S + 1/2)} \quad (3.14)$$

where S donates the diffusion direction of the solute to the layers which can be calculated by:

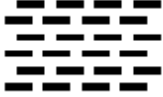
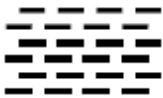
$$S = 1/2(3\cos^2 \theta - 1) \quad (3.15)$$

As the  $\theta$  denotes the angle between diffusion direction and the orientation of solute so its value may have a value between 0 and 1 (Bharadwaj, 2001).

All models based on the assumptions and orientation of the filler is listed in Table 3.4. These models allow us to predict the aspect ratio with the assumption of good level dispersion of the silicate layers. Therefore, these models can only be applicable to dilute or semi dilute LS containing composite systems. The estimated aspect ratio is normalized for the overall polymer-clay system. The higher length width ratio means higher degree of dispersion of silicate layers and the aspect ratio of the layered silicate was found in the range of 10 to 1000 (Paul and Robeson, 2008; Sun, 2008).

Zenkiewicz and coworkers (2008) studied water vapor, oxygen and carbon dioxide transmission rates through polylactide nanocomposites films with the addition of the natural and organomodified clay. Transmission rates of water vapor, oxygen and carbon dioxide of organomodified clay nanocomposites were reduced with the ratio of 43%, 39% and 82%, respectively. Besides the reduction ratio of the natural clay nanocomposite was improved as 25%, 4% and 76% in water vapor oxygen and carbon dioxide transmission rates respectively. Increment in clay content resulted in continuous decrease in transmission rates.

Table 3.4. Permeability models for nanocomposites  
(Source: Sun, 2008)

Models	Filler Type	Array/ Orientation	Dimension	Aspect ratio	Formulas
Nielsen	Ribbon 	Regular array / oriented	2D	w/l	$\frac{P}{P_o} = \frac{1-\phi}{1+(\alpha/2)\phi}$
Cussler- regular array	Ribbon 	Regular array / oriented	2D	w/l	$\frac{P}{P_o} = \frac{1-\phi}{1+(\frac{\alpha}{2}\phi)^2}$
Cussler- random array	Ribbon 	Random array / oriented	2D	w/l	$\frac{P}{P_o} = \frac{1-\phi}{(1+\frac{\alpha}{3}\phi)^2}$
Bharadwaj	Ribbon 	Random array / non-oriented	2D	w/l	$\frac{P}{P_o} = \frac{1-\phi}{1+\frac{\alpha}{3}\phi(S+1/2)}$

Moreover, Rhim and coworkers (2009) reported continuous decrease in water vapor permeability of nanocomposites prepared by organomodified clay but, increase in permeability of nanocomposites was obtained for unmodified clay containing samples. Koh and coworkers (2008) investigated modifier effect on the oxygen and carbon dioxide permeability and polymer type. They reported that the concentration of the modifier affect the molecular interaction between the polymer matrix and silicates layers. Therefore, different nanocomposite structures were obtained with the different type of modifier and the permeability of the nanocomposites was decreased with respect to dispersion degree of the silicates layers in polymer matrix. Effect of length and width ratio (aspect ratio) on the permeability and degree of dispersion on polymer matrix was studied by Ray and Okomato (2009). It was found that layered silicates having higher aspect ratios gave better dispersion where exfoliated structures were obtained. Oxygen barrier properties were also improved with an increase in aspect ratio.

### 3.5.2. Thermal Properties of PLA-LSN

Thermal improvements are achieved by crosslinking between polymer chains and clay sheets and molecular chains are confined inside the interlayer distance of clay sheets. Generally, decrease in melting temperature was observed by addition of nanofiller in polymer matrix. , but different results were also responses seen in the literature owing to relation between the polymer matrix and clay (Koh, 2006; Mittal, 2010) .

As volatile components are not generated during the decomposition, thermal stability is improved and also formation of the char is supported (Mittal, 2010). Koh and coworkers (2008) compared the thermal degradation behavior of polylactide nanocomposites with the pure polylactide. It is observed that pure polymer leaves fewer residues than its nanocomposites therefore; thermal resistance was increased with the increase of clay content. Thellen and coworkers (2006) reported that the onset of thermal degradation of pure polylactide was approximately 9 °C lower than its nanocomposite. Paul and coworkers (2003) have reported enhancement in thermal stability of PLA nanocomposites with increasing clay content, up to clay loading of 5wt%. With further increase of filler content, a decrease in thermal stability was observed. This was explained by the relative extent of exfoliation as a function of the amount of organomodified layered silicates. However, Wu and coworkers (2006) studied thermal stability of the polylactide nanocomposites and decrease in onset temperature was also observed although even flocculated structure was obtained.

In the literature, mostly decrease in melting temperature was observed with the incorporation of clay, Peterson and Oksman (2006) did not observe any change in melting temperature of polylactide nanocomposites. However, glass transition temperature and enthalpy of melting decreased with an increase in clay content. So, crystallinity degree was decreased by the filler addition (degree of crystallization). Lewitus and coworkers (2006) did not report any change in glass transition temperature, but cold crystallization temperature of nanocomposites decreased around 14-15°C with respect to pure polylactide owing to nucleation effect on the degree of crystallization with the use of clay.

Consequently, thermal behavior of the nanocomposites depends on polymer type and clay type as for each polymer clay system give different response in thermal

analysis. In addition to this, the degree of exfoliation also affects the thermal stability of the nanocomposites (Peterson and Oksman 2006).

### **3.5.3. Mechanical Properties of PLA-LSN**

Mechanical properties of conventional polymer which are improved by adding fillers with dimensions in the micrometer range and are related to volume fraction, shape and the size of the filler particles (Mittal, 2010). Whatever the size of the filler is, rigid fillers in a soft polymer matrix are resistant to stretching to maximum extension owing to their high modulus and adequate bonding between the two phases. The first evidence of the improvement in polymer nanocomposites was mechanical improvement reported by Toyota research group on a Nylon-6/montmorillonite composite. By the addition of only a small filler volume compared traditional polymers, the greater reinforcing effect was obtained as the larger the surface of the filler was in contact with the polymer matrix. The mechanical properties can include Young's modulus, yield stress, ultimate stress and strain etc. The improvement in the mechanical performances of nanocomposites is due mainly to the nanosized dimensions of the fillers which results in an extremely large aspect ratio and strong polymer-filler interactions that may affect the effectiveness of load transfer between the nanofillers and the polymer matrix. In addition, the type of the filler surface treatment governs the degree of particle dispersion in the matrix and, thus plays a key role in the mechanical performances of the final nanocomposite (Mittal, 2010). The nanocomposite stiffness (Young's modulus) is increased by a significant factor over that of the neat matrix when a uniform dispersion is achieved in nanoscale size. However, nonlinear mechanical properties such as tensile strength, elongation at break or impact strength. This may be explained by the fact that the Young's modulus is evaluated at low strains, whereas other properties are determined beyond catastrophic break where the loading transfer between the matrix and filler important (Paul and Robeson, 2008; Mittal, 2010)

Rhim and coworkers (2009) investigated the tensile strength values of polylactide nanocomposites. Maximum 20% and 17% decrease was observed in tensile strength and elongation at break of nanocomposites, respectively with respect to pure polylactide. Effects of filler type and loading on mechanical properties of

polylactide layered silicate nanocomposites were studied by Koh and coworkers (2008). It was observed that the improvement in modulus of elasticity and tensile strength was changing depending on the each polymer clay system. Generally modulus increased, however, tensile strength decreased with the addition of clay. But if the the clay was superior compatible with the polymer matrix increase could be seen. On the other hand Lewitus and coworkers (2006) observed that Young's modulus and tensile strength of polylactide nanocomposites were increased with the addition of clay due to the high aspect ratio of silicate layers leading to large surface area between the silicate layers and polymer matrix.

In the case of dynamic mechanical studies of polylactide-layered silicate nanocomposites, the storage modulus increases upon dispersion of a layered silicate in a polymer. This increase is generally larger above the glass transition temperature, and for exfoliated polylactide nanocomposites structures is probably due to the creation of a three-dimensional network of interconnected long silicate layers, strengthening the material through mechanical percolation. Above the glass transition temperature, when materials become soft, the reinforcement effect of the clay particles becomes more prominent, due to the restricted movement of the polymer chains. Generally, a decrease of  $\tan\delta$  peaks was observed. This indicates glass transition suppression by the presence of the clay. (Peterson and Oksman, 2006 ; Lewitus, 2006 , Ray and Bousmina 2005).

#### **3.5.4. Rheological Properties of PLA-LSN**

The rheological properties of the nanocomposites is vital importance as there are difficulties in polymer processing owing to increase of the viscosity with the addition of the clay. Also, rheological material functions are strongly influenced by the structure and the interfacial properties. The dispersion state of the clays can be studied at two levels:

- The macroscopic level: It includes the measurements of the rheological properties of the bulk blend.
- The microscopic level: It investigates the detailed dynamics of the individual particles

Therefore, rheology can be used as a tool that is complementary to traditional methods of nanocomposite characterization (Paul and Robeson, 2008; Mittal, 2010).

Based on the rheological studies done in the literature, it was found that polymer nanocomposites were very often have solid-like behavior owing to the physical jamming percolation of the randomly distributed silicate layers, at surprisingly low volume fraction, due to their anisotropy at lower shear rates. On the other hand, at high shear rates, shear thinning behavior was usually observed. As the alignment of silicate layers moved towards the direction of flow at high shear rates. Also, complex viscosity, loss and storage modulus of the nanocomposites was increasing by increasing angular frequency owing to clay addition. At lower frequency, behavior is sensitive to the structure of the percolation state of the silicate layers within the nanocomposite (Ray, 2002; Ray, 2003; Ray 2006, Wu 2006; Gu, 2007; Ahmed, 2010).

## CHAPTER 4

### EXPERIMENTAL STUDY

#### 4.1. Materials

Two kinds of poly (L-lactides) (PL65 and GF) were used to prepare the films. PL65 with inherent viscosity (i.v.) of  $6.74 \text{ dl g}^{-1}$ , density ( $\rho$ ) of  $1.24 \text{ g/cm}^3$  and GF with inherent viscosity (i.v.) of  $1.02 \text{ dl g}^{-1}$ , density ( $\rho$ ) of  $1.25 \text{ g/cm}^3$  were supplied from Purac Biomaterials (Netherlands) and Good Fellow (England). Chloroform was used as solvent obtained from Merck. To prepare polylactide nanocomposite (PLANC) films, commercial organomodified montmorillonites: Cloisite 10A, Cloisite 93 A and unmodified natural montmorillonite, Nanofill 116, from Southern Clay-Rockwood were used as nanofillers (Table 4.1.).

Table 4.1. Properties of Montmorillonite

Clay Type	Density ( $\text{g/cm}^3$ )	Organic modifier	Cation Exchange Capacity ( $\text{m}_{\text{eq}}/100\text{g clay}$ )
Cloisite 10A	1.90	2MBHT	125
Cloisite 93A	1.88	M2HT	90
Nanofill 116	2.86	No modification	116

## **4.2. Preparation of Polylactide (PLA) and Polylactide Nanocomposites (PLANC) Films**

Pure polylactide films were prepared by solution casting method by using chloroform containing 3 (w/v) % polylactide from Purac (PL65-P) and 7.5 (w/v) polylactide from Good Fellow (GF-P) at room temperature. Films were cast on the glass plates and then kept at 60° C in the vacuum oven for 24 hour to ensure complete solvent removal.

Nanocomposite films were prepared by solution intercalation method. Initially clays were swollen in chloroform by mixing for 24 hours while polylactide dissolved in chloroform then clay solution was sonicated with ultrasonic probe sonicator (MISONIX 20±0.05 kHz) for an hour to increase interlayer distance between the layers. After clay and polymers solutions were mixed for an hour and sonication process was again introduced in order to improve dispersion of clays in the polymer matrix. The amount of clay in PLANC was varied between 1 wt% to 10 wt%. Finally, films were cast on the glass plates and then kept at 60° C in the vacuum oven for 24 hour to ensure complete solvent removal.

## **4.3. Determination of Thickness of PLA and PLANC Films**

An electronic digital micrometer (293-821, Mitutoyo) with 0.001m sensitivity was used to measure the thickness of PLA and PLANC films. Each analyzed sample in permeability measurements and mechanical tests were measured by taking at least ten different measurements randomly.

## **4.4. Structural Characterizations of PLANC Films**

### **4.4.1. Fourier Transform Infrared (FTIR) Analysis of PLA and PLANC Films**

FTIR analysis gave information on the chemical structures of the nanocomposites, presence of polylactide and montmorillonite. IR spectra were taken in the range of 400 to 4000 cm<sup>-1</sup> with a FTIR Shimadzu 8201 Model.

#### 4.4.2. X-Ray Diffraction (XRD) Analysis of PLANC Films

The structure of clay and nanocomposites were characterized by Phillips X'Pert Pro MRD (Cu K $\alpha$  radiation ( $\lambda=1.54$  nm),40 kV,40 mA) between 2° and 8°. Interlayer distance between the silicate layers was determined with Braggs' Law:

$$\lambda = 2d \sin \theta \quad (4.1)$$

where:

$\lambda$ =wavelength of X-ray

$\theta$ =diffraction angle

d =interlayer distance

#### 4.5. Permeability of Measurements

##### 4.5.1. Determination of Relative Humidity Effect on Thickness of PLA and PLANC Films

Three samples were used for each PLA and PLANC film thickness measurements. Films were kept at 60° C in the vacuum oven for 2 days to ensure complete water removal. Ten measurements on each sample were done to determine average thickness of the dried samples. After that, films put into relative humidity chamber at 90% RH and 37.8 °C for one day. Then wet samples were measured ten times to find average thickness of the wet films. Change in thickness was calculated by the following formulas:

$$\Delta thickness(\%) = \frac{(WTF - DFT)}{DFT} 100 \quad (4.2)$$

where WTF and DFT denote wet film thickness and dry film thickness, respectively.

#### 4.5.2. Water Vapor Permeability Measurements of PLA and PLANC Films

The water vapor transmission rates of the PLA and PLANC films were measured with Mocon Permatran-W model 3/33 water vapor permeation measurement system. Measurements were performed at conditions of 37.8 °C and 90% relative humidity with 100 cm<sup>3</sup>/min nitrogen gas flow rate (ASTM F1249 standard).

To analyse water vapor barrier performance PLA or PLANC film samples, a film is placed in a test cell. Test cells are divided into two chambers separated by the sample material. The inner chamber is filled with nitrogen (carrier gas) and the outer chamber with water vapor (test gas). Molecules of water diffuse through the film to the inside chamber and are conveyed to the sensor by the carrier gas. The computer monitors the increase in water vapor concentration in the carrier gas and it reports that value on the screen as the water vapor transmission rate.

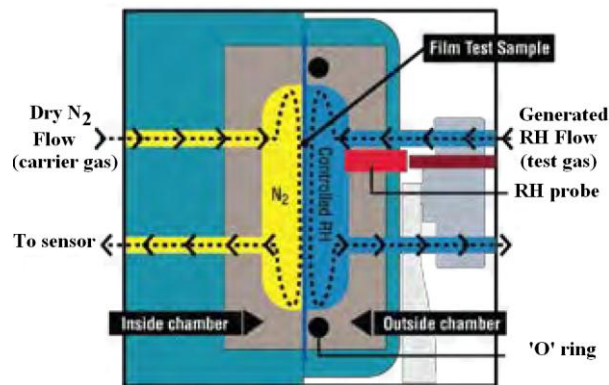


Figure 4.1. Illustration of water vapor permeability experiment  
(Source: Mocon Manual Book)

By using water vapor transmission rate, (WVTR), permeance and permeability can be calculated from the following formulas:

$$Permeance = \frac{WTR}{S(R_1 - R_2)} \quad (4.3)$$

$$Permeability = Permeance \times Thickness \quad (4.4)$$

where:

$\Delta P$  = Vapor pressure difference in inches of mercury

$R_1$  = Relative humidity at the source expressed as a fraction

( $R_1 = 1.00$  for a 100% RH chamber, and for 90% RH chamber  $R_1 = 0.90$ )

$R_2$  = Relative humidity of the vapor sink expressed as a fraction

( $R_2 = 0$  for the 0% RH chamber (dry side))

$S$  = Vapor pressure of water at the test temperature.

#### 4.5.3. Oxygen and Carbon dioxide Permeability Measurements of PLA and PLANC Films

The oxygen permeability of the films was measured according to the ASTM D3985 standard using gas permeation instrument, Lyssy L100-5000 (PBI Dansensor, Denmark) based on the manometric testing principle. In the manometric testing method, a pressure difference (driving force) across the sample is created by maintaining the test gas at atmospheric pressure in the upper chamber, while vacuum is applied in the lower measuring chamber. While the gas permeates through the sample, the pressure in the lower measuring chamber increases. The instrument measures the time required for the lower chamber pressure to increase from a predefined lower limit to a pre-defined upper limit. The measured time interval is then transformed into the gas permeability rate expressed in  $\text{ml/m}^2/\text{day}$ . Gas permeabilities of the films were determined at constant temperature ( $23\text{ }^\circ\text{C}$ ) and relative humidity (0% RH) conditions with  $5\text{--}10\text{ cm}^3/\text{min}$  gas flow.

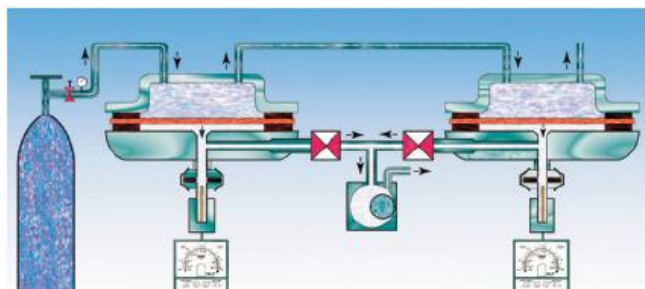


Figure 4.2. Illustration of gas permeability experiment

(Source:PBI Dansensor)

#### **4.6. Thermal Analysis of PLA and PLANC Films**

Glass transition and melting temperature of the PLA and PLNC were measured by differential scanning calorimetry DSC, TA instruments Q10 under nitrogen flow of 50 L/min with the heating rate 10°C/min. Crystallization temperature of the PLA and PLNC were determined with the following procedure. Initially films were heated up to 200 °C with the heating rate 10°C/min, then they were cooled down to 0 °C with the cooling rate 2°C/min and finally, they were heated up to 200 °C with the heating rate 10°C/min again.

Thermal stability and onset degradation temperature of PLA and PLANC were investigated with Perkin Elmer Diamond TG/ DTA from room temperature to 1000 °C with the heating rate 10°C/min. The analyses were performed in a dry nitrogen atmosphere.

#### **4.7. Mechanical Property Determination of PLA and PLANC Films**

According to ASTM D-882 standard modulus of elasticity, tensile strength percent elongation at break, yield strength and percent elongation at yield were determined with texture analyzer (TA XT Plus) equipped with a 5 kgf load cell in tensile mode. Tested films were cut in 10 mm width and 80 mm in length and put into relative humidity chamber at 50% RH and 23 °C for three days. The initial gauge length and testing speed were fixed at 50 mm and 5 mm/min, respectively. At least five films were tested and the average was reported.

Glass transition temperatures, loss modulus, storage modulus of films were determined using a dynamic mechanical analyzer (Q800, TA Instruments). Dynamic mechanical analysis (DMA) was performed in tension mode at a frequency of 1 Hz and an amplitude of 15 µm from 35 °C to 150 °C at a heating rate of 3 °C/min

#### **4.8. Rheological Measurements of PLA and PLANC Films**

Melt rheological measurements were performed by a parallel plate rheometer, TA instruments. Measurements were conducted by using a set of 25 mm diameter parallel plates with a sample thickness of 1 mm.

The limits of linear viscoelastic properties of PLA and PLANCs were determined by dynamic strain sweeps that were performed at 170°C and a frequency of 10 rad s<sup>-1</sup>. The strain amplitude was fixed to 1% to obtain reasonable signal intensities even at elevated temperature to avoid the nonlinear response.

For dynamic frequency measurements were performed at 170 °C which was chosen as the most representative of a typical processing temperature of PLA. The storage modulus, loss modulus and complex viscosities were determined. Steady-shear viscosity measurements were conducted at 170 °C at 0.01, 0.05 and 0.1 s<sup>-1</sup>.

#### **4.9. Contact Angle Measurements of PLA and PLANC Films**

To determine the surface wettability property of the films, contact angle measurements were performed using Attension Theta Optical Tensiometer, KSV. During the analyses, 6 µl of water were dropped on the film surface. Contact angles of left and right sides were determined by computer programme digitally and the mean value of both sides was calculated and ten replications of the analyses were done for each sample and obtained mean values of the replications were reported.

#### **4.10. Color Measurements of PLA and PLANC Films**

The color measurement of PLA and PLANC was performed using a color measurement device (Avantis, AvaSoft 6.2). The color change between the pure polylactide and polylactide nanocomposites was determined by using white paper as a background for color measurements of the films. In the Hunter system, color is represented as a position in a three-dimensional sphere, where the vertical axis L indicates the lightness (ranging from black to white), and the horizontal axes, indicated by a and b, are the chromatic coordinates (ranging from a: greenness to redness and b:

blueness to yellowness). Hunter L, a, and b values were averaged from five readings across for each coating replicate. The total color difference ( $\Delta E$ ) can be calculated by the following equation;

$$\Delta E = \sqrt{(\Delta L)^2 + (\Delta a)^2 + (\Delta b)^2} \quad (4.5)$$

## CHAPTER 5

### RESULTS AND DISCUSSIONS

The aim of the study was to investigate the effects of nanoclay type, nanoclay content and polymer molecular weight on the barrier, mechanical, surface, optical and thermal properties of layered silicate polylactide nanocomposite by achieving intercalated or exfoliated structures. Structural characterization of the nanocomposites was conducted by FTIR, SEM and XRD analysis. Besides, rheological properties were also examined to see the effect of nanoclay addition on the processability of PLANCs.

Poly lactide nanocomposites (PLANCs) were prepared by solution intercalation method by using layered silicates as nanofiller. In order to open clay stackings (step I) and obtain further penetration of PLA chains into clay galleries (step II), sonication process was applied in the preparation steps of the nanocomposites as explained in Section 4.2. Sonication time of both steps was optimized with the help of XRD analysis. From XRD chromatograms of PLANC samples (Figures A1 and A2), it is evident that  $2\theta$  values of nanocomposites decreased with increasing sonication time from 5 min to 60 min due to the opening of clay layer stackings (increase of the interlayer distance between the silicate layers) and better penetration in polymer chains into interlayer space. Therefore, sonication time of the two steps was set to an hour.

Effects of organomodification of clay and molecular weight of PLA on the properties of nanocomposites were studied by using two different organomodified clays (Cloisite 10A and Cloisite 93A) and PLA polymers (PLA65 and GF-PLA) with different molecular weights, Resulting films were named according to their clay content in PLA polymer and its polymer and clay types and coded as shown in Table 5.1

Table 5.1. Sample codes of prepared films according to polymer and nanoclay type and nanoclay content.

Sample Code	Polymer Type	Clay Type	Clay Amount (%)
PL65-P	Purac	-	0
PL65-10A-2	Purac	Cloisite 10A	2
PL65-10A-5	Purac	Cloisite 10A	5
GF-P	Good Fellow	-	0
GF-10A-1	Good Fellow	Cloisite 10A	1
GF-10A-2	Good Fellow	Cloisite 10A	2
GF-10A-5	Good Fellow	Cloisite 10A	3
GF-10A-7	Good Fellow	Cloisite 10A	7
GF-10A-10	Good Fellow	Cloisite 10A	10
GF-93A-1	Good Fellow	Cloisite 93A	1
GF-93A-2	Good Fellow	Cloisite 93A	2
GF-93A-5	Good Fellow	Cloisite 93A	5
GF-93A-7	Good Fellow	Cloisite 93A	7
GF-93A-10	Good Fellow	Cloisite 93A	10
GF-NF-2	Good Fellow	Nanofil 116	2
GF-NF-5	Good Fellow	Nanofil 116	5

## 5.1. Structural Characterizations

Structural characterization of the PLA nanocomposites was performed by using FTIR, SEM and XRD analysis in order to understand the interactions between the silicate layers and polymer matrix and also their effect on the properties of the films.

### 5.1.1. Fourier Transform Infrared (FTIR) Analysis

In any composite system, the interaction of filler with the polymer matrix can be examined by FT-IR spectroscopy. Appearance of new bands is the evidence of this interaction. Figure 5.1 shows the chemical structure of all silicate layers used in this study. Layered silicates give a large band in the region  $750\text{-}1350\text{ cm}^{-1}$  due to the several Si-O-Si bonds between the layered silicate platelets as seen in Figure 5.1. All bands detected by FT-IR analysis are consistent with the literature results discussed in Section 3.3 in Chapter 3. Cervantes-Uc and coworkers determined organomodifier presence in organomodified layered silicates from the bands which were located at  $2842$  and  $2924\text{ cm}^{-1}$ . These bands were assigned to C-H vibrations of methylene groups (asymmetric stretching, symmetric stretching respectively) owing to chemical

structure of the surfactant. Organomodified clays, Cloisite 10A and 93A, show two bands between 2800 and 3000  $\text{cm}^{-1}$  which can be attributed to organomodifier presence. However, nanofill 116 does not show these bands since it is an unmodified layered silicate.

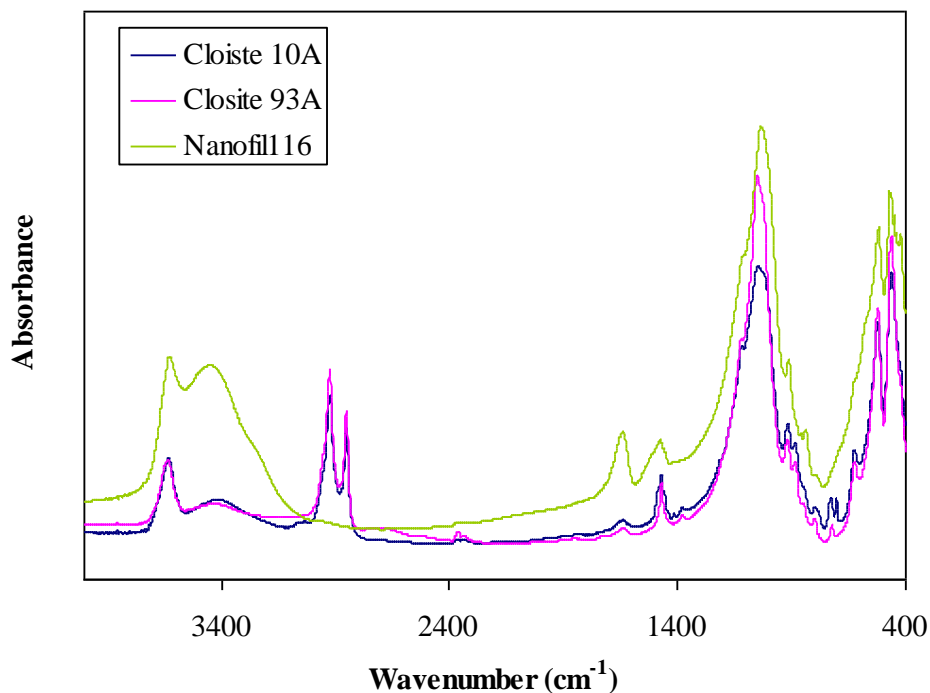


Figure 5.1. FTIR spectra of Cloisite 10A, Cloisite 93 A and Nanofill 116.

Figure A.2.5 in appendix A. illustrates the characteristic bands of PL65-P and GF-P polymers in the range of 800  $\text{cm}^{-1}$  to 1800  $\text{cm}^{-1}$  wavenumber region. Vibrations of the helical backbone with  $\text{CH}_3$  rocking modes were observed between 800 and 1000  $\text{cm}^{-1}$ . The  $\nu\text{O-C}$  asymmetric mode and  $\text{C-O}$  stretching modes of the ester groups appeared at 1090  $\text{cm}^{-1}$  and 1225  $\text{cm}^{-1}$ .  $\text{CH}_3$  bands were seen at the region between 1500 and 1360  $\text{cm}^{-1}$ . Besides, at the same region clay has  $\text{O-H}$  bending at 1639  $\text{cm}^{-1}$ , stretching vibration of  $\text{Si-O-Si}$  at 1040  $\text{cm}^{-1}$  and  $\text{Al-OH-Al}$  deformation at 917  $\text{cm}^{-1}$  (Figure 5.1.). Moreover, between 2800 and 3000  $\text{cm}^{-1}$  IR bands of PL65-P and GF-P were observed indicating the  $\text{CH}$  stretching region of PLA. These bands were overlapped with organoclay bands between 2800 and 2900  $\text{cm}^{-1}$ . Hence, degree of exfoliation can not be followed by the FTIR spectra of the PLANCS.

However, by comparing FTIR spectra of pure PLA and all PLANCS films in Figures A.2-5, it was seen that determinative nanoclay bands were located at 525 and 465  $\text{cm}^{-1}$  owing to  $\text{Al-O}$  stretching and  $\text{Si-O}$  bending of nanoclays, respectively.

Therefore, wavenumber versus percent absorbance graphs were drawn to investigate effect of clay addition on these bands for all polymer-clay systems (Figures 5.2-5.5). It was obviously seen that the percent absorbance of the polymer nanocomposites at 525 and 465  $\text{cm}^{-1}$  increased with the addition of the clay. That indicates the presences of nanoclays in PLA matrix.

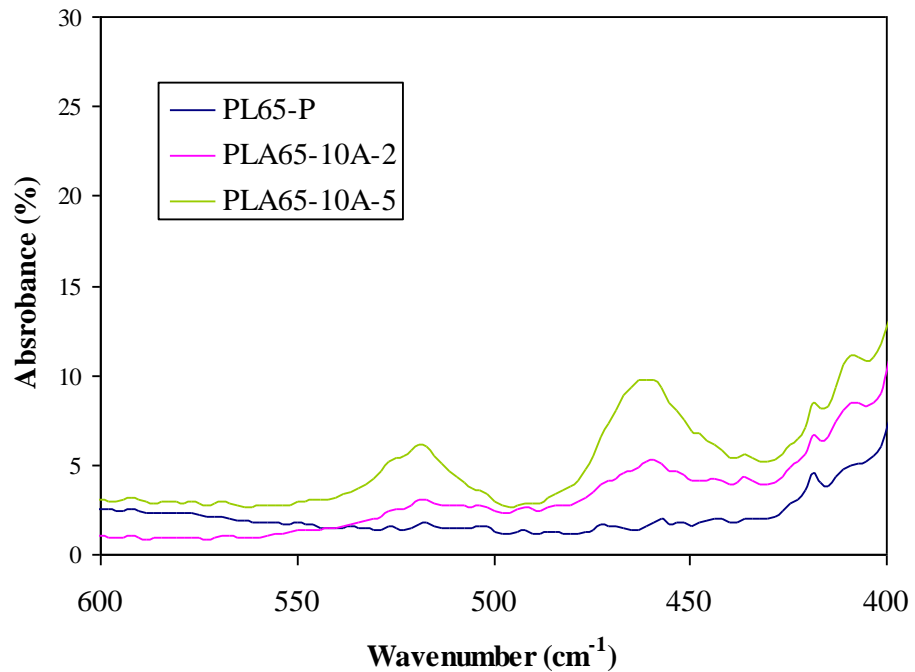


Figure 5.2. Percent FTIR spectra of PL65-P and PL65-10A nanocomposite films in 400-600 $\text{cm}^{-1}$  region.

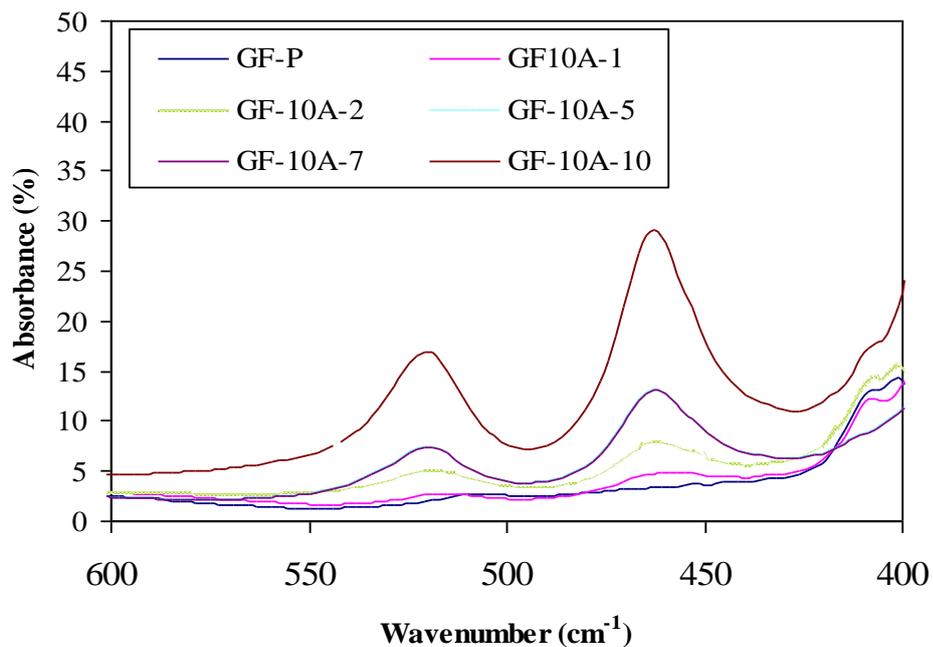


Figure 5.3. Percent FTIR spectra of GF-P and GF-10A nanocomposite films in 400-600 $\text{cm}^{-1}$  region.

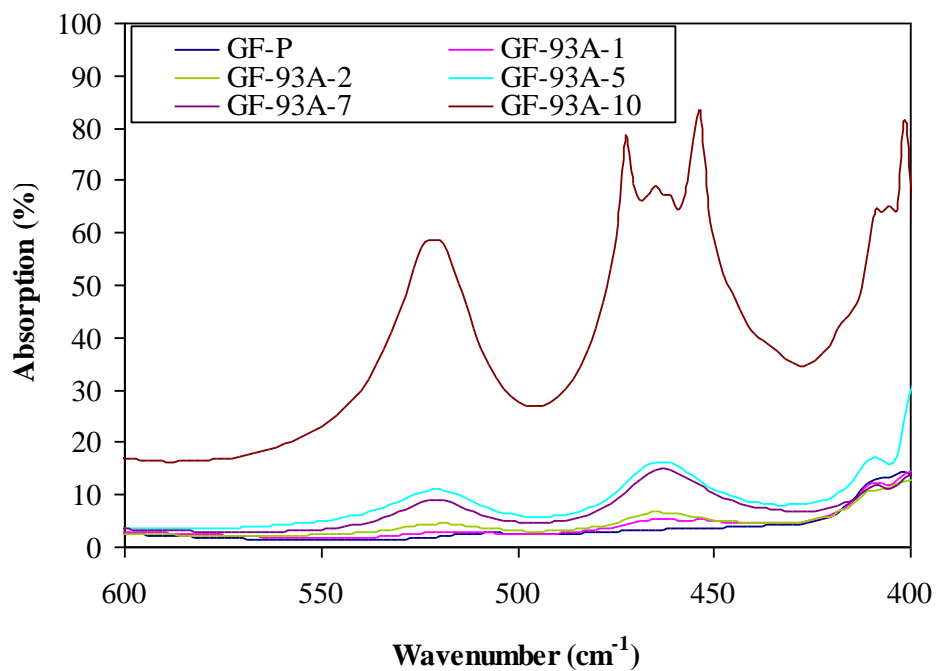


Figure 5.4. Percent FTIR spectra of GF-P and GF-93A nanocomposite films in 400-600 $\text{cm}^{-1}$  region.

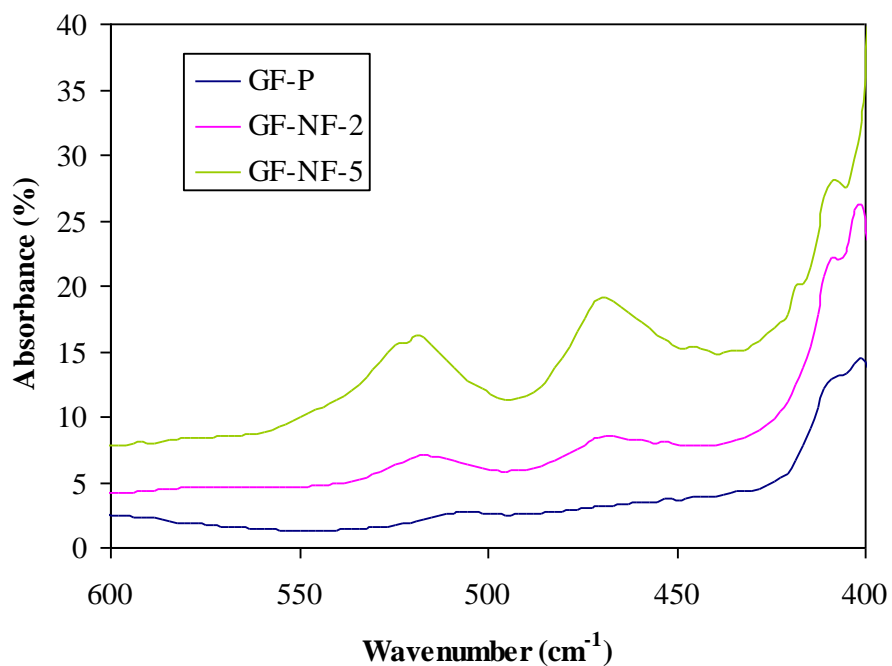


Figure 5.5. Percent FTIR spectra of GF-P and GF-NF nanocomposite films in 400-600 $\text{cm}^{-1}$  region.

### 5.1.2. X-Ray Diffraction (XRD) Analysis

X-Ray diffraction is the most commonly used technique to characterize the structure of nanocomposites. The distance between layers of the silicate can be

determined by utilizing Bragg's law (Equation 4.1.). If there is no change in basal reflections of the layered silicate polymer nanocomposites with respect to characteristic peak of nanoclay, it can be said that phase separated structure is obtained owing to incompatibility between the layered silicate and polymer matrix. Intercalated structures can be determined by monitoring peak shifts to lower angles and/or broader peaks as the spacing of the organoclays increases. Exfoliated structures do not give diffraction peaks since distances between layered silicate platelets are higher than the detection limit of XRD (Koo, 2006; Pavlidou and Papaspyrides, 2006; Mittal 2010).

Figures 5.6 and 5.7 show the XRD patterns of Cloisite 10A, Cloisite 93A and Nanofil 116 clays. Their basal spacing (d-spacing) were calculated as 1.92nm, 2.36 nm and 1.026 nm, respectively from their characteristic diffraction peaks at  $2\theta$  values of 4.65, 3.72 and 8.65, respectively by using Bragg's law (Equation 4.1).

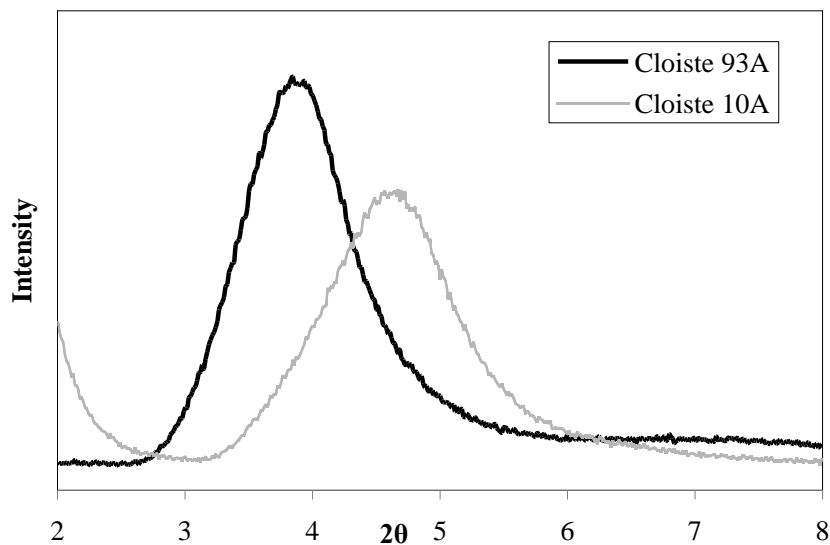


Figure 5.6. XRD patterns of Cloisite 10A and Cloisite 93A.

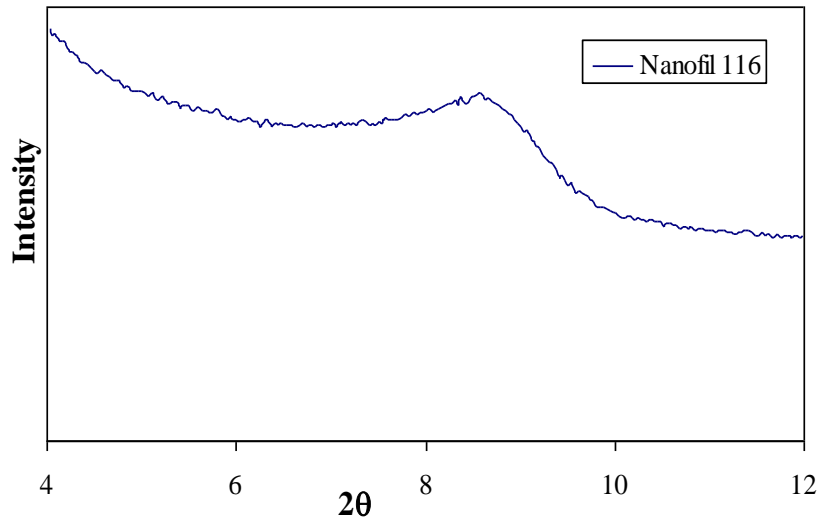


Figure 5.7. XRD pattern of Nanofil 116.

Figure 5.8 shows the XRD results of PLA65-10A nanocomposites. Comparing the structures of these films, as seen in Figure 5.8, the characteristic peak of the clay disappeared in the XRD spectrum for PLA65-10A nanocomposite films when the clay content was below 5wt%, which may be attributed to the complete delamination of clay platelets (exfoliated structure). The diffraction peaks of the nanocomposite films containing 5wt % and 7wt% clay shifted to lower angles with broader peaks showing intercalated flocculated structure. PLA65-10A-10 sample showed a peak broadening between  $2\theta$  values of 2.89 and 5.20 that indicated intercalated and partially agglomerated structure. These results indicate that high interaction between the layered silicates and polymer matrix was achieved and penetration of the polymer chains into layered silicates became more expressed by the increase of the clay amount as layered silicates aggregated due to particle interaction.

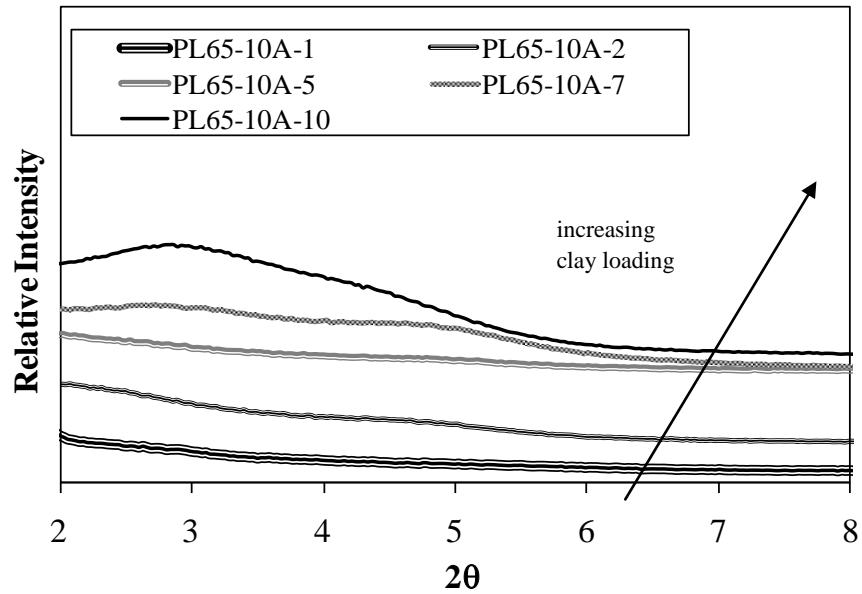


Figure 5.8. XRD patterns of PL65-10A nanocomposites with different clay contents.

Figure 5.9 illustrates the XRD patterns of GF-10A nanocomposite films. The characteristic peak of the clay was not observed in the XRD spectra of GF-10A-1 nanocomposites. Peaks of the GF-10A nanocomposite films were shifted towards left up to the clay content 10wt%. The movement of the basal reflection of clay to lower angle indicates the formation of an intercalated nanostructure. As the peak position is the same as that of the organoclay, the structure of GF-10A-10 nanocomposite might be as phase separated structure.

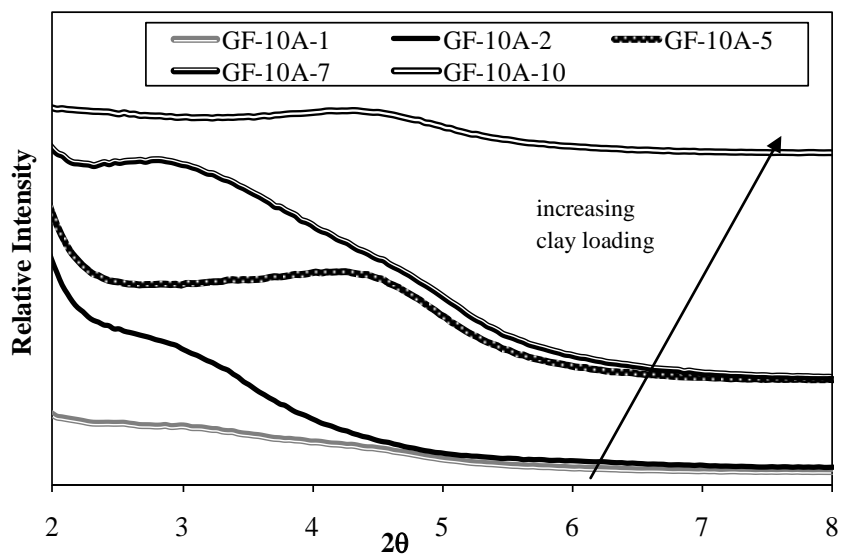


Figure 5.9. XRD patterns of GF-10A nanocomposites with different clay contents.

In Figure 5.10, the XRD patterns of GF-93A nanocomposites are shown. The basal spacing of GF-93A nanocomposites are determined as 1.90 nm ( $2\theta = 4.62^\circ$ ), 2.83 nm ( $2\theta = 3.15^\circ$ ) and 1.80 nm ( $2\theta = 4.83^\circ$ ) for 1 wt %, 5 wt %, 7 wt % and 10 wt % clay contents, respectively. According to these results, increase in basal spacing of layered silicates was not large enough for the penetration of the polymer chains into the layered silicates. . This showed that the level of dispersion of clay particles in polymer matrix was not good as compared to PLA-65 polymer nanocomposite systems.

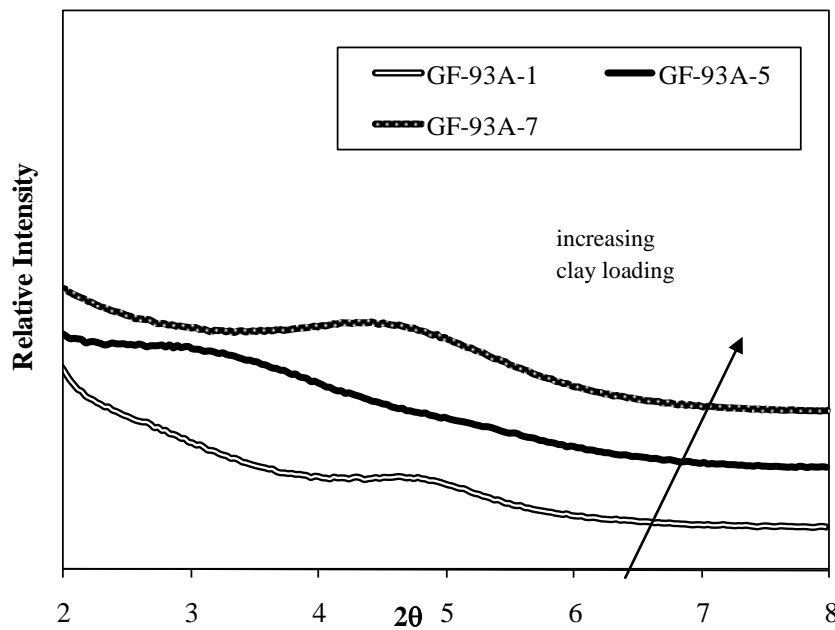


Figure 5.10. XRD patterns of GF-93A nanocomposites with different clay contents.

No intercalation of PLA occurs in the case of structure of GF-NF nanocomposites determined to be phase separated (Figure 5.11). Natural clay is immiscible with PLA due to surface energy differences or polarity differences. Interlayer distance of the GF-NF nanocomposites with 2wt% and 5wt% platelets were calculated as 1.43 and 1.49 nm, respectively. The intercalated structure could not be achieved as the interlayer distance between silicate galleries were small for intercalation, even though interaction exists between PLA and natural clay.

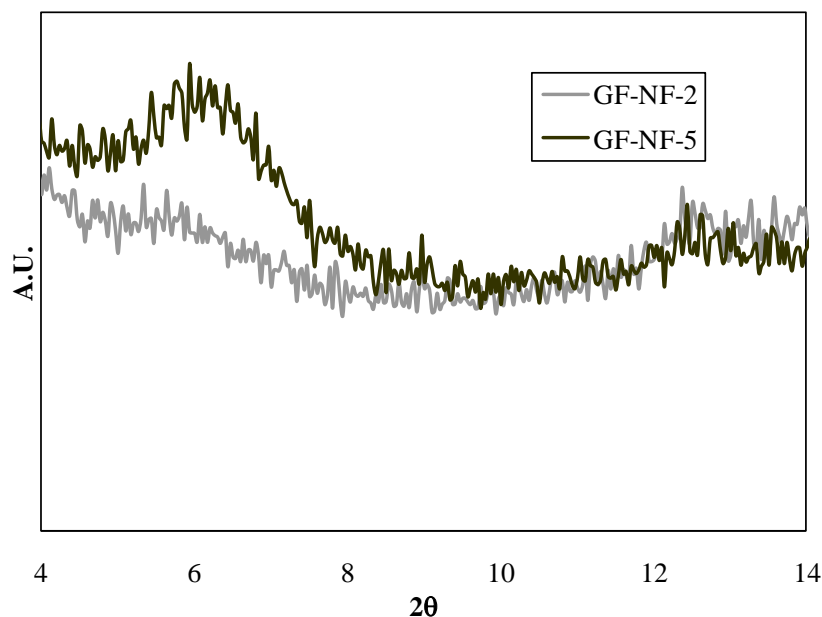


Figure 5.11. XRD patterns of GF-NF nanocomposites with different clay contents.

By comparing the XRD spectra of PL65-10A, GF-10A, GF-93A and GF-NF nanocomposites it was seen that best results were obtained at PL65-10A nanocomposite system as interfacial interaction between the PL65 and Cloisite 10A was higher than others owing to nature of the polymer, presence of organic modifier and modifier type. Inherent viscosity of PL65 is greater than GF polylactide which indicates molecular weight of PL65 is higher than molecular weight of GF. In the literature, the penetration of the chains of the low molecular weight polymers into the basal spacing was easy; however, the chance of bond capability between the layered silicate and polymer chain was higher when the molecular weight was higher (Fornes 2001; Koo, 2006; Mittal. 2010). This could be the main reason of the better morphological structure was obtained for PL65-10A nanocomposites with respect to other PLANC's. Besides, the better morphological structures were obtained at PLANCs prepared with the Cloisite 10A nanoclays compared to other clays used in this work as organomodification increased compatibility of layered silicates with polymer matrix. Due to the presence of organomodifiers, the more hydrophobic structure of the nanoclays was obtained; hence electrostatic forces between the layered silicates were reduced.

## **5.2. Transport Properties of PLANCs**

Transport properties of prepared films were investigated by measuring water vapor, oxygen, and carbon dioxide transmission rates through PLA and PLANCs films. Water vapor (WVP), oxygen (OP) and carbon dioxide (CP) permeability of each film was calculated by using equations 4.2 and 4.3.

### **5.2.1. Effect of Relative Humidity on Thickness of PLANCs**

Swelling in polymeric materials is important in several aspects. Water molecules may act as plasticizers relaxing interactions between polymeric chains and may have dramatic changes in permeability properties especially for hydrophilic polymers, but solution of transport properties in polymer assumes that thickness of polymer film is constant. To make sure that this assumption is valid for our polymer system studied, swelling degree of the prepared films were investigated. Average swelling degree of the PLA and PLANCs were determined by measuring thickness of the films before and after humidification. Average swelling degree of the PLA and PLANCs were calculated to be between 0.5 % to 2.0 %. Average swelling degrees of prepared films were tabulated in Table A.2. From the results, it was seen that the thickness of the films did not change significantly. This can also be accepted as an indication of hydrophobic character of PLA. Therefore permeability calculations were done by assuming no change in the initial thickness.

### **5.2.2. Water Vapor Permeability**

Water vapor permeability (WVP) is one of the important properties for industrial usage of polymers especially in food packaging applications. In the literature significant improvements on water vapor permeability were obtained with incorporation of layered silicates up to critical clay loading when good level of dispersion of layered silicates in the polymer matrix were achieved (Alexandre et al., 2009).

The results of WVP analysis were plotted in Figure 5.12. The water vapor permeability of PL65-P and GF-P are calculated as 2.84 and 0.15 g m/m<sup>2</sup> day mmHg, respectively. WVP of base polymers were observed to be different owing to degree of crystallinity and molecular weight of the pure polymers and they were consistent with the literature seen in Table 2.2 in Chapter 2. Effect of organomodification of nanoclays on WVP was also investigated. While WVP of samples prepared by organomodified nanoclays decreased significantly; WVP of the GF-NF films prepared by the incorporation of pristine nanoclay; increased by 64% with respect to pure polymer. Therefore, it can be said that organomodification significantly affected the molecular interaction between the layered silicates and polymer matrix leading to enhancement of the water barrier performances of polymers as hydrophilic character of natural clay turns toward hydrophobic by organomodification in accordance with study of Yano and coworkers (1997). Yano and coworkers (1997) modified natural clay in order to reduce hydrophilicity of montmorollinite as it was negatively charged due to sodium ions. Intercalated structure of layered silicates were obtained in polyimide matrix and decrease in permeability coefficient of water vapor was observed. Also, Rhim and coworkers (2009) showed that water vapor permeability of polylactide increased with the addition pristine nanoclay whereas with the organomodified nanoclay addition decreased the permeability due to the increase in diffusing path length of water vapor in polymer matrix.

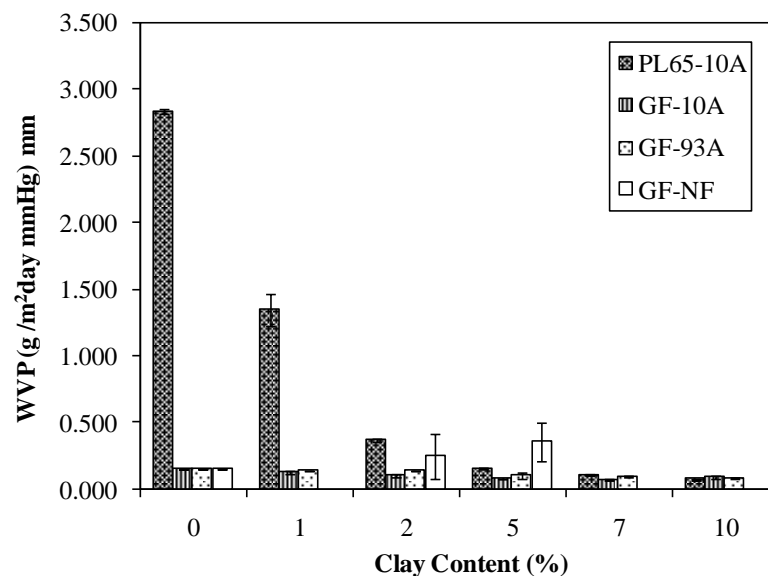


Figure 5.12. Water vapor permeabilities of PL65-10, GF-10A, GF-93A and GF-NF nanocomposites films with respect to clay content.

In Figure 5.13, it was observed that the permeability values of PL65-10A nanocomposites are lower than PL65-P. Moreover, the higher the clay content the lower the water vapor permeability of PL65-10A nanocomposites. The percent of maximum decrease in water vapor permeability of nanocomposite films was achieved as 97% in PL65-10A-10 nanocomposite. Decrease in permeabilities is believed to be due to the presence of ordered dispersed particle layers with large aspect ratios in the polymer matrix, thus water vapor travels through the film to follow a tortuous path through the polymer matrix surrounding the clay particles by increasing the effective path length for diffusion (Ray and Okomato, 2009).

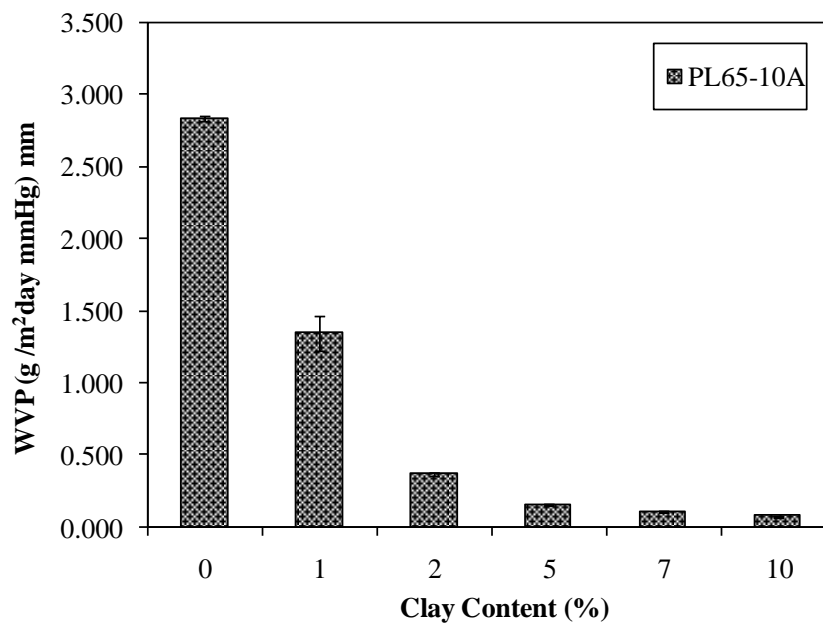


Figure 5.13. Water vapor permeabilities of PL65-10A nanocomposites films with respect to clay content.

Figure 5.14 shows the effect of organomodification type on the WVP for GF-10A, GF-93A and GF-NF nanocomposites systems. Results of analyses indicated a continuous decrease in WVP of GF-10A and GF-93A nanocomposites with increased clay content up to critical clay loading. In case of GF-10A and GF-93A nanocomposite systems, the percent of maximum decrease were determined to be 53% and 45% for 7wt% and 10wt% nanoclay loading, respectively.

The results showed that vapor permeability of GF-10A and GF-93A nanocomposites were systematically decreased with increasing clay content and when the clay loading is as much as 7 wt% and 10 wt%, respectively. It was obviously seen that both polymer type and the organomodification type affect the improvement of water vapor barrier properties of polymer nanocomposite. However, the permeability

of the GF-NF films increased by 64% with respect to pure polymer. Therefore, organomodification significantly improved the molecular interaction between the layered silicates and polymer matrix leading to enhancement of the water barrier performances of polymers (Yano et al., 1997).

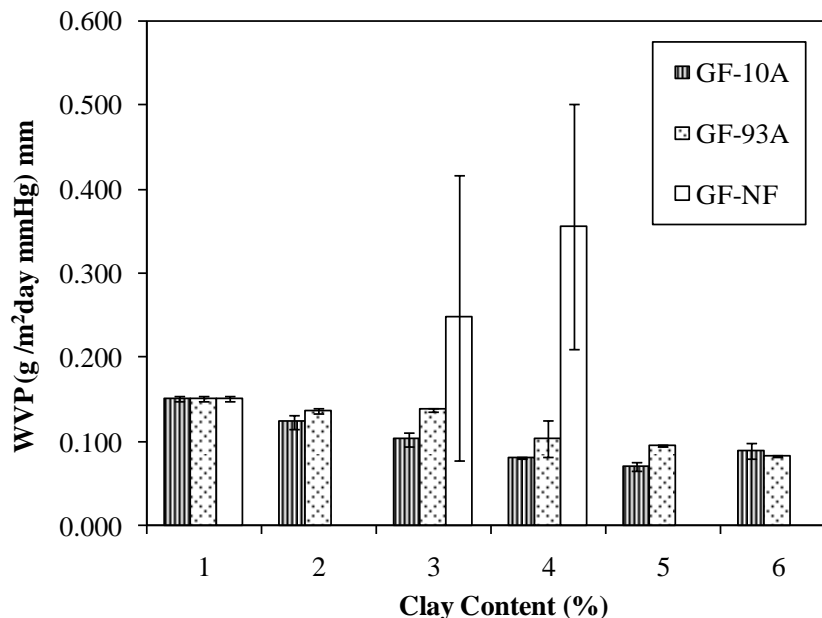


Figure 5.14. Water vapor permeabilities of GF-10A, GF-93A and GF-93A nanocomposites films with respect to clay content.

### 5.2.3. Oxygen Permeability

Oxygen permeability plays an important role in packaging application to control shelf-life of the foods, drinks and goods. Moreover, corrosion which is known as a gradual wearing away of a metal by a chemical or oxidizing process, can be prevented by using the polymers as coating materials. Therefore, when a polymer film has a low oxygen permeability coefficients, the oxidation is retarded and the shelf-life of the product extends. (Sangaj and Malshe 2004; Siracusa et al., 2008).

Maiti and coworkers (2002) studied oxygen permeability (OP) of polylactide nanocomposite and 60 % improvement in OP was obtained with the addition of the modified montmorillonite due to the good level of dispersion. OP of prepared films was given in the Figure 5.15. OP of PL65-P and GF-P were calculated as  $5.33 \times 10^{-5}$  and  $3.11 \times 10^{-5}$  ml m/m<sup>2</sup> day atm, respectively. Incorporation of organoclays resulted in significant OP decreases depending on the polymer and nanofiller type up to critical clay loading except natural clay loaded composites.

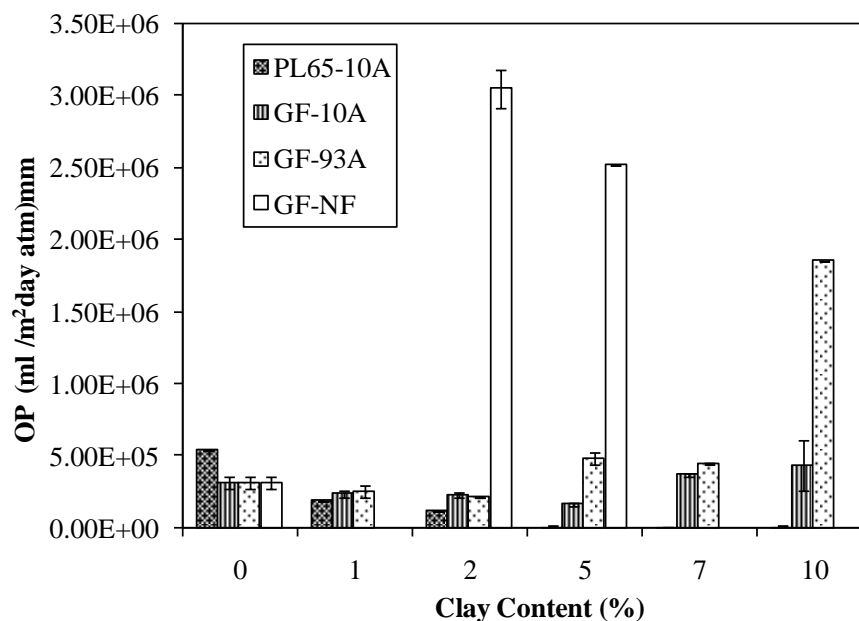


Figure 5.15. Oxygen permeabilities of PL65-10A, GF-10A, GF-93A and GF-NF nanocomposites films with respect to clay content.

Figure 5.16 illustrates the OP of PL65 nanocomposite films. Incorporation of organomodified nanoclays into PLA polymer decreased OP by 99 %, besides; oxygen permeability of PL65-10A nanocomposite was decreasing continuously with clay concentration. It was clearly understood that in nanocomposite system molecular pathway of the oxygen molecule was increasing due to dispersion state of silicate layers in polymer matrix indicating that interfacial area between the silicate layers and polymer chain was larger (Ray, 2003). These results showed the similar behavior as WVP results.

In Figure 5.17, OP of GF-10A, GF-93A and GF-NF nanocomposites systems were seen. OP of GF-10A and GF-93A nanocomposite films were decreased by 47% and 32%, respectively. Besides, oxygen permeability of GF-10A and GF-93A nanocomposites were systematically decreased with increasing clay content and when the clay loading is as much as 5 wt% and 2 wt%, respectively which means there was no good interaction between silicate layers and polymer matrix owing to polymer type. Moreover, OP of GF-NF nanocomposite films were increased instead of decreasing as expected with the addition of clay that indicated agglomeration state.

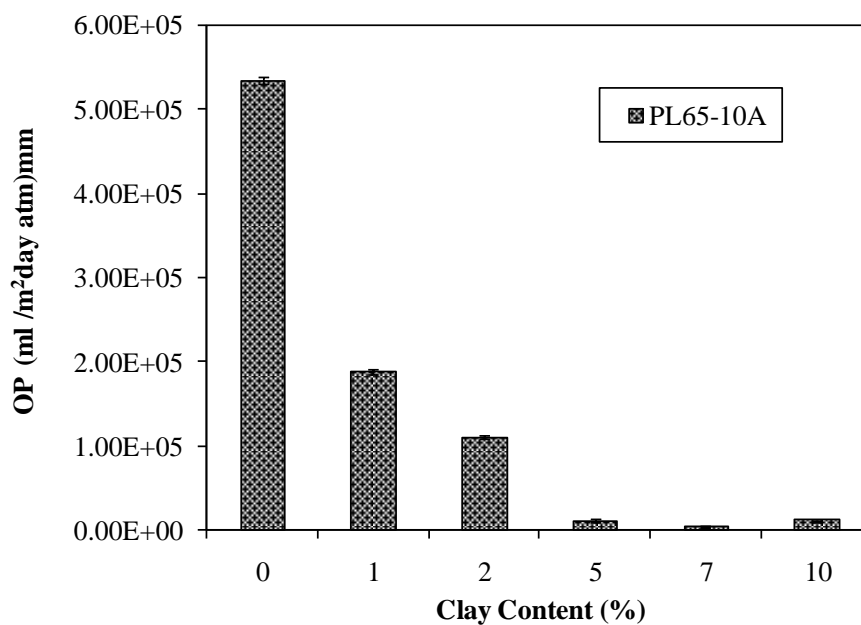


Figure 5.16. Oxygen permeabilities of PL65-10A nanocomposites films with respect to clay content.

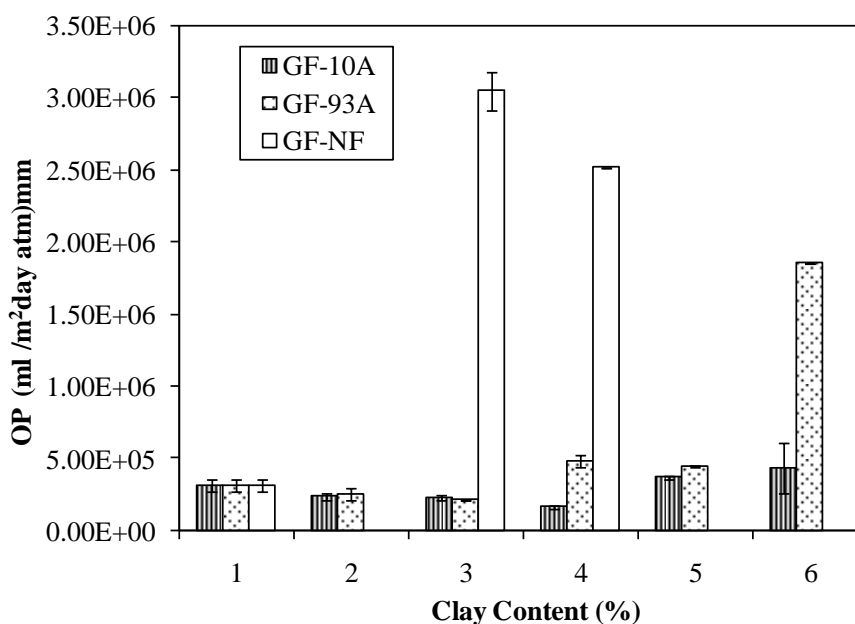


Figure 5.17. Oxygen permeabilities of GF-10A, GF-93A and GF-NF nanocomposites films with respect to clay content.

All in all, oxygen and water vapor permeability behavior of PLANC films were nearly the same due to same tortuous path of the polymer matrix.

## 5.2.4. Carbon Dioxide Permeability

Carbon dioxide permeation from the polymer films are also important in food packaging, and coating applications like oxygen and water vapor (Siracusa et al., 2008). Figure 5.18 shows permeability of PLA and PLANCs films. The carbon dioxide permeability of PL65-P and GF-P are calculated as  $1.64 \times 10^{-6}$  and  $5.99 \times 10^{-5}$  ml  $m^{-2}$  day atm, respectively.

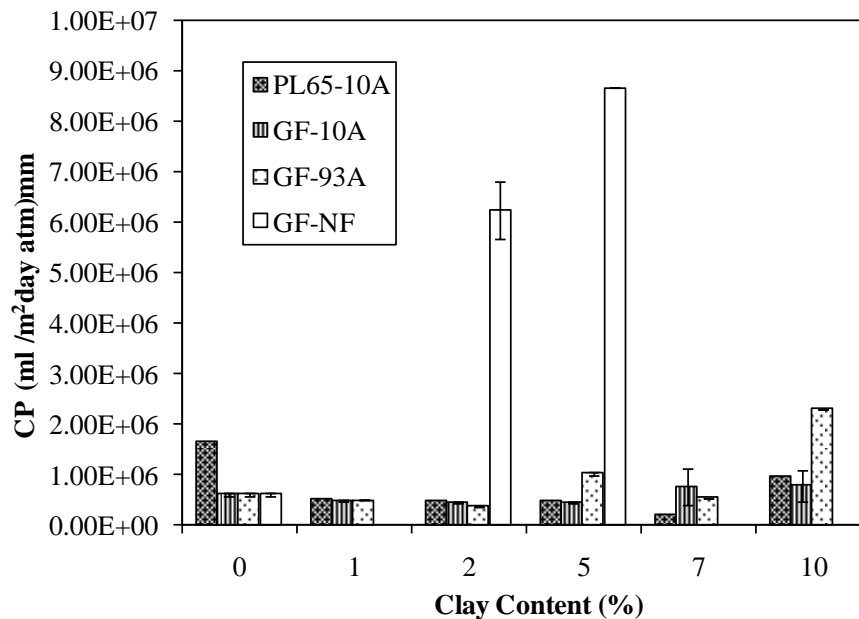


Figure 5.18. Carbon dioxide permeabilities of PL65-10A, GF-10A, GF-93A and GF-NF nanocomposites films with respect to clay content.

Żenkiewicz and Richert (2008) studied carbon dioxide permeability of polylactide layered silicate nanocomposites and 22 % decrease in carbon dioxide permeability was observed with the incorporation of Cloisite 30B. In accordance with literature, in Figures 5.19 and 5.20, maximum percent improvement of carbon dioxide barrier in PL65-10A, GF-10A and GF-93A was achieved as 89%, 26% and 15% respectively. In PL65-10A nanocomposite, decrease in the carbon dioxide permeability was obtained for all clay loadings, however 1 the GF-10A-7 nanocomposites films have not been achieved good level dispersion of clays in polymer matrix. Besides carbon dioxide permeability of GF-10A and GF-93A nanocomposites were systematically decreased with increasing clay content and when the clay loading is as much as 5 wt % and 2 wt %, respectively (Figure 5.19) which means there is no good interaction between silicate layers and polymer matrix owing

to polymer type. Moreover, carbon dioxide permeability of GF-NF nanocomposite was higher than PLA films.

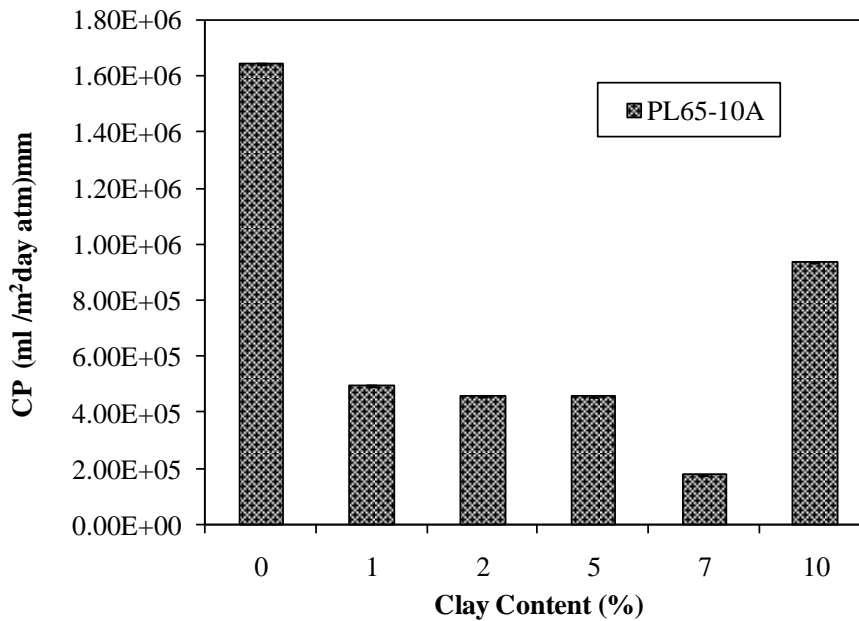


Figure 5.19. Carbon dioxide permeabilities of PL65-10A, GF-10A, GF-93A and GF-NF nanocomposites films with respect to clay content.

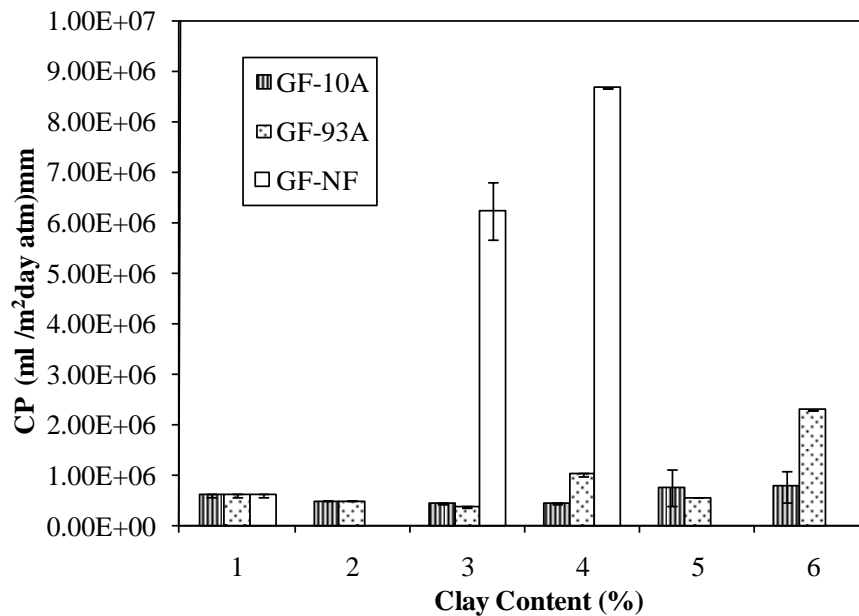


Figure 5.20. Carbon dioxide permeabilities of GF-10A, GF-93A and GF-NF nanocomposites films with respect to clay content.

Besides, XRD results showed that PL65 nanocomposites had exfoliated and flocculated intercalated structure, intercalated structures were obtained in GF-10A and

GF-93A nanocomposite films and phase separated structure were occurred in GF-NF composites. Best improvement in barrier properties was achieved at PL65 nanocomposites. Therefore, we can say that permeability data of the nanocomposites were in good agreement with XRD results.

### **5.2.5. Permeability Models**

The dramatic improvements in barrier properties of polymer nanocomposites are attributed to formation of a tortuous path by the incorporation of nano-size fillers (Herrera-Alonso, 2009; Choudalakis, 2009). That is, when impermeable nanoparticles are incorporated into a polymer, the permeating molecules are forced to wiggle around them in a random walk, and hence diffuse through a tortuous pathway. The degree of exfoliation or intercalation in the polymer matrix is the most important factor that affects the barrier properties of the layered silicate nanocomposite films. However, for each nanoclay-polymer system, permeability properties may differ with several factors such as clay content, orientation of fillers etc. Hence, it is impossible to comment on degree of exfoliation by using permeation data alone. At this point, predictive theoretical permeability models may be helpful. Experimental permeability data can be fit to various phenomenological models, predicting the permeability of polymer systems filled with nanoclays as a function of clay concentration and aspect ratio of silicate layers (Sun, 2007). Effective aspect ratio utilized in prepared nanocomposites can be predicted by using the models, and comments can be made by comparing predicted aspect ratio with literature data.

Several permeability models discussed in details in Chapter 3 (given in Table 3.4) were fitted to experimental WVP, OP and CP data of PL65-10A and GF-10A nanocomposites as the assumption of models is good level dispersion of silicate layers in polymer matrix. Cussler-random model is the well-fitted model, also aspect ratio was calculated between 498-574. In the case of GF-10A nanocomposite system, the well-fitted model was found as Nielsen model with the aspect ratio of 243-382. Higher aspect ratio indicates intercalation or exfoliation structure in polymer layered silicate nanocomposite system.

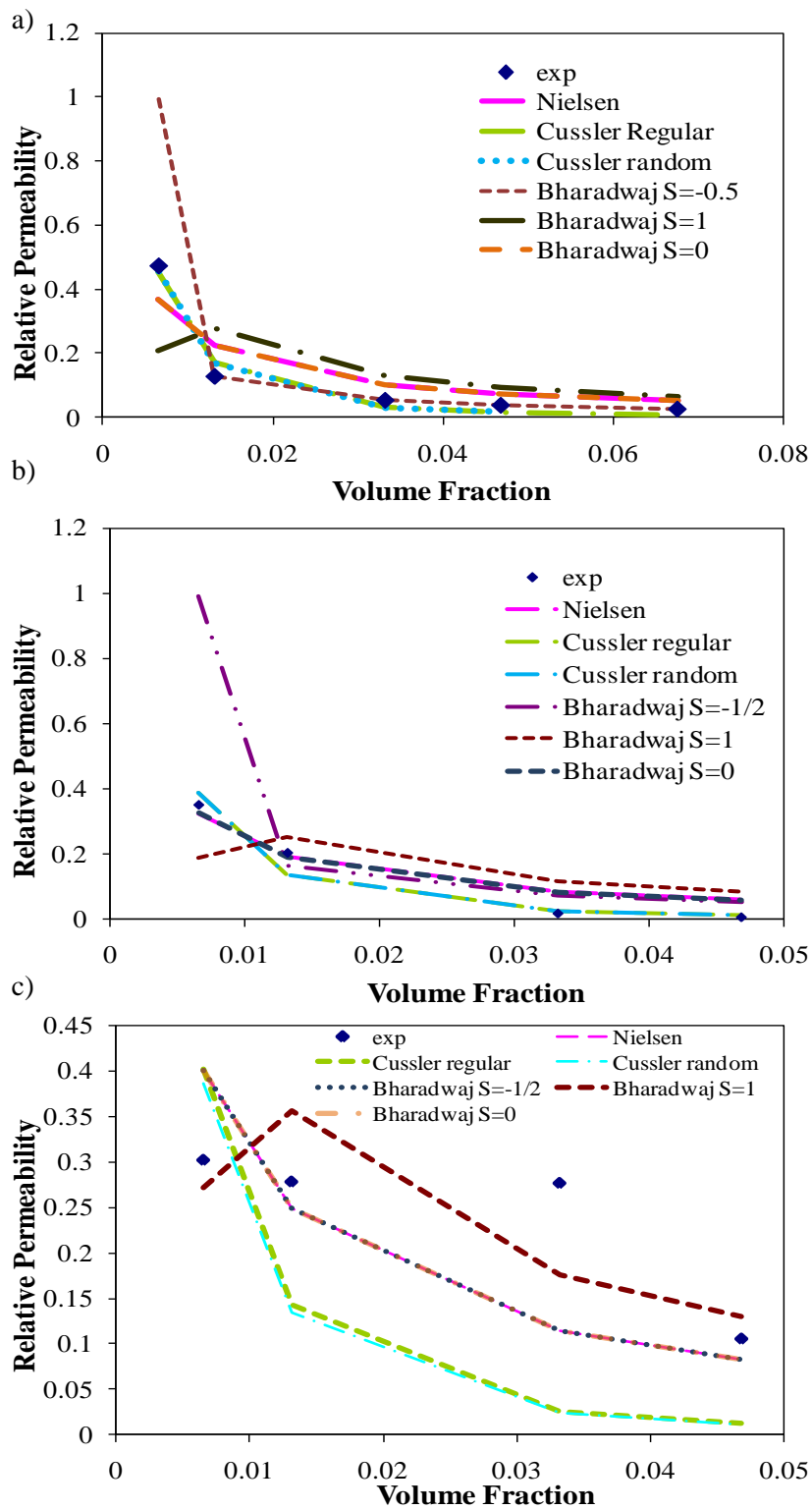


Figure 5.21. Permeability models fitted to experimental (a) water vapor (b) oxygen and (c) carbon dioxide permeability of PL65-10A nanocomposite films.

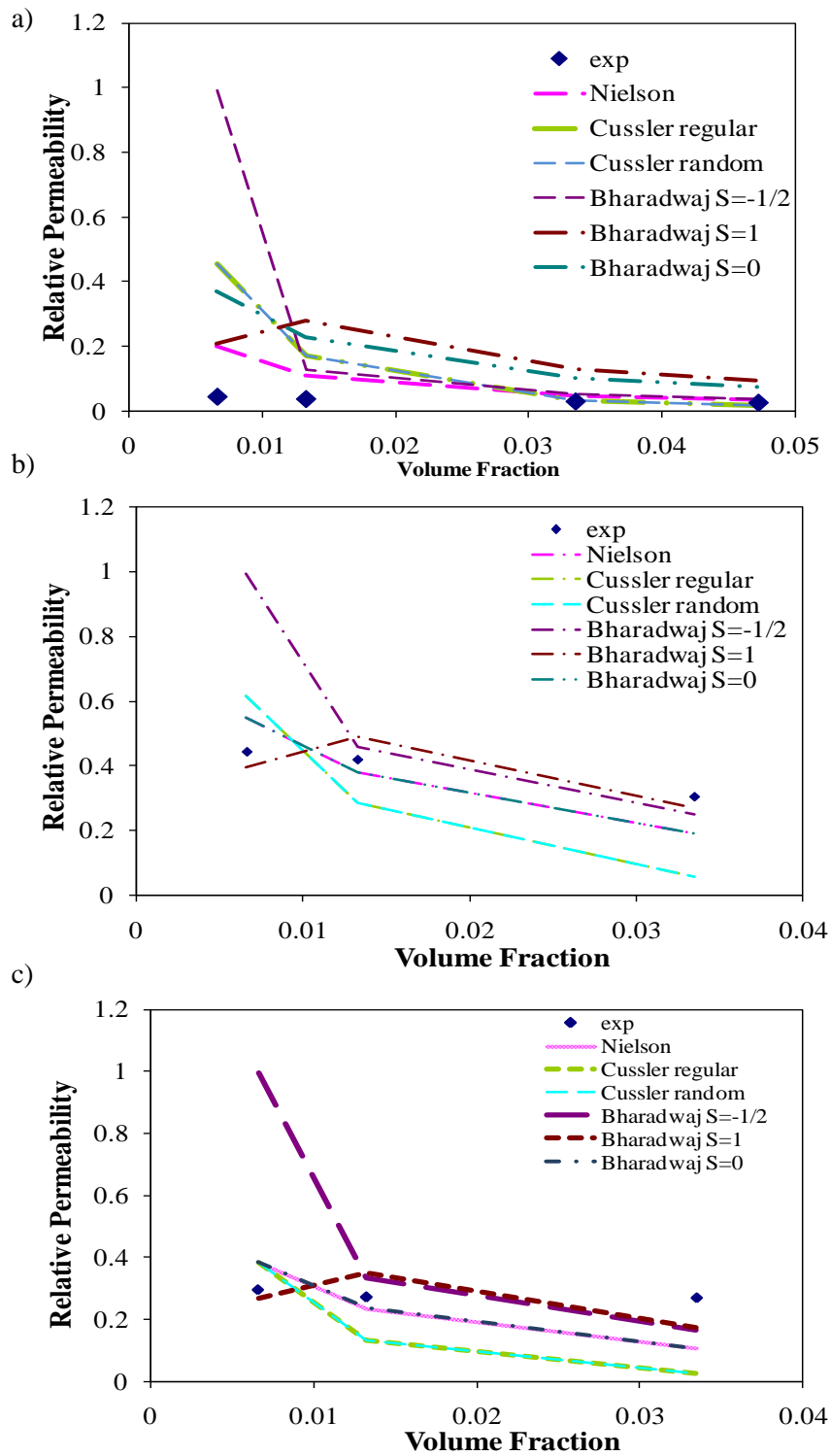


Figure 5.22. Permeability models fitted to experimental (a) water vapor (b) oxygen and (c) carbon dioxide permeability of GF-10Ananocomposite films.

### **5.3. Thermal Analysis**

Thermal properties of the PLA and PLANCs were investigated using differential scanning microscopy (DSC) and thermogravimetric analysis (TGA).

#### **5.3.1. Differential Scanning Calorimetry (DSC) Analysis**

DSC analyses of the prepared nanocomposite samples showed no significant effect of organomodification or nanoclay content in thermal properties of nanocomposites compared to pure PLA films. As can be seen from the DSC results given together in the Table 5.2; only small variations in glass transition, melting and crystallization temperatures as well as degree of crystallinity of PLA nanocomposites were observed. However, crystallization temperature of PL65 nanocomposites were decreasing with clay loading that indicates nucleation effect due to the large surface area for the nanofiller (Mittal, 2010). Moreover, glass transition of the GF-93A nanocomposite films were increased about 10 °C, but same trends were not achieved at other nanocomposite systems, therefore this increment was caused by organomodifier type. Furthermore melting temperature, of GF-10A and GF-93A nanocomposite films were slightly decreased by the incorporation of the clay into the polymer matrix while significant change was not observed in the other composite systems. As it is mentioned in Chapter 3, there was no restricted relationship between the DSC results and dispersion of state and amount of clay. Table 5.2 tabulates DSC results of PLA and PLANC's films.

Table 5.2. DSC results of PLA and PLANCs films

<b>Sample</b>	<b>T<sub>g</sub></b> <b>(°C)</b>	<b>T<sub>m</sub></b> <b>(°C)</b>	<b>H<sub>m</sub></b> <b>(J/g)</b>	<b>X<sub>c</sub></b> <b>%</b>	<b>T<sub>c</sub> (°C)</b> <b>cold</b>
PL65-P	62.07	164.07	33.46	36.0	121.43
PL65-10A-2	61.24	164.55	34.47	37.1	111.04
PL65-10A-5	61.01	166.82	30.82	33.1	111.86
GF-P	59.35	169.94	36.97	39.8	101.1
GF-10A-1	61.78	163.41	36.18	38.9	102.15
GF-10A-2	61.66	163.68	35.38	38.1	102.53
GF-10A-5	61.41	163.35	34.27	36.9	108.27
GF-10A-7	61.93	162.56	42.93	46.2	101.96
GF-10A-10	51.36	159.41	33.99	36.5	100.8
GF-93A-1	51.79	163.58	33.55	36.01	102.75
GF-93A-2	61.46	163.10	34.53	37.1	103.10
GF-93A-5	62.41	162.67	33.32	35.8	110.56
GF-93A-7	67.67	162.91	33.30	35.8	101.96
GF-93A-10	60.72	162.07	35.86	38.6	101.1
GF-NF-2	57.30	169.76	44.38	47.7	108.97
GF-NF-5	56.90	170.56	36.68	39.4	109.98

### 5.3.2. Thermogravimetric Analysis (TGA)

Thermogravimetric analysis (TGA) was conducted to determine the effect of nanocomposites on PLA thermal stability. TGA analyses were done under nitrogen atmosphere with a temperature increment of 10°C/min. Discussions and comparisons on thermal stability of PLANCs were done according to:

- the onset temperature of thermal degradation ( $T_{\text{onset}}$ )
- end temperature of thermal degradation ( $T_{\text{end}}$ )
- the yield of charred residue (char %)
- 10wt% loss temperature ( $T_{0.1}$ )
- 50wt% loss temperature ( $T_{0.5}$ )

To see the nanoclay and polymer interaction clearly, TGA analysis of the nanoclays were conducted. The thermogravimetric weight loss curves of the nanoclays

used in this study can be seen in Figure 5.23. From the decomposition pattern of the nanoclays was different for each sample owing to organomodifier presence and type. Onset decomposition temperatures of organomodifiers were generally observed at 200°C in the literature (Koo, 2006; Mittal, 2010). In accordance with literature, decomposition of the organoclays started around 200-250 °C and the percent weight loss of the Cloisite 10A and 93A were observed as 45% and 42%, respectively. Nanofil 116 loss only 8% of its weight up to 656 °C, then weight gain were observed due to the presence of oxygen and metal species in the clay as clay might act as catalyst to the oxidative cleavage of alkenes to produce aldehydes at elevated temperatures (Cervantes-Uc, 2007).

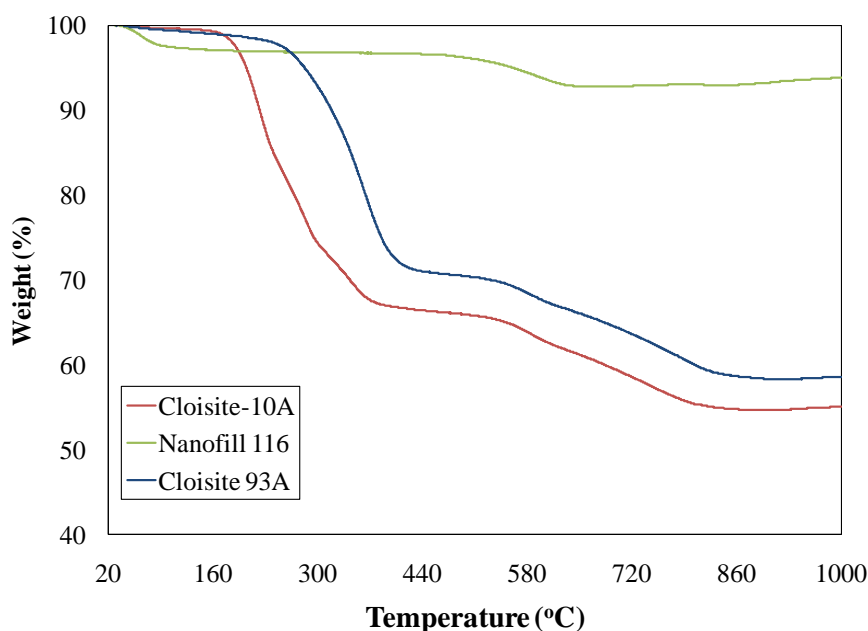


Figure 5.23. TGA results of Cloisite 10A, Cloisite 93A and Nanofil 116.

PL65-10A nanocomposites showed enhancement in thermal stability compared to pure PLA. TGA indicated an increase of 28 and 31 °C in the  $T_{\text{onset}}$  value of 2 wt% and 5wt% organomodified nanoclay containing PL65-10A nanocomposites, respectively. Similar improvements were also seen for  $T_{\text{end}}$ ,  $T_{0.1}$  and  $T_{0.5}$ . In case of onset temperature of GF-10A and GF-93A nanocomposites, maximum temperature improvement was only 10 °C. The reason of less significant property improvements for GF-10A and GF-93A nanocomposites was probably due to poorer dispersion in silicate layers in polymer matrix. Therefore, it can be said that better dispersion of the layered silicates in the matrix of PL65 nanocomposites is responsible for significant

thermal stability. Besides, high molecular interaction between silicate layers and polymer chains also contributes to thermal stability improvements as reported in several studies (Mittal, 2010). Besides these, in GF-10A nanocomposites,  $T_{\text{onset}}$  values of 10wt % clay addition decreased due to presence of more organomodifier leading polymer matrix to become destabilize as ammonium cations tended to decompose to produce ammonia and olefein (Mittal, 2010).

On the contrary, PLANCs prepared by the incorporation of unmodified natural montmorillonite exhibited 12 °C and 14 °C decreases on the  $T_{\text{onset}}$  for GF-NF-2 and GF-NF-5 nanocomposite films, respectively. Similar decreases were also observed for  $T_{\text{end}}$ ,  $T_{0.1}$  and  $T_{0.5}$ . Alteration of thermal stability of PLA nanocomposites can be attributed poor bonding between unmodified nanoclays and PLA matrix due to inefficient dispersion of nanoclays in the matrix.

Mittal (2010) summarized that the presence of nanofiller led in degradation reactions before the onset of thermal degradation of neat polymer; therefore, char formation increased and rate of mass loss in degradation was slowed down. But, ammonium alkyl salts in the clays showed catalytic activity towards the degradation reactions. Moreover, there could be no interaction between the layered silicates and polymer chains if the expected char residue is equal to obtained one. Therefore; GF-10A-1 and PL65-10A-2 nanocomposites, higher char formation was obtained than the expected due to interaction between the organomodifier and polymer chains indicating fully exfoliated structure. However, low char residue was obtained than expected with the addition of nanoclay. For instance, the expected char residue of GF-10A-5 nanocomposite film was expected as 3.7% but obtained value was 0.58 corresponding partially exfoliated and intercalated structure. Furthermore, it was seen that in GF-10A-7, GF-93A-7 and NF-10A-5 nanocomposite films char residue was found as expected which showed lower interaction between layered silicate and polylactide chains.

Table 5.3. TGA results of PLA and PLANCs films.

<b>Sample</b>	<b>T<sub>onset</sub></b> <b>(°C)</b>	<b>T<sub>end</sub></b> <b>(°C)</b>	<b>Char</b> <b>%</b>	<b>T<sub>0.1</sub> (°C)</b> <b>10%mass loss</b>	<b>T<sub>0.5</sub> (°C)</b> <b>50%mass loss</b>
PL65-P	274.60	346.66	1.181	301.33	326.58
PL65-10A-2	305.76	369.92	3.230	324.86	347.59
PL65-10A-5	302.42	376.01	2.436	321.33	348.53
GF-P	308.1	368.55	0.917	325.51	348.03
GF-10A-1	312.89	473.98	7.253	330.61	353.30
GF-10A-2	310.27	375.93	0.973	334.36	352.59
GF-10A-5	313.00	376.87	0.600	321.91	349.13
GF-10A-7	318.14	735.04	4.650	332.61	353.50
GF-10A-10	316.70	379.76	2.009	334.79	356.17
GF-93A-1	306.20	373.54	0.530	329.79	350.89
GF-93A-2	310.96	368.04	3.739	332.59	349.16
GF-93A-5	316.40	370.11	2.746	333.50	349.51
GF-93A-7	316.58	383.48	4.563	336.34	365.94
GF-93A-10	318.56	380.23	2.788	333.381	356.15
GF-NF-2	296.91	359.78	0.566	315.63	338.73
GF-NF-5	294.15	362.39	5.158	315.73	339.37

Consequently, thermal stability of the PL65-10A, GF-10A and GF-93A nanocomposite systems increased with incorporation of the clay owing to the dispersion of the clay and surfactant presence in the polymer matrix.

#### 5.4. Mechanical Analysis

Mechanical properties were important properties of polymer to determine application area and design process. Mechanical properties are generally investigated by the help of short-term tests such as tensile testing, dynamic mechanical analysis etc. Tensile testing and dynamic mechanical analysis in tensile mode was performed to investigate the stiffness and temperature dependency on the mechanical properties of the PLA and PLANCs.

### 5.4.1 Tensile Test

Generally, Young's modulus and tensile strength values of layered silicate nanocomposites increases with the addition of nanoclay up to critical clay loading whereas elongation at break values decreases (Koo, 2006; Mittal, 2010). However, Lewitus and coworkers (2006) achieved 45% increase in elongation at break values with addition of 5wt% Cloisite 25A into polylactide matrix. Moreover, Koh and coworkers (2008) observed different behavior of Young's modulus and tensile strength of PLANCs with the addition of different organomodified nanoclays due to the interaction between the organomodifier and polymer chain. The tensile strengths and strength at breaks of the PLA and PLANC films with different clay contents and types were presented in Table 5.4. The values showed that, the tensile strength of the PLANCs increased remarkably with the clay content and possessed a maximum value for a critical clay loading. Above this critical loading, the strength values of all the PLANCs decreased. Improvements or decreases in the tensile strength can be attributed to level of nanoclay dispersion in the PLA matrix. The tensile strength and strength at break values increased as a result of incorporation of 1wt% organomodified nanoclay as can be seen for GF-10A and GF-93A nanocomposite films. Further nanoclay addition into PLA matrix resulted in decreased improvement efficiency or alteration of base polymer mechanical properties. Such decreases can be attributed to poorer dispersion of nanoclays as it was proven by the XRD results. The most significant improvements for tensile strength were obtained for PL65-10A nanocomposites as in the case of permeability properties. This can be attributed to better interactions between matrix and nanoclays as a result of more effective dispersion of fillers.

Table. 5.4. Tensile strength, strength at break, elongation at break and Young's Modulus of PLA and PLANCs films

Sample	Tensile		Elongation	Young's Modulus
	Strength (MPa)	Strength @break (MPa)	@break (%)	
PL65-P	54.79±2.02	47.30±6.22	4.12±1.50	26.43±1.06
PL65-10A-2	60.05±3.89	59.83±2.10	5.36±1.00	27.21±2.82
PL65-10A-5	61.44±3.68	57.74±4.86	6.67±2.60	30.02±1.71
GF-P	54.24±3.73	45.36±3.22	16.56±6.77	24.26±1.69
GF-10A-1	58.11±1.58	53.11±4.52	3.07±0.28	25.94±1.23
GF-10A-2	53.70±3.08	50.12±3.38	4.56±1.49	27.70±1.75
GF-10A-5	45.78±1.86	43.27±1.32	3.85±1.51	28.08±0.76
GF-10A-7	41.78±2.17	41.76±2.55	1.71±0.97	32.90±3.65
GF-10A-10	30.16±4.58	29.74±4.95	1.27±0.15	25.07±2.38
GF-93A-1	56.34±1.59	50.09±1.02	6.71±1.66	25.54±0.42
GF-93A-2	49.04±2.49	46.58±4.26	4.31±1.34	26.09±0.39
GF-93A-5	46.33±2.32	45.10±2.03	4.31±1.34	28.51±1.93
GF-93A-7	42.52±1.98	40.40±14.19	4.40±0.99	26.59±1.19
GF-93A-10	36.09±3.45	35.89 ±14.19	1.98±0.46	23.43±3.59
GF-NF-2	50.31±2.54	48.59±1.99	3.91±0.70	24.43±1.41
GF-NF-5	48.97±1.46	48.99±4.34	5.15±3.14	22.31±4.88

The most promising feature of nanocomposites in terms of mechanical properties is the Young's modulus improvements. Several authors reported significant modulus improvements obtained by nanocomposites (Zewitus, 2006; Mittal, 2010). The Young's modulus increased continuously with increasing clay content up to 7 wt% for GF-10A and 5 wt% for GF-93A nanocomposite films, respectively as can be seen in the Table 5.4. This behavior was ascribed to the resistance exerted by the clay itself and to the orientation and aspect ratio of the intercalated silicate layers (Mittal, 2010). Additionally, the stretching resistance of the oriented backbone of the polymer chain in the gallery was also reported to contribute to modulus enhancements (Mittal, 2010). Further incorporation of nanoclays lead to decreases in improvements

due to more intercalated structure of nanocomposites as it was also evidenced by XRD analysis. Most significant effect of ineffective dispersion and phase separation on modulus of nanocomposites was observed for GF-NF samples prepared by unmodified nanoclay. Modulus of nanocomposite films altered compared to base PLA films. Such modulus diminishing was attributed to incompatibility of hydrophilic montmorillonite with hydrophobic matrix observed in several studies (Mittal, 2010). Besides, stiffness of PLA has been shown to be improved when nanocomposites are formed with layered silicates up to critical clay loading. It was understood that high aspect ratio of layered silicate layers results in high interfacial area to volume and increase in the mechanical properties with very low filler content are expected. Furthermore, beyond the critical clay loading the additional silicates are already affected by other silicate layers, and thus it was expected that the enhancement of modulus would be much less dramatic.

A characteristic drawback of composite applications is that elasticity of the polymeric films is sacrificed for property improvements. Nanocomposites often exhibit the same drawback in a lesser content than conventional composites (Koh, 2008; Rhim, 2009). The elongation at break values of the nanocomposite films prepared by using various clays was tabulated in Table 5.4. The elongation at break of pure PLA clearly decreased with the incorporation of nanoclays and also elasticity decreases become more expressed by the increase in the nanoclay loading. Interestingly, elongation at break of PLA65-10A nanocomposites exhibited significant increases, a 50% increase for 5wt% organomodified nanoclay loading. Elasticity increase is in good accordance with superior barrier improvements observed in PLA65-10A samples and can be attributed to facile interactions between polymer and nanoclays (Mittal, 2010).

#### **5.4.2. Dynamic Mechanical Analysis (DMA)**

Glass transition temperature of the nanocomposites and temperature dependence on storage ( $G'$ ) and loss modulus ( $G''$ ) and  $\tan \delta$  of PLNCs were investigated by dynamic mechanical analysis. Glass transition temperatures ( $\tan \delta$  values in Figures 5.24 and 5.25) of all nanocomposite increased with the addition of the clay.(Table 5.5.)

In Table 5.5 glass transition temperature of nanocomposites were seen and glass transition temperature increased with the addition of clay. Figures 5.24 and 5.25 show the change in storage modulus, loss modulus and  $\tan\delta$  values of PLANCs with respect to temperature. As seen in the figures, below  $T_g$ , the enhancement of  $G'$  is clear in the PLA65-10A, GF-10A and GF-93A nanocomposites. Furthermore, above  $T_g$ , all the three nanocomposites systems exhibited much higher enhancement of  $G'$  as compared to that of pure PLA owing to reinforcement by layered silicates and high temperature. Strong enhancement of modulus was observed above  $T_g$ , as the materials become soft leading to reinforcement effect of the clay particles negligible. Besides in GF-NF composite system, decrease in storage modulus that was due to the phase separated structure.

Table 5.5. Glass transition temperature values of PLA and PLANCs from DMA

<b>Sample</b>	<b>Tg(°C)</b>	<b>Sample</b>	<b>Tg(°C)</b>
GF-P	69.86	GF-93A-1	-
GF-10A-1	72.44	GF-93A-2	70.02
GF-10A-2	75.26	GF-93A-5	77.90
GF-10A-5	77.09	GF-93A-7	78.65
GF-10A-7	78.15	GF-93A-10	79.85
GF-10A-10	80.02	PL65-P	75.20
GF-NF-2	75.20	PL65-10A-2	78.91
GF-NF-5	81.37	PL65-10A-5	81.37

On the other hand, above  $T_g$  the enhancement of  $G''$  of PLACNs is much higher compared to that of below  $T_g$  indicating plastic response to the deformation was important in the presence of clay as material becomes soft. However, there is no significant shift and broadening of  $\tan \delta$  curves with incorporation of the layered silicates. This could be explained as the unrestricted segmental motions at the organic–inorganic interface neighborhood of intercalated PLACNs (Ray and Bousmina, 2005; Mittal 2010). It is obvious that choosing appropriate polymer-clay pair and clay content in polymer were more effective in improvement of the dynamic mechanical properties of PLANC films.

Mittal (2010) summarized that  $G'/G$  gave the information about the structure of nanocomposites. Higher ratio was attributed to presence of filler in the matrix leading to solid-like behavior. Decrease in the ratio showed the agglomeration of the filler in the polymer matrix which did not contribute the mechanical properties. For GF-10A and GF-93A nanocomposites  $G'/G$  ratio increased up to 7wt% and 5wt% clay amount, respectively. For PL65-10A nanocomposite system, this ratio increased whereas in NF-10A nanocomposite system, it did not as natural clay particles aggregated in PLA matrix. Based on all DMA results, it was seen that  $G'/G$  ratio increased with respect to pure polymer up to critical clay amount when the exfoliation of nanoclay is achieved due to an interfacial interaction between polymer matrix and clay layers.

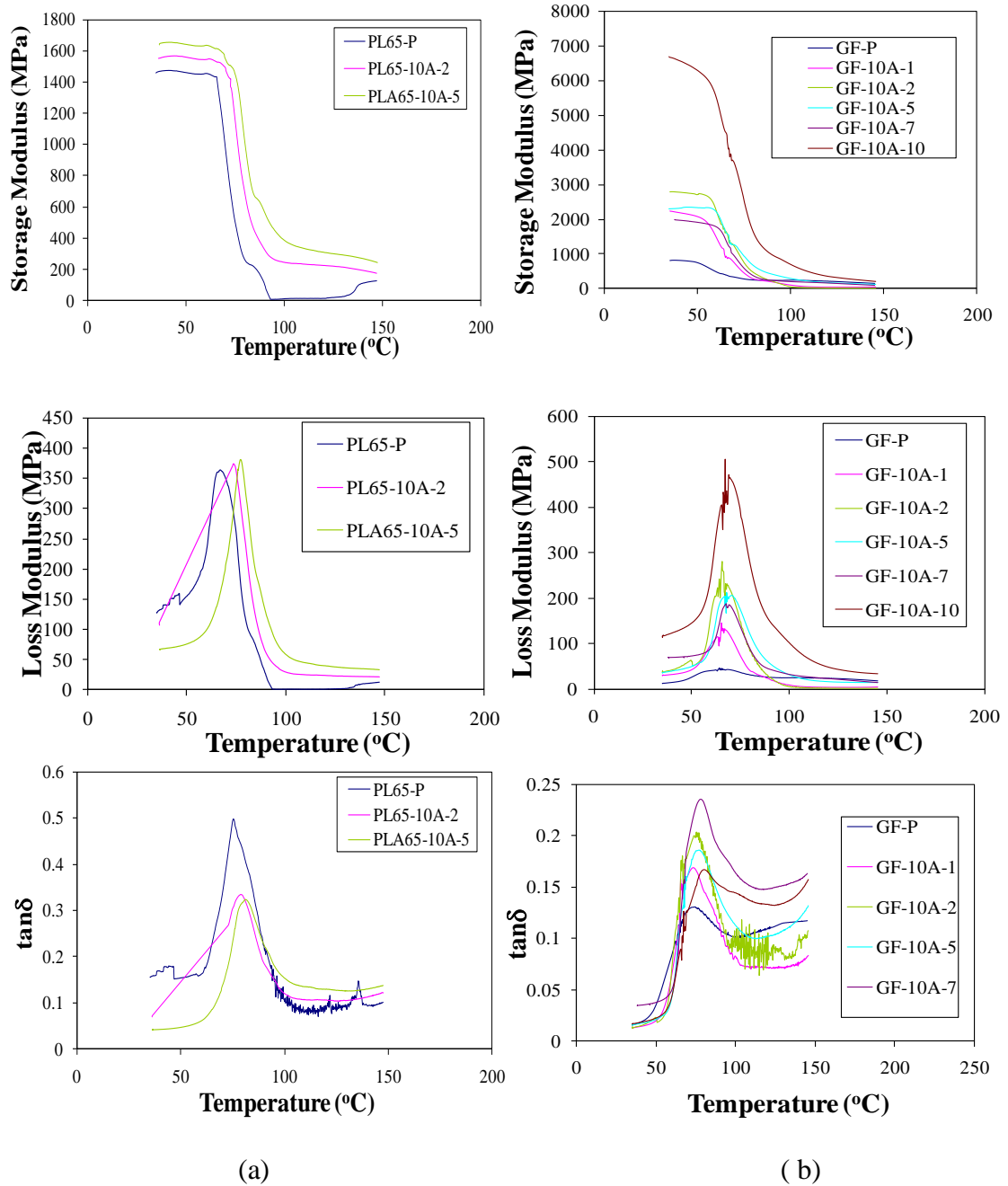


Figure 5.24. Temperature dependence of storage modulus ( $G'$ ), loss modulus ( $G''$ ), and their ratio ( $\tan \delta$ ) for (a) PL65-10A nanocomposites (b) GF-10A nanocomposites.

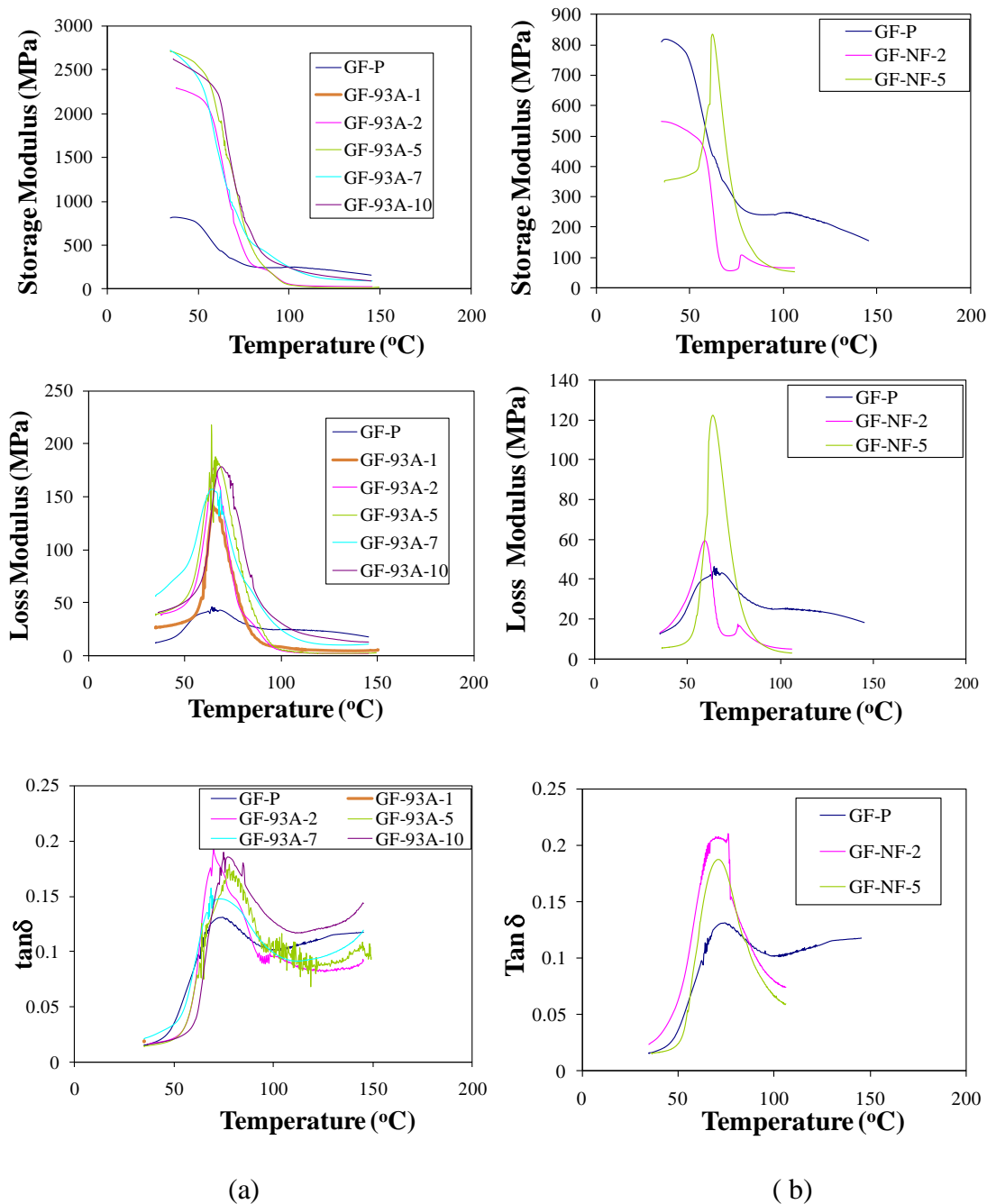


Figure 5.25. Temperature dependence of storage modulus ( $G'$ ), loss modulus ( $G''$ ), and their ratio ( $\tan \delta$ ) for (a) GF-93A nanocomposites (b) GF-NF nanocomposites.

## 5.5. Rheological Analysis

Rheological measurements were performed to investigate the viscoelastic properties of GF-10A nanocomposite system only above the melting temperature defined as 170°C.

Initially dynamic strain sweep test was performed to investigate the linear and nonlinear region of GF-P and GF-10A nanocomposite systems, illustrated in Figure 5.26. As seen in the figure, nonlinear region started where decrease in the storage modulus was observed. It is seen that nonlinear region of the nanocomposite differed with the addition of the clay. According to these results, %strain was set below %10 to perform linear viscoelastic measurements.

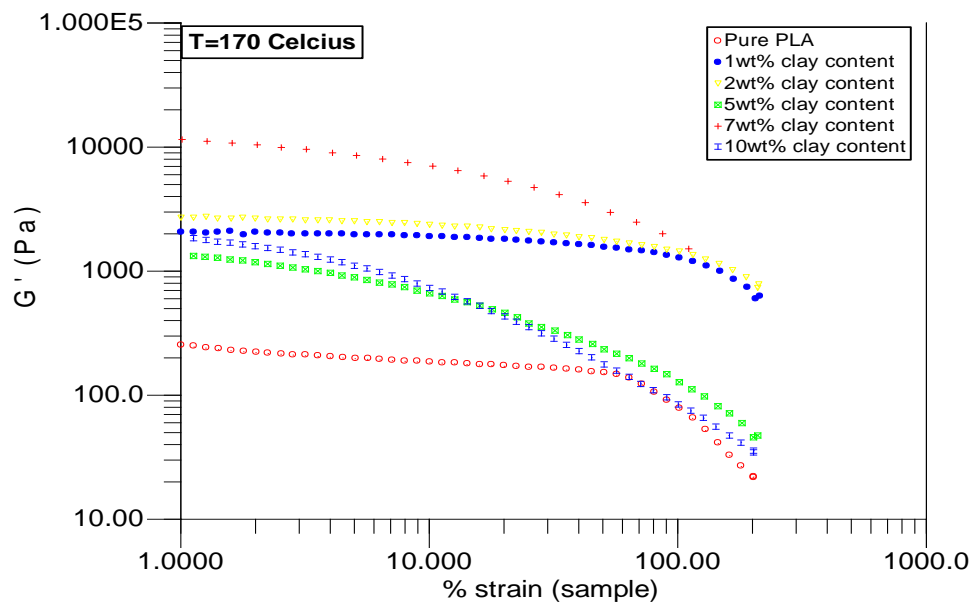


Figure 5.26. Storage modulus of GF-P and GF-10A nanocomposites as a function of %strain.

Figures 5.27-5.29 show the angular frequency dependency of storage modulus, loss modulus, and complex viscosity for GF-P and GF-10A nanocomposites. The modulus of the nanocomposites increased with increasing clay loading at all frequencies. This showed that materials exhibited a pseudo-solid-like behavior with the addition of the clay. At high frequencies, storage and loss modulus of GF-10A nanocomposites remained same as GF-P and unaffected with frequency changes. However, at low frequencies, storage modulus and loss modulus increased monotonically with increasing clay content. As layered silicates can resist through the flow at lower frequencies, but at higher frequencies layered silicates involves in flow (Ray and Bousima, 2005).

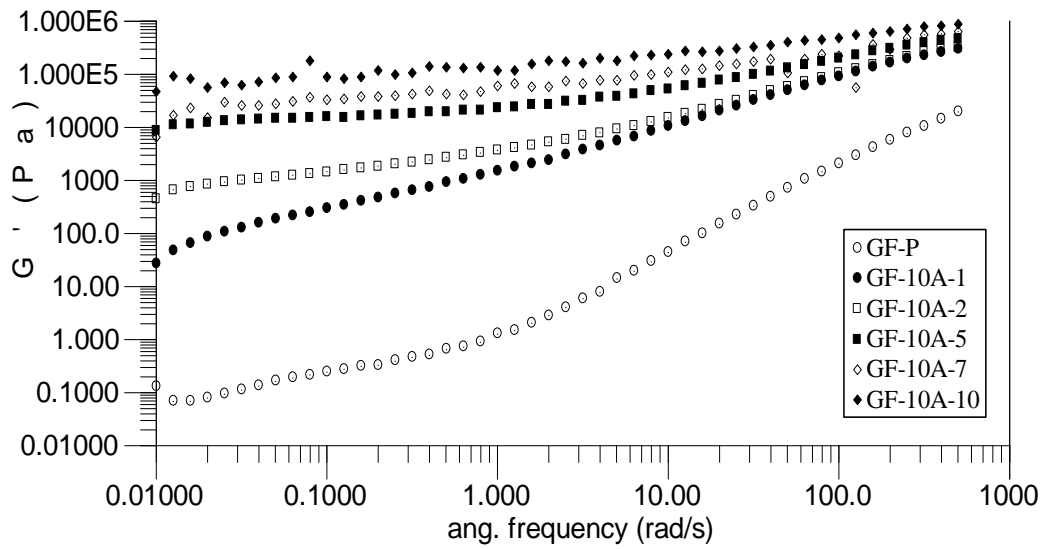


Figure 5.27. Storage modulus of GF-P and GF-10A nanocomposites as a function of angular frequency at 170 °C.

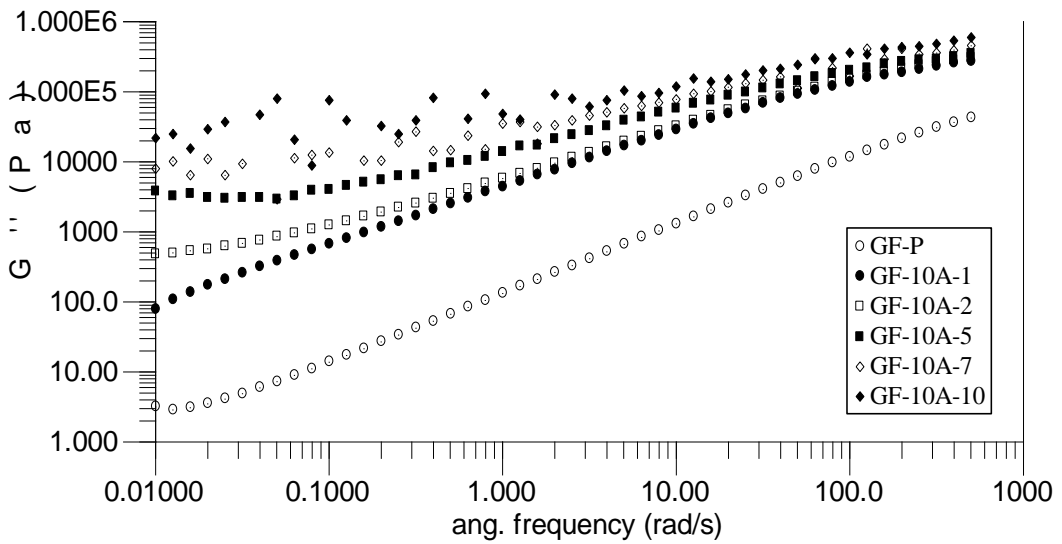


Figure 5.28. Loss modulus of GF-P and GF-10A nanocomposites as a function of angular frequency at 170 °C.

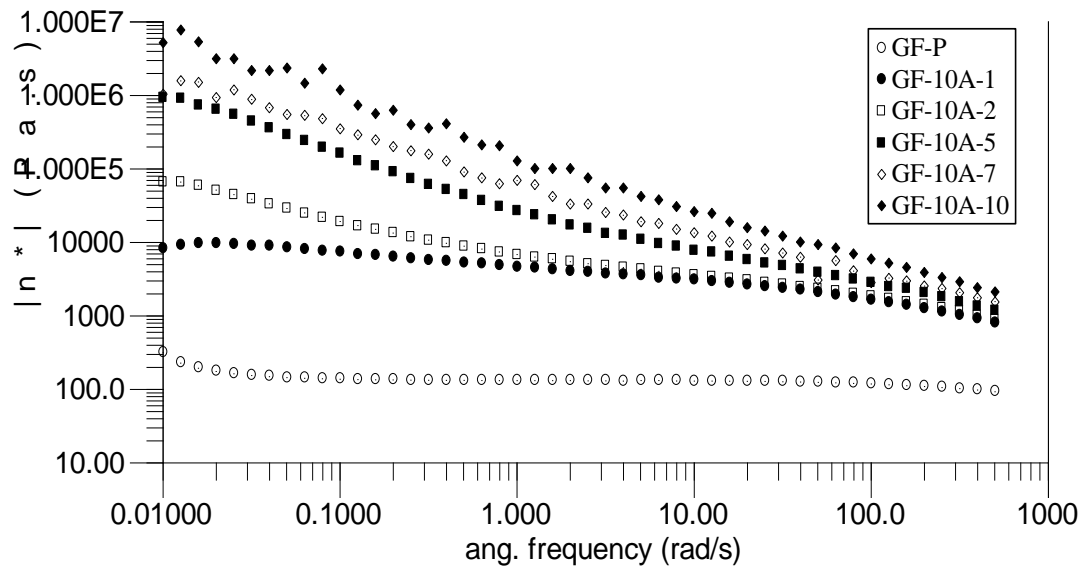


Figure 5.29. Complex viscosity of GF-P and GF-10A nanocomposites as a function of temperature.

Ray and Okamoto (2003) explained that slope of storage modulus ( $G'(\omega)$ ) and loss modulus ( $G''(\omega)$ ) were lower than neat polylactide due to the solid-like behavior of the nanocomposites. In Table 5.6, it was seen that slopes of nanocomposites were decreasing with the addition of nanoclay indicating pseudo-solid-like behavior in accordance with literature studies (Ray and Okamoto, 2003; Gu, 2007).

Table 5.6. Terminal regions of slopes of  $G'(\omega)$  and  $G''(\omega)$

Sample	$G'(\omega)$	$G''(\omega)$
GF-P	0.93	0.83
GF-10A-1	0.83	0.76
GF-10A-2	0.62	0.43
GF-10A-5	0.44	0.29
GF-10A-7	0.35	0.26
GF-10A-10	0.19	0.18

Figure 5.30 shows the shear rate dependence of viscosity for GF-P and GF-10A nanocomposites measured at 170°C. GF-P showed almost Newtonian behavior at all shear rates however, the GF-10A nanocomposites exhibited non-Newtonian behavior. At very low shear rates, the shear viscosity of the GF-10A nanocomposites initially exhibited increase in the viscosity with respect to time and this indicated the

rheopexy as observed at very low shear rates as layered silicate nanocomposite were mostly strongly correlated the mesoscopic structure of the layered silicates which depended on not only the strength of the polymer-clay interaction but also inherent viscoelastic properties of layered silicates (Mittal, 2010) Additionally, at very high shear rates, the steady shear viscosities of GF-10A nanocomposites are lower than pure PLA. These observations suggest that the silicate layers are strongly oriented towards the flow direction at high shear rates. In accordance with this study, Ray and Okamoto (2003) and Gu and coworkers (2007) also studied steady shear viscosity of PLANCs as a function of shear rate and shear thinning behavior were found with the addition of nanoclay at higher shear rates.

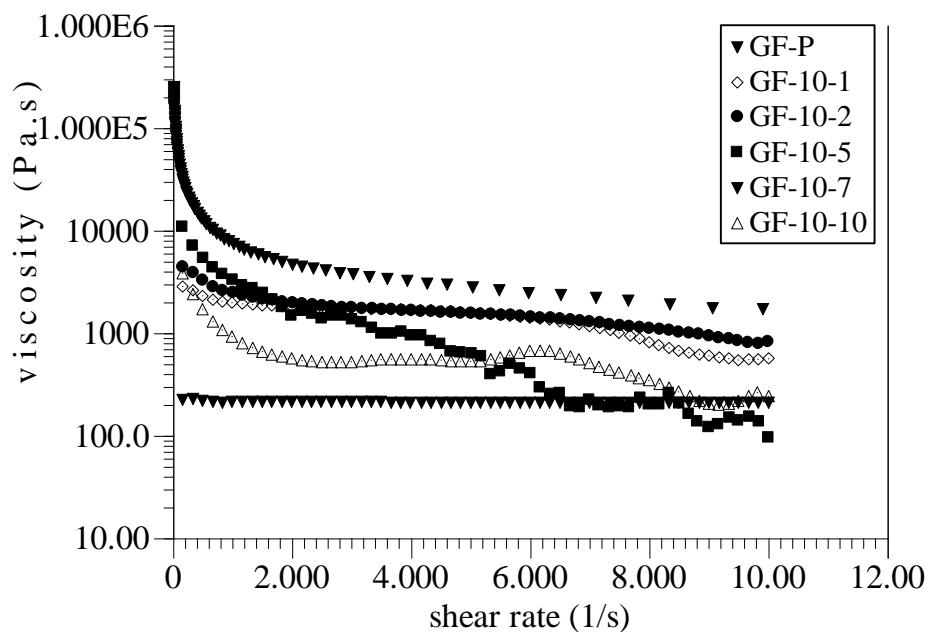


Figure 5.30. Shear Viscosity of GF-P and GF-10A as a function of shear rate.

The steady shear rheological behavior of GF-P and GF-10A nanocomposites are shown in Figures 5.31-5.36. The shear viscosity of GF-10A nanocomposites were improved at all shear rates with time for all clay loadings, and at a fixed shear rate it increased monotonically with increasing clay loadings. On the other hand, all GF-10A nanocomposites exhibited strong rheopexy behavior, and this behavior was obviously seen at low shear rate  $0.001 \text{ s}^{-1}$ , while viscosity of GF-P decreased at all shear rates. The same behavior was observed by Ray and Okamoto (2003) in PLANCs films as the planer alignment of layered silicates towards the flow direction under steady shear rate.

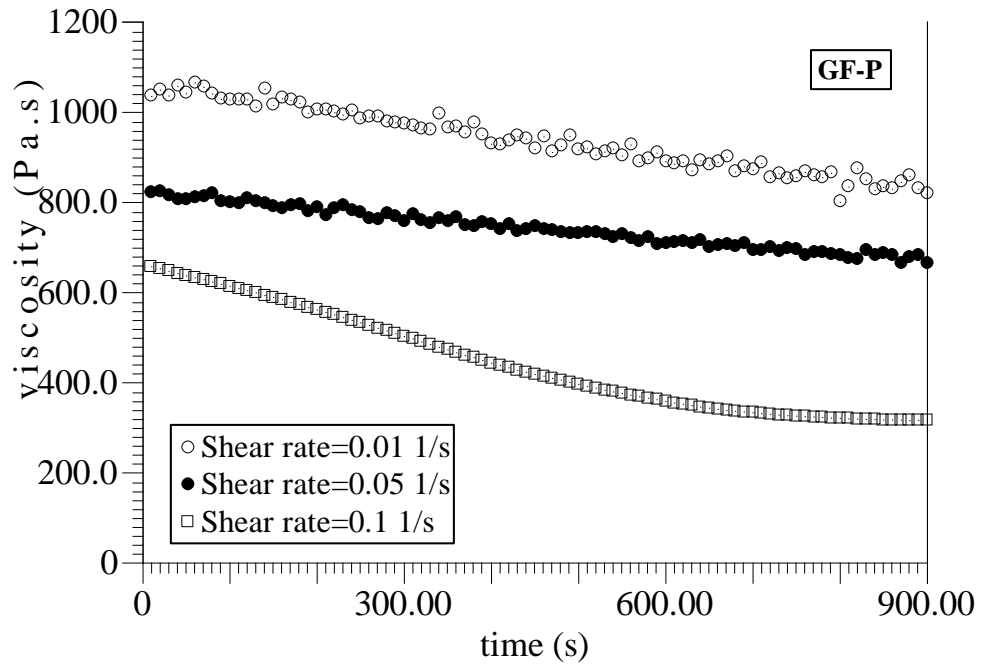


Figure 5.31. Steady shear viscosity of GF-P as a function of time.

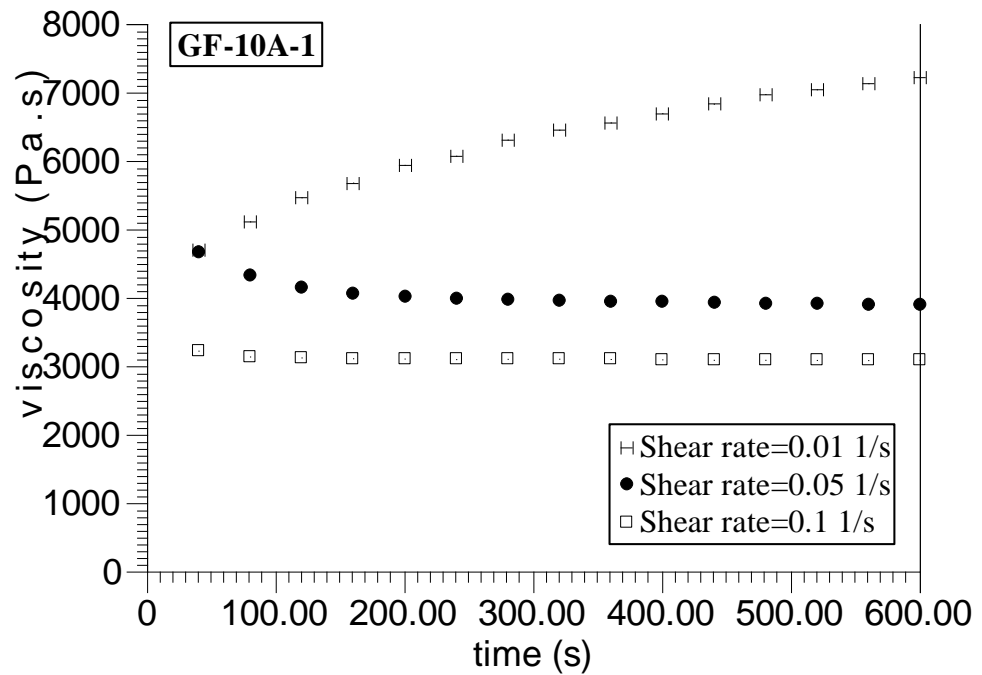


Figure 5.32. Steady shear viscosity of GF-10A-1 as a function of time.

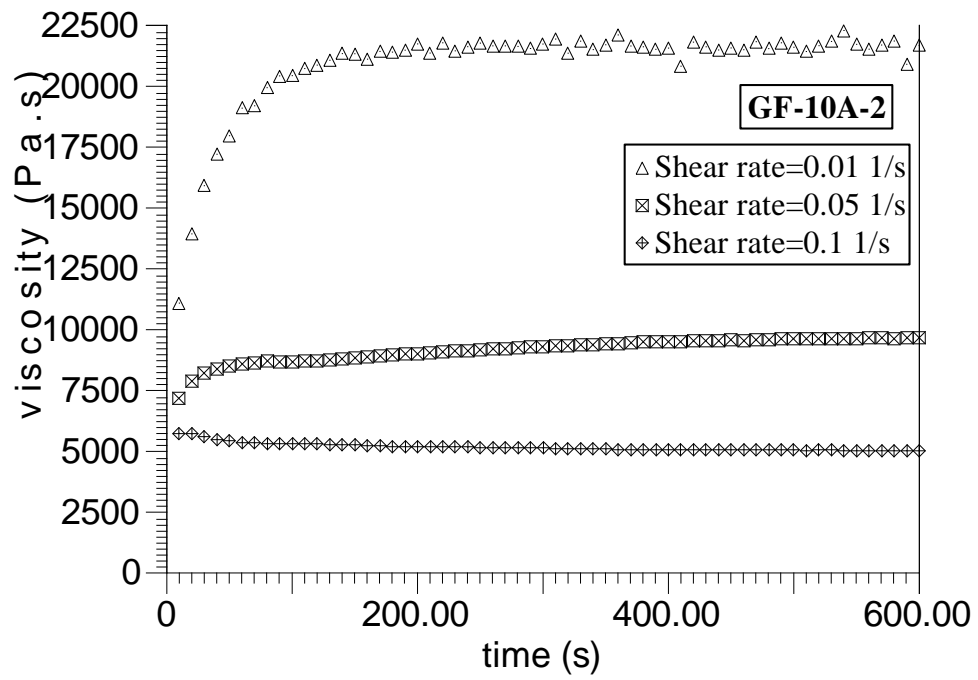


Figure 5.33. Steady shear viscosity of GF-10A-2 as a function of time.

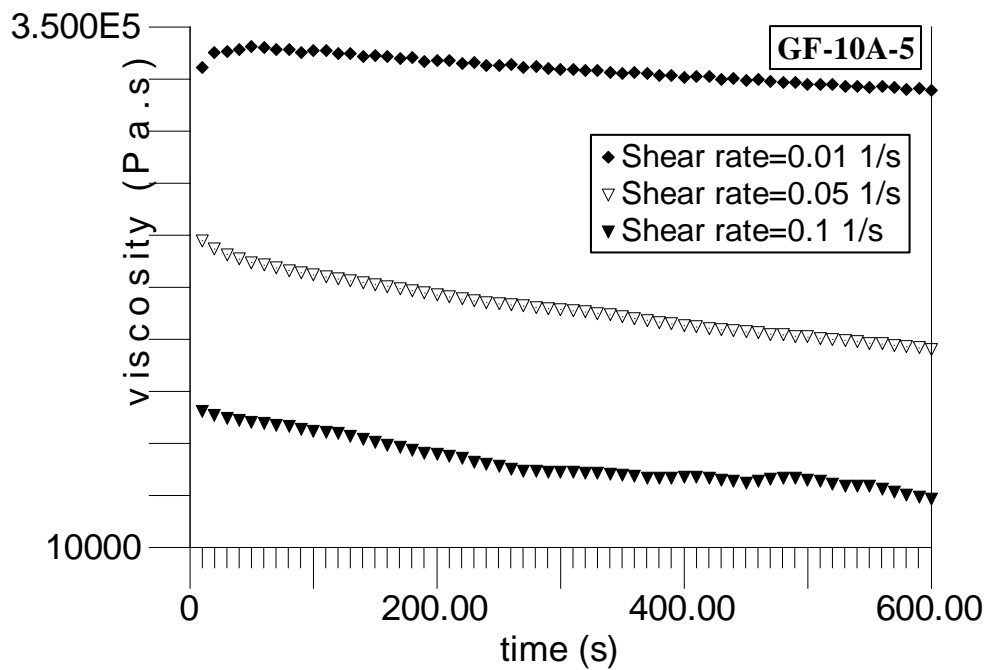


Figure 5.34. Steady shear viscosity of GF-10A-5 as a function of time.

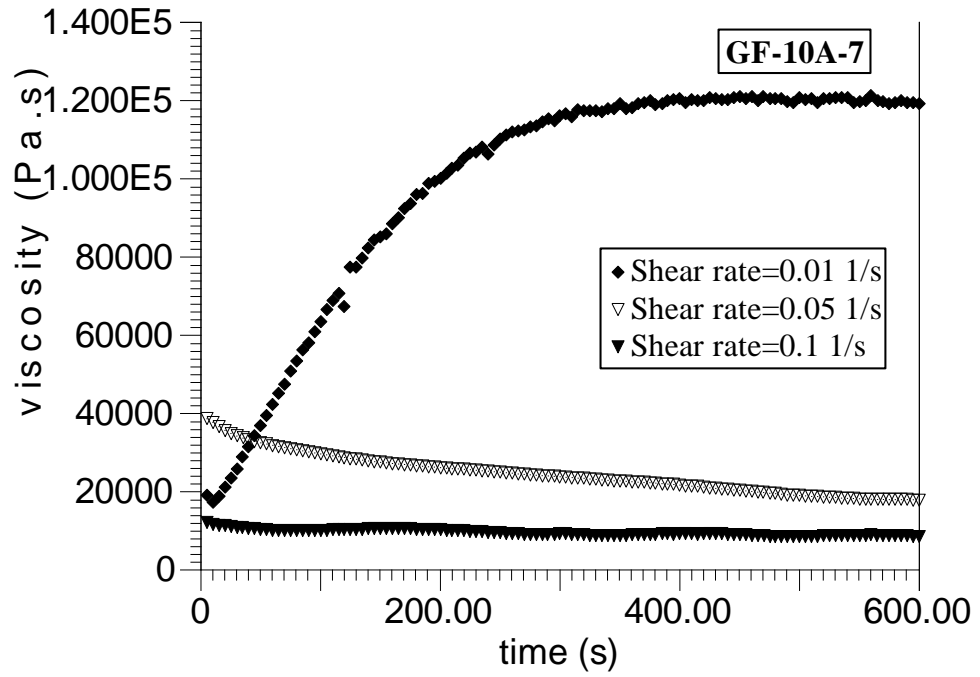


Figure 5.35. Steady shear viscosity of GF-10A-7 as a function of time.

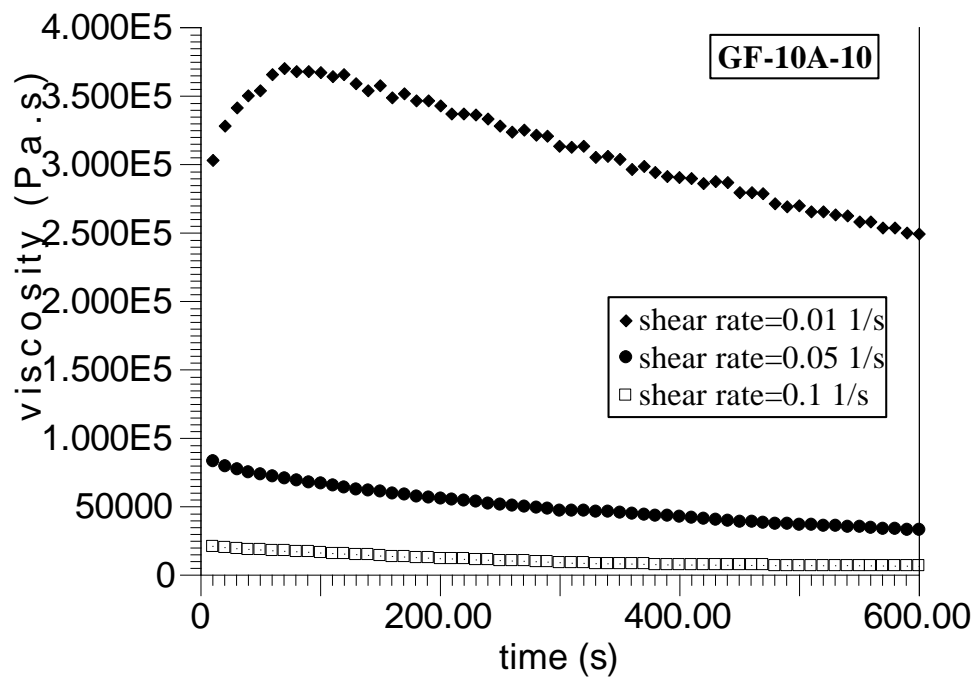


Figure 5.36. Steady shear viscosity of GF-10A-10as a function of time

## 5.6. Contact Angle Measurements

Contact angle measurements were performed to observe the effects of clay type and clay amount on surface hydrophobicity of PLA and PLANC films. Contact angle is the measure of wettability of a substance. While hydrophobicity of the surface increases, contact angle tends to increase. Measured water contact angles of the PLA and PLANC films are given in Table 5.7. Surface hydrophobicity of neat PLA obtained from Goodfellow Company was observed as higher than neat PLA supplied by Purac Company as the contact angle of the GF-P was measured higher than the other due to molecular weight difference of the polylactide as hydroxyl group increased while the molecular weight increased leading to increase in hydrophilicity (Sangaj and Malshe, 2004). In case of PL65-10A, GF-10A and GF-93A nanocomposite, the degree of surface hydrophobicity increased with increasing clay content. However, contact angles of GF-NF composite films were decreasing due to the phase separated structure. Although the PL65 polymer is more hydrophilic compared to GF polymer, the improvement in contact angles from hydrophilic to hydrophobic surface is more effective with the addition of clay for PL65-10A nanocomposites. Moreover, the degree of surface hydrophobicity was consistent with water vapor permeability measurement of PLA and PLA nanocomposite films. Since degrees of surface hydrophobicity increased while the permeabilities of PLA and PLA nanocomposite films decreased. That showed the linear relationship between contact angle changes and water vapor permeabilities due to changes in the nanocomposite structure in the polymer matrix.

Table 5.7. Contact angles measured for PLA and PLANC films

<b>Sample</b>	<b><math>\theta</math>(mean value)</b>	<b>Sample</b>	<b><math>\theta</math>(mean value)</b>
GF-P	78.31 $\pm$ 1.58	PL65-P	46.09 $\pm$ 7.30
GF-10A-1	78.85 $\pm$ 3.87	PL65-10A-1	68.70 $\pm$ 2.19
GF-10A-2	78.93 $\pm$ 1.20	PL65-10A-2	71.80 $\pm$ 0.93
GF-10A-5	83.72 $\pm$ 2.80	PL65-10A-5	74.37 $\pm$ 2.78
GF-10A-7	83.37 $\pm$ 1.55	PL65-10A-7	86.36 $\pm$ 3.76
GF-10A-10	81.00 $\pm$ 1.95	PL65-10A-10	83.38 $\pm$ 1,20
GF-93A-1	84.11 $\pm$ 2.84	GF-NF-2	61.58 $\pm$ 7.11
GF-93A-2	86.69 $\pm$ 6.96	GF-NF-5	66.60 $\pm$ 5.52
GF-93A-5	86.27 $\pm$ 2.50		
GF-93A-7	80.49 $\pm$ 3.12		
GF-93A-10	80.63 $\pm$ 3.21		

## 5.7. Color Measurement

The color of films is important property for packaging and coating applications requiring visibility. Besides, color measurements helped to determine dispersion of clay in the nanocomposite films (Hong, 2004). The results of the color measurements of the prepared PLA and PLANC films were shown in Table 5.8. As can be seen from the Table 5.8, the incorporation of Cloisite 10A and 93A in PLA matrix had almost no effect on the color of the films. It is generally known that  $\Delta E < 3-4$  means that the color change can not be detected by naked human eye (Oguzlu and Tihminlioglu, 2010). Therefore, the results indicated that the dispersion of clay in the polymer matrix can be assumed to be uniform especially up to 10 wt% loaded samples. However,  $\Delta E$  values GF-NF composite were observed to be significantly greater than 3, which can be attributed to poorer dispersion of nanoclays in the PLA matrix. When PL65-10A nanocomposite was compared with other nanocomposite systems, it was seen that less color difference of the PL65-10A05 nanocomposites was observed indicating better dispersion have achieved in PL65-10A nanocomposites. Addition to these, significant changes in the color of PLANCs are also in good accordance with the poorer properties of PLANCs prepared by using unmodified natural montmorillonite.

Table 5.8. The total color difference ( $\Delta E$ ) and color parameters of PLA and PLANCs

<b>Sample</b>	<b>L</b>	<b>A</b>	<b>b</b>	<b><math>\Delta E</math></b>
PL65-P	85.83±0.45	4.09±0.08	-8.98±0.14	-
PL65-10A-2	85.60±0.11	4.06±0.09	-8.68±0.20	0.41±0.20
PL65-10A-5	84.57±0.17	3.91±0.05	-8.03±0.25	0.27±1.59
GF-P	88.88±0.19	0.41 ±0.07	0.97±0.52	-
GF-10A-1	88.63±0.09	0.46 ±0.05	0.88±0.92	0.32±0.11
GF-10A-2	88.61±0.14	0.44±0.08	0.92±0.20	0.36±0.11
GF-10A-5	88.37±0.11	0.16±0.07	1.93±0.19	1.11±0.21
GF-10A-7	89.02±0.11	0.23±0.05	1.45±0.11	0.55±0.09
GF-10A-10	89.00±0.09	0.41±0.04	1.11±0.15	0.25±0.06
GF-93A-1	88.89±0.09	0.50±0.04	1.06±0.04	0.15±0.05
GF-93A-2	88.07±0.24	0.36±0.05	1.26±0.17	0.88±0.21
GF-93A-5	88.53±0.03	0.17±0.05	1.73±0.23	0.88±0.20
GF-93A-7	88.51±0.17	-0.02±0.04	2.54±0.30	1.68±0.29
GF-93A-10	88.27±0.06	0.06±0.05	2.06±0.08	1.30±0.06
GF-NF-2	86.41±0.49	3.17±0.05	-6.28±0.33	8.16±0.29
GF-NF-5	86.74±0.25	2.96±0.05	-5.66±0.11	7.42±0.11

## CHAPTER 6

### CONCLUSION

Throughout the research study, polylactide clay nanocomposite (PLANC) films were investigated as an alternative to conventional polymer composites. The purpose of the study was to examine the effect of nanoclay content, presence and type of organomodifier and nature of the polymer on barrier, thermal, mechanical and rheological properties and also surface and optical properties.

During the research study, FTIR- and XRD analysis were performed to characterize the PLANC films. FTIR analysis was used to be sure about presence of nanoclay in PLA matrix. It was seen that, percent absorbance of the Al-O stretching and Si-O bending at 525 and 465  $\text{cm}^{-1}$  was increasing with the increasing of the clay content. Structure of the nanocomposite had significant influence on the physical properties of the nanocomposites as the dispersion of the clay in polymer matrix and interfacial area between the silicate and polymer chain are larger than conventional microcomposites. XRD analysis was performed to determine exfoliation degree of the nanocomposites and exfoliated structure was observed in PL65-10 nanocomposites films and intercalated structures were obtained GF-10A and GF-93A up 5wt%.

Water vapor, oxygen and carbon dioxide permeabilities were measured to investigate the barrier properties of the nanocomposites. Nanoclay addition improved barrier properties of pure PLA. Best improvement in barrier properties was achieved in PL65-10A nanocomposites films as the molecular interaction between the layered silicates and polymer chains were higher than others. It was obviously seen from XRD results and permeability measurements that the structure of the nanocomposites significantly affected permeability of the PLANCs. As permeation of the water vapor or gas molecules followed a tortuous path through the polymer matrix by increasing the effective path length for diffusion. To get an idea about the tortuosity in PLANCs experimental permeability data were fitted to various permeability models and length width ratio of the PL65-10A and GF-10A are found between 498-574 and 243-382, respectively.

No significant change in DSC results were investigated during the study, However, thermal stability of the PL65-10A, GF-10A and GF-93A nanocomposite systems increased with incorporation of the clay owing to the dispersion of the clay and surfactant presence in the polymer matrix. Tensile strength and Young's modulus of the GF-10A and GF-93A were improved by the addition of organomodified montmorillonite up to critical clay amount 7wt%. However, mechanical properties of GF-NF nanocomposite were decreasing due to bad level dispersion of silicate layers in polymer matrix. In dynamic mechanical analysis glass transition temperatures of PLANCs were increasing with increasing of clay amount. Below  $T_g$  storage modulus of PL65-10A, GF-10A and GF-93A nanocomposites were improved due to reinforcement effect of the silicate layers.

In rheological measurements it was seen that GF-10A nanocomposites showed solid-like behavior at lower shear rates due to the presence of clay content as they resisted through the flow. Besides, those GF-10A nanocomposites showed shear thinning behavior at higher shear rates leading to improvements on the processability of nanocomposite.

In conclusion, excellent barrier and thermal properties of PL65-10A nanocomposite films were investigated combined with mechanical properties analysis with respect to other nanocomposite systems studied. Despite the best properties were achieved for PL65-10A nanocomposite GF-10A nanocomposites, physical properties of GF-10A and GF-93A nanocomposites were developed up to critical clay amount. Therefore, this study showed that industrial usage of polylactide polymers can be extended with incorporation of the nanoclays into polymer matrix using nanotechnology.

## REFERENCES

- Agrawal, A.; Saran, A. D.; Rath, S. S., Khanna, A. Constrained nonlinear optimization for solubility parameters of poly(lactic acid) and poly(glycolic acid)—validation and comparison *Polymer*, **2004**, 45, 8603–8612.
- Ahmed, J.; Varshney, S. K.; Auras, R., Rheological and Thermal Properties of Polylactide/Silicate Nanocomposites Films *Journal Of Food Science*, **2010** 75, 75:2, N17–N24.
- Ahmed, J.; Zhang J.-X.; Song, Z.; Varshney, S. K. Thermal Properties of Polylactides Effect of Molecular Mass and Nature of Lactide Isomer, *Journal of Thermal Analysis and Calorimetry*, **2009**, 95:3, 957–964.
- Alexandre, M.; Dubois, P. Polymer - Layered Silicate Nanocomposites: Preparation, Properties and Uses of A New Class of Materials, *Materials Science and Engineering*, **2000**, 28, 1-63.
- Auras, R. A.; Singh, S. P. ; Singh J. J., Evaluation of Oriented Poly(lactide) Polymers vs. Existing PET and Oriented PS for Fresh Food Service Containers, *Packaging Technology and Science*, **2005**, 18, 207–216.
- Auras, R. A.; Harte, B.; Selke, S.; An Overview of Polylactides as Packaging Materials, *Macromolecular Bioscience* **2004**, 4, 835–864.
- Bharadwaj, R.K. Modelling the Barrier Properties of Polymer-Layered Silicate Nanocomposites, *Macromolecules*, **2001**, 34, 9189-9192.
- Burgentzle, D.; Duchet, J.; Gerard, J.F.; Jupin, A.; Fillon B. Solvent Base Nanocomposite Coatings I. Dispersion of Organophilic Montmorillonite Inorganic Solvents, *Journal of Colloid and Interface Science*, **2004**, 278,26-39.

- Cervantes-Uc, J. M.; Cauich-Rodríguez, J. V.; Vázquez-Torres, H.; Garfias-Mesías, L.F.; Paul, D. R. Thermal degradation of commercially available organoclays studied by TGA–FTIR, *Thermochimica Acta*, **2007**, 457, 92-102.
- Chiellini, E.; Solaro, R. *Biodegradable Polymers and Plastics*, Kluwer Academic, **2003**, 67-73, 185-211.
- Choudalakis, G.; Gotsis, A.D. Permeability of Polymer/Clay Nanocomposites: A Review. *European Polymer Journal*, **2009**, 45, 967-984.
- Crank, J. Mathematics of Diffusion, *Oxford University Press*, 2<sup>nd</sup> Ed., **1956**.
- DeRocher, J.P.; Gettelfinger, B.T.; Wang, J.; Nuxoll, E.E.; Cussler, E.L. Barrier Membranes with Different Sizes of Aligned Flakes, *Journal of Membrane Science*, **2005**, 254, 21-30.
- Drieskens, M.; Peeters R.; Mullens, J.; Franco, D.; Lemstra, P. J.; Hristova-Bogaerds, D. G. Structure versus properties relationship of poly(lactic acid). I. Effect of crystallinity on barrier properties, *Journal of Polymer Science Part B: Polymer Physics*, **2009**, 47: 22, 2247–2258.
- Eitzman, D.M.; Melkote, R.R.; Cussler, E.L. Barrier Membranes with Tippe Impermeable Flakes, *AIChE Journal*, **1996**, 42:1, 2-9.
- Gedde, U.W. *Polymer Physics*, 1<sup>st</sup> ed., Chapman and Hall, **1995**.
- Gontard, N.; Thibault, R., Cuq B.; and Guilbert, S. Influence of Relative Humidity and Film Composition on Oxygen and Carbon Dioxide Permeabilities of Edible Films, *Journal of Agricultural Food Chemistry*, **1996**, 44, 1064-1069.
- Goodwin, J. W.; Hughes, R. W. *Rheology for chemists, an introduction*, Royal Society of Chemistry, 2<sup>nd</sup> ed., **2000**.

- Gu, S.; Ren J., Dong B. Melt Rheology of Polylactide/Montmorillonite Nanocomposites, *Journal of Polymer Science: Part B: Polymer Physics*, **2007**, 45, 3189–3196.
- Herrera-Alonso, J.M.; Marand, E.; Little, J.C.; Cox, S.S. Transport Properties in Polyurethane/Clay Nanocomposites as Barrier Materials: Effect of Processing Conditions, *Journal of Membrane Science*, **2009**, 337, 208-214.
- Janjarasskul, T.; Krochta, J. M. Edible Packaging Materials, *Annual Review of Food Science and Technology*, **2010**, 1:415–48.
- Ke, Y.C.; Stroeve, P. *Polymer-Layered Silicate and Silica Nanocomposites*, Elsevier B.V., 1<sup>st</sup> ed., **2005**.
- Koh, H.C. J.; Parka, S.M.; Jeonga, A.; Hwanga H. Y, TaekHong Y., Yong H. S., Yong N. S., Preparation and gas permeation properties of biodegradable polymer/layered silicate nanocomposite membranes, *Desalination*, **2008**, 233, 201–209.
- Koo, J. *Polymer Nanocomposites: Processing, Characterization, and Applications*, 1<sup>st</sup> ed., McGraw-Hill, New York, 2006.
- Kolybaba, M.; Tabil, L.G.; Panigrahil, S.; Crerar, W.J.; Powell, T.; Wang, B.; Biodegradable Polymers: Past, Present and Future, *The society for engineering in argicultral, food and biological systems*, **2003**, RRV03-0007.
- Krevelen, D.W.; Nijenhuis, K.T. *Properties of Polymers*, Elsevier B.V., 4<sup>rd</sup> ed., **2009**
- Letcher T.M. Thermodynamics, Solubility and Environmental Issues, Elsevier B.V, 1<sup>st</sup> ed., **2007**, 343-369.
- Lewitus D., McCarthy S., Ophir A., Kenig S., The Effect of Nanoclays on the Properties of PLLA-modified Polymers Part 1: Mechanical and Thermal Properties *Journal of Polymers and the Environment*, **2006**, 14, 171-177.

- Lopez-Rodriguez N., Lopez-Arraiza A., Meaurio E., Sarasua J.R. Crystallization, Morphology, and Mechanical Behavior of Polylactide/Poly( $\epsilon$ -caprolactone) Blends, *Polymer Engineering and Science*, **2006**, 46, 1299-1308.
- Lu, C.; Mai, Y.W. Permeability Modeling of Polymer-Layered Silicate Nanocomposites, *Composites Science and Technology*, **2007**, 67, 2895-2902.
- Mark, J.E. Physical properties of polymer handbook, *Springer Science Business Media, LLC* 2<sup>nd</sup> ed, **2007**, 289-305.
- Mittal, V. *Optimization of Polymer Nanocomposite Properties*, Wiley-VHC Verlag GmbH&Co, **2010**.
- Mohanty, A.; Misra, M.; Drzal, L.T. *Natural Fibers Biopolymers and Biocomposites*, CRC Press, **2005**, Chapter 16.
- Naira, L.S.; Laurencina, C.T.; Biodegradable polymers as biomaterials, *Progress in Polymer Science*, **2007**, 32, 762–798
- Nielsen, L.E. Models for the Filled Polymer System, *Journal of Macromolecular Science: Part A – Chemistry*, **1967**, 1:5, 929-942
- Oguzlu, H.; Tihminlioglu, F. Preparation and Barrier Properties of Chitosan-Layered Silicate Nanocomposite Films, *Macromolecular Symposia*, **2010**, 298:1, 91-98.
- Okamoto M., Biodegradable Polymer/Layered Silicate Nanocomposites A Review, *Handbook of Biodegradable Polymeric Materials and Their Applications*, **2005**, 1, 1-45
- Paul, M.; Alexandre, M.; Degée, P.; Henrist, C.; Rulmont, A.; Dubois, P.; New nanocomposite materials based on plasticized poly(L-lactide) and organomodified montmorillonites: thermal and morphological study, *Polymer*, **2003**, 44, 443-450

- Paul, D.R.; Robeson, L.M. Polymer Nanotechnology: Nanocomposites. *Polymer*, **2008**, 49, 3187-3204
- Pavlidou, S.; Papaspyrides, C.D. A review on Polymer-Layered Silicate Nanocomposites, *Progress in Polymer Science*, **2008**, 33, 1119–1198
- Peterson, L.; Oksman, K. Biopolymer Based Nanocomposites: Comparing Layered Silicates and Microcrystalline Cellulose as Nanoreinforcement. *Composites Science and Technology*, **2006**, 66, 2187-2196
- Rasal., R; M., Janorkar A. V., Hirt D. E., Poly(lactic acid) modifications, *Progress in Polymer Science*, **2010**, 35 338–356
- Ray, S. S.; Yamada, K.; Okamoto, M.; Ueda, K. Polylactide-Layered Silicate Nanocomposite: A Novel Biodegradable Material, *Nano Letter*, **2002**, 2: 10, 1093–1096.
- Ray S. S., Maiti P., Okamoto M., Yamada K., and Ueda K., New Polylactide/Layered Silicate Nanocomposites. 1. Preparation, Characterization, and Properties, *Macromolecules* **2002**, 35, 3104-3110.
- Ray S. S., Okamoto M. New Polylactide/Layered Silicate Nanocomposites, Melt Rheology and Foam Processing, *Macromolecular Material Engineering*, **2003**, 288, 936–944.
- Ray, S. S.; Bousmina, M. Biodegradable Polymers and Their Layered Silicate Nanocomposites: In Greening the 21<sup>st</sup> Century Materials World. *Progress in Materials Science*, **2005**, 50, 962–1079.
- Ray, S.S; Bousmina, M.M. *Biodegradable Polymers/Layered Silicate Nanocomposites Polymer Nanocomposites*,, 1<sup>st</sup> ed, Woodhead Publishing Cambridge, 2006, 57-129.

- Ray, S.S.; Okamoto, M. Polymer/Layered Silicate Nanocomposites: A Review from Preparation to Processing. *Progress in Polymer Science*, **2003**, 28, 1539-1641.
- Ray, S.S.; Okamoto, M.; Biodegradable Polylactide and Its Nanocomposites: Opening a New Dimension for Plastics and Composites, *Macromolecular Rapid Communications* **2003**, 24, 815–840.
- Rhim, J.; Hong, S.; Ha, C. Tensile, water vapor barrier and antimicrobial properties of PLA/nanoclay composite films, *Food Science and Technology*, **2009**, 42, 612-617.
- Sangaj, N. S.; Malsh, V. C. Permeability of polymers in protective organic coatings, *Progress in Organic Coatings*, **2004**, 50:1,28-39
- Shen, L.; Haufe J.; Patel\ M.K.; Product overview and market projection of emerging bio-based plastics, *EuropeanBioplastics*, 2009, 1-191
- Siracusa, V.; Rocculi, P.; Romani., S.; Rosa, M.D. Biodegradable polymers for food packaging: a review, *Trends in Food Science & Technology*, **2008**, 19, 634-643
- Smith, P. G, *Introduction to Food Process Engineering*, Springer Science Bussiness Media LLC, 2011
- Sun, L.; Boo, W.J.; Clearfield, A.; Sue, H.J.; Pham, H.Q. Barrier Properties of Model Epoxy Nanocomposites, *Journal of Membrane Science*, **2008**, 318, 128-136
- Fornes, T. D.; Yoon, P. J.; Keskkula, H.; Paul, D. R. Nylon 6 nanocomposites: the effect of matrix molecular weight, *Polymer*, **2001**, 42: 25, 09929-09940
- Thellen, C.; Orroth, C.; Froio, D.; Ziegler, D.; Lucciarini, J.; Farrell, R. Influence of montmorillonite layered silicate on plasticized poly(l-lactide) blown films *Polymer*, **2005**, 46, 11716-11727.

- Tjong, S. C. Structural and Mechanical Properties of Polymer Nanocomposites: A Review, *Journal of Material Science and Engineering*, **2006**, 53: 73–197.
- Tsuji, H.; Fukui I. Enhanced thermal stability of poly(lactide)s in the meltbyenantiomeric polymer blending *Polymer*, **2003**, 44, 2891–2896
- Tsuji, R. O.; Hiroyuki D.; Koichi F. Water Vapor Permeability of Poly(lactide)s: Effects of Molecular Characteristics and Crystallinity, *Journal of Applied Polymer Science*, 99, **2006**, 2245–2252
- WEB\_1 [http://www.plastics.ca/\\_files/file.php?fileid=filehchYqdhbjw&filename=file\\_BIODEGRADABLE\\_POLYMERS\\_A\\_REVIEW\\_24\\_Nov.\\_2000.\\_Final.pdf](http://www.plastics.ca/_files/file.php?fileid=filehchYqdhbjw&filename=file_BIODEGRADABLE_POLYMERS_A_REVIEW_24_Nov._2000._Final.pdf)
- WEB\_2 <http://www.unitedcomposites.net/usapages/whycomposites2.htm>
- Weber\ J.C.; Biobased Packaging Materials for the Food Industry: Status and Prospectives, *KVL*, 1-136.
- Wu, D.; Wu, L.; Wu, L.; Zhang, M. Rheology and thermal stability of polylactide/clay nanocomposites, *Polymer Degradation and Stability*, **2006**, 91:12, 3149-3155
- Yang, S.; Wu, Z; Yang, W.; Yang, M. Thermal and mechanical properties of chemical crosslinked polylactide (PLA). *Polymer Testing*, **2008**, 27:8 , 957-963
- Yang, W.; Ko., S.; Wang, P.; Shih, Chang, M.; Jian, G.J. Preparation of Polystyrene/Clay Nanocomposite by Suspension and Emulsion Polymerization, *Polymer Composites*, **2008**, 29, 409-414
- Żenkiewicz, M.; Richert, J. Permeability of polylactide nanocomposite films for water vapour, oxygen and carbon dioxide, *Polymer Testing*, **2008**, 27:7, 835-840

## APPENDIX A

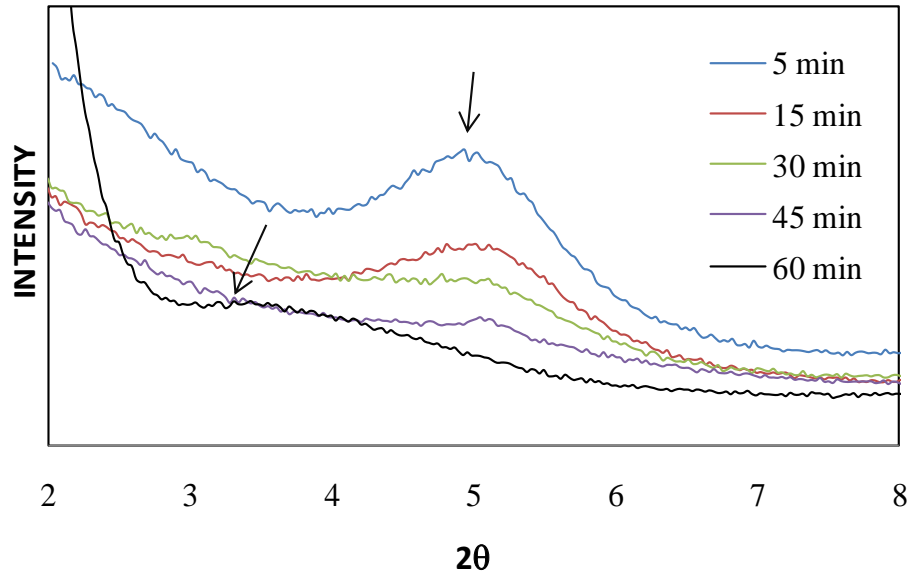


Figure A.1. XRD patterns of PLANCs according to clay solution sonication time.

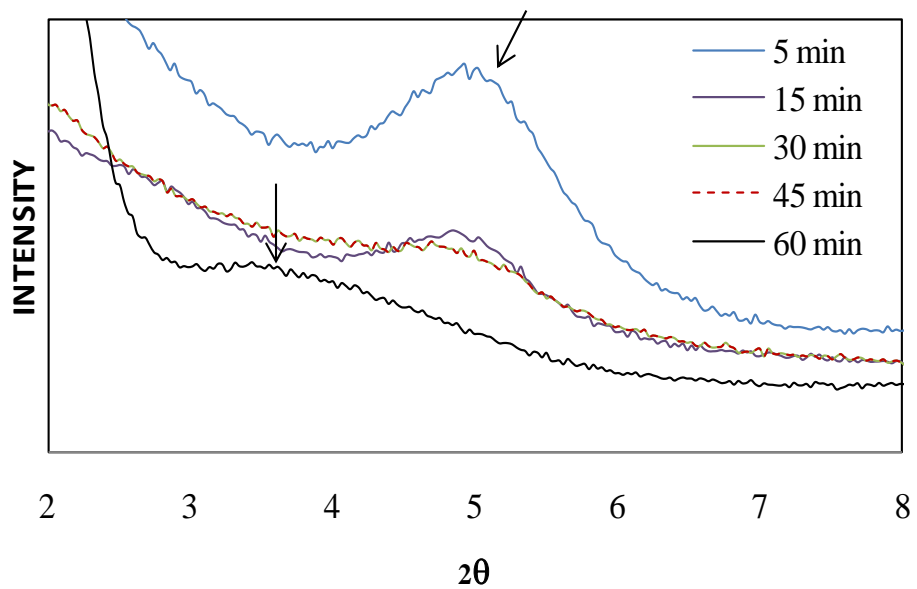


Figure A.2. XRD patterns of PLANCs according to polymer-clay solution sonication time.

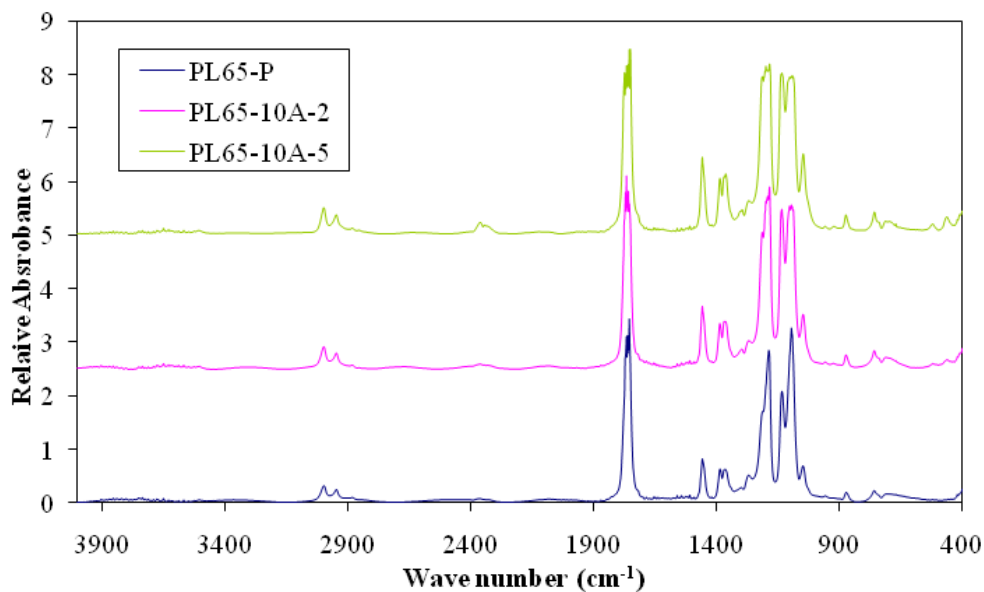


Figure A.3. FTIR spectra of PL65-P and PL65-10A nanocomposite films in 400-600 $\text{cm}^{-1}$  region

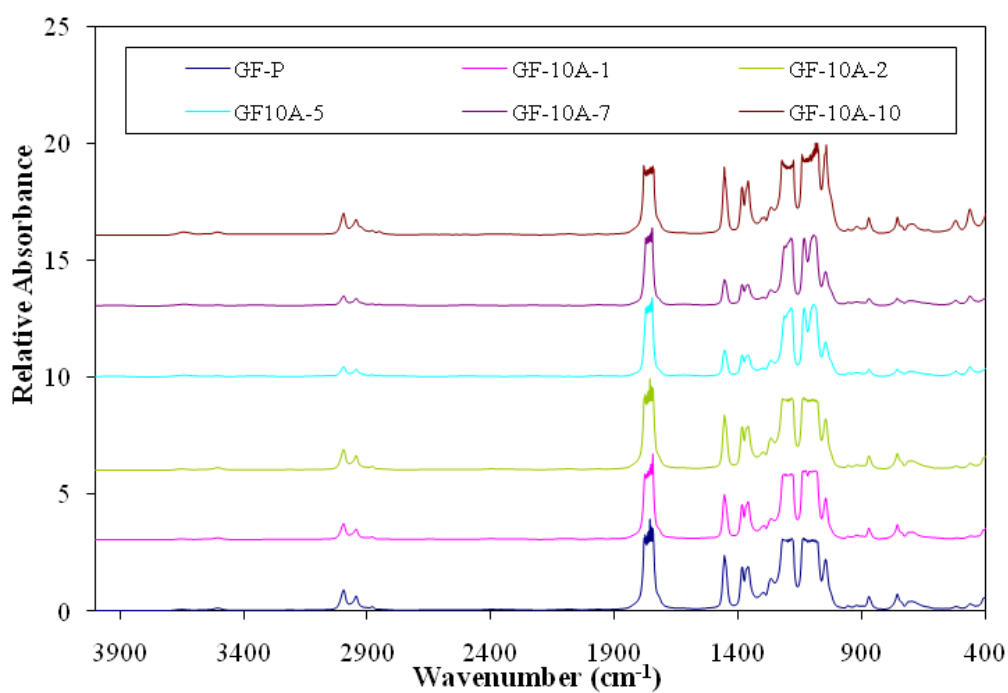


Figure A.4. FTIR spectra of GF-P and GF-10A nanocomposite films in 400-600 $\text{cm}^{-1}$  region

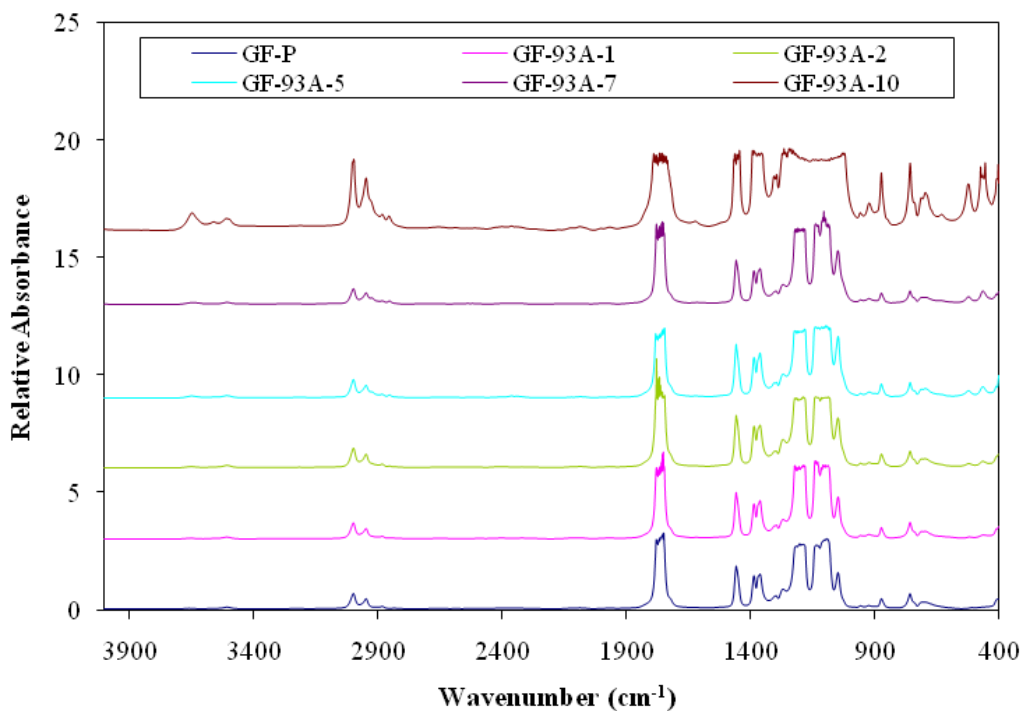


Figure A.5. FTIR spectra of GF-P and GF-93A nanocomposite films in 400-600 $\text{cm}^{-1}$  region

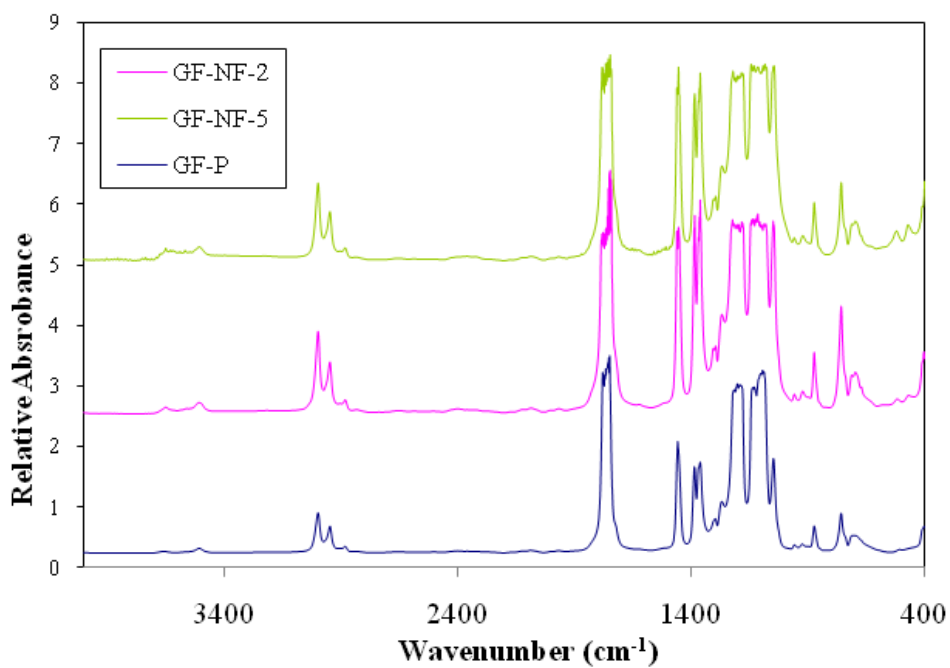


Figure A.6. FTIR spectra of GF-P and GF-NF composite films in 400-600 $\text{cm}^{-1}$  region

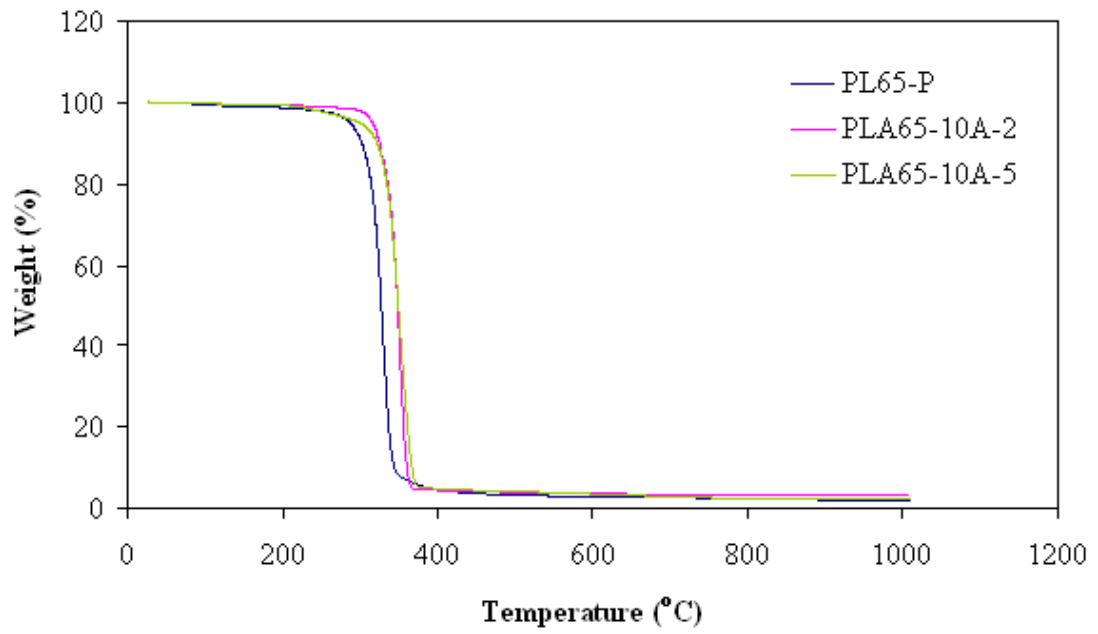


Figure A.7. TGA results of PL65-P and PL65-10A nanocomposite films

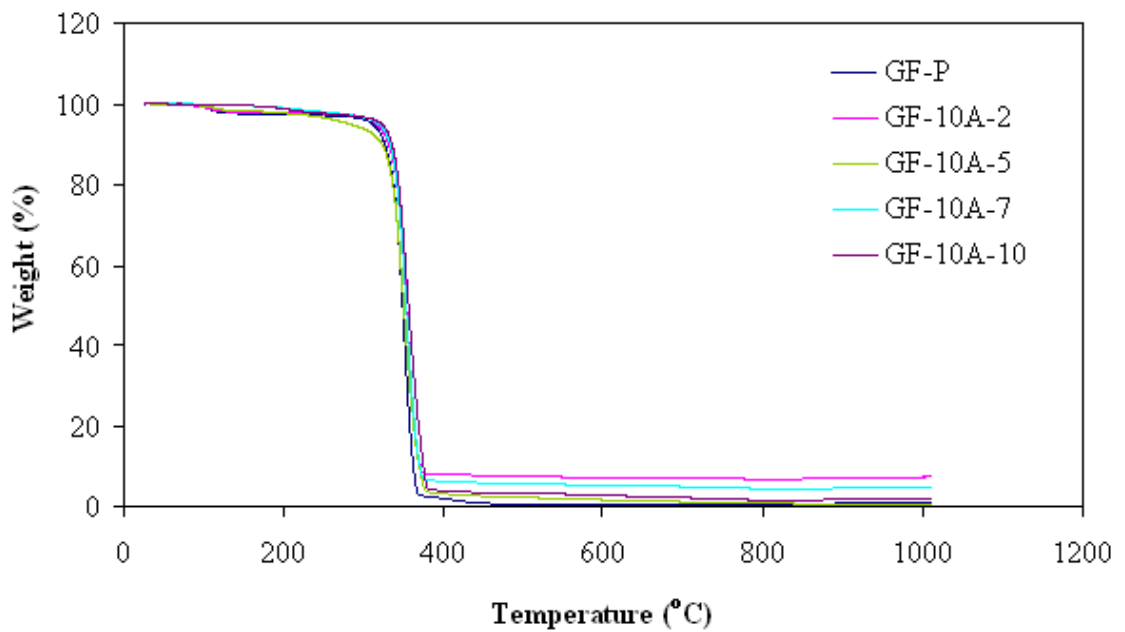


Figure A.8. TGA results of GF-P and GF-10A nanocomposite films

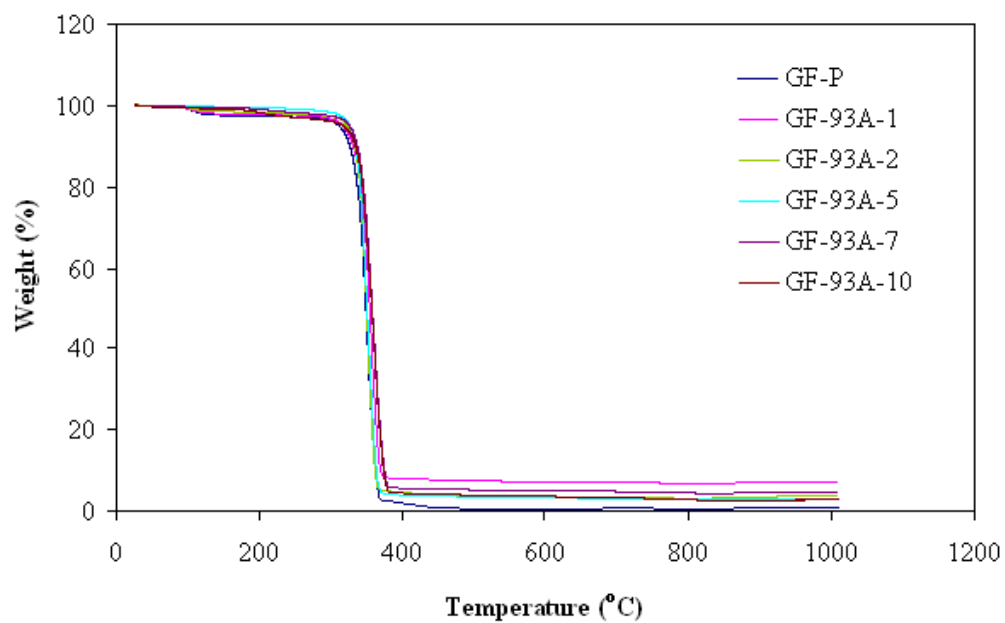


Figure A.8. TGA results of GF-P and GF-93A nanocomposite films

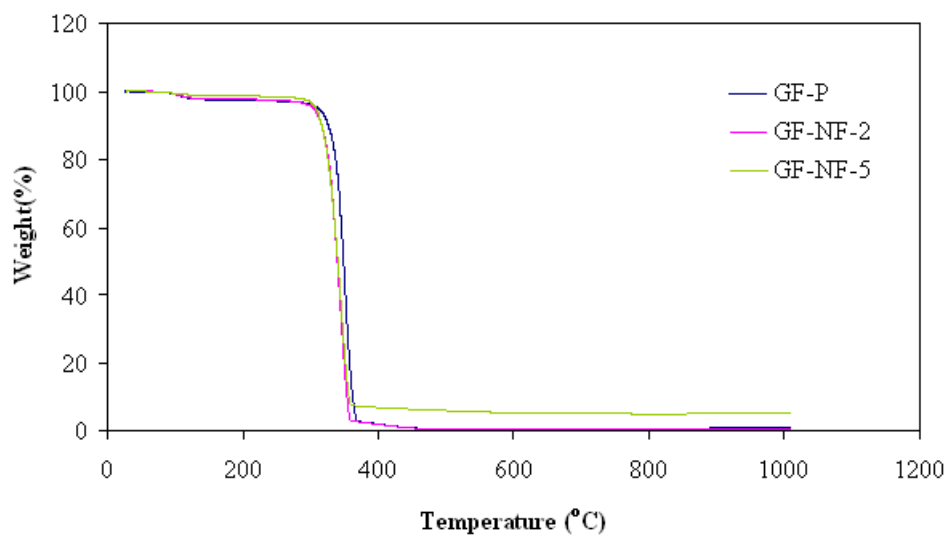


Figure A.9. TGA results of GF-P and GF-NF nanocomposite films

Table A.1. Swelling degree of PLA and PLANCs

Sample	Dry film thickness( $\mu\text{m}$ )	Wet film thickness( $\mu\text{m}$ )	Thickness change (%)	Avg. thickness change(%)	Sample	Dry film thickness( $\mu\text{m}$ )	Wet film thickness( $\mu\text{m}$ )	Thickness change (%)	Avg. thickness change(%)
GF-P	25.80 $\pm$ 1.23	26.00 $\pm$ 2.86	0.78	1.70 $\pm$ 0.81	GF-93A-1	20.20 $\pm$ 0.63	20.27 $\pm$ 0.90	0.36	0.75 $\pm$ 0.59
	18.50 $\pm$ 0.53	18.91 $\pm$ 0.70	2.21			22.10 $\pm$ 1.66	22.42 $\pm$ 1.56	1.43	
	18.80 $\pm$ 0.63	19.20 $\pm$ 1.32	2.13			22.00 $\pm$ 2.83	22.10 $\pm$ 2.47	0.45	
GF-10A-1	35.40 $\pm$ 0.97	35.50 $\pm$ 1.27	0.28	0.81 $\pm$ 0.73	GF-93A-2	22.70 $\pm$ 1.25	22.91 $\pm$ 1.04	0.92	0.88 $\pm$ 0.41
	35.64 $\pm$ 0.67	35.82 $\pm$ 0.75	0.51			21.90 $\pm$ 0.74	22.00 $\pm$ 1.13	0.46	
	39.60 $\pm$ 1.71	40.25 $\pm$ 0.97	1.64			22.30 $\pm$ 1.16	22.58 $\pm$ 0.67	1.27	
GF-10A-2	23.80 $\pm$ 0.79	24.42 $\pm$ 1.16	2.59	1.43 $\pm$ 1.20	GF-93A-5	26.30 $\pm$ 1.83	26.36 $\pm$ 1.69	0.24	0.85 $\pm$ 0.54
	23.50 $\pm$ 1.35	23.55 $\pm$ 0.93	0.19			24.20 $\pm$ 0.92	24.45 $\pm$ 0.82	1.05	
	31.20 $\pm$ 2.78	31.67 $\pm$ 2.57	1.50			31.80 $\pm$ 3.22	32.20 $\pm$ 2.30	1.26	
GF-10A-5	26.10 $\pm$ 2.76	26.45 $\pm$ 3.24	1.36	2.15 $\pm$ 1.51	GF-93A-7	43.40 $\pm$ 3.50	43.67 $\pm$ 2.00	0.61	0.83 $\pm$ 0.57
	21.00 $\pm$ 0.82	21.82 $\pm$ 1.40	3.90			43.56 $\pm$ 1.01	44.20 $\pm$ 1.03	1.48	
	26.50 $\pm$ 2.76	26.82 $\pm$ 2.86	1.20			48.70 $\pm$ 6.73	48.90 $\pm$ 4.86	0.41	
GF-10A-7	21.92 $\pm$ 3.09	22.18 $\pm$ 0.60	1.21	1.28 $\pm$ 0.95	GF-93A-10	30.60 $\pm$ 6.04	31.00 $\pm$ 6.20	1.31	2.60 $\pm$ 1.25
	20.80 $\pm$ 1.99	21.27 $\pm$ 1.42	2.27			37.30 $\pm$ 5.33	38.30 $\pm$ 5.17	2.68	
	22.10 $\pm$ 3.21	22.18 $\pm$ 0.75	0.37			17.10 $\pm$ 1.79	17.75 $\pm$ 2.26	3.80	
GF-10A-10	34.10 $\pm$ 2.69	34.55 $\pm$ 1.13	1.31	1.79 $\pm$ 0.81	PL65-P	8.70 $\pm$ 1.16	8.77 $\pm$ 0.93	0.80	1.70 $\pm$ 1.07
	30.00 $\pm$ 4.74	30.82 $\pm$ 4.40	2.73			8.00 $\pm$ 0.00	8.23 $\pm$ 0.44	2.88	
	39.20 $\pm$ 4.32	39.73 $\pm$ 1.85	1.35			8.10 $\pm$ 0.74	8.21 $\pm$ 0.80	1.41	
GF-NF-2	35.70 $\pm$ 0.95	36.00 $\pm$ 1.66	0.84	0.54 $\pm$ 0.29	PL65-10A-2	11.00 $\pm$ 0.47	11.08 $\pm$ 0.86	0.70	1.05 $\pm$ 0.70
	39.90 $\pm$ 0.57	40.00 $\pm$ 0.85	0.25			10.80 $\pm$ 0.79	11.00 $\pm$ 0.95	1.85	
	40.20 $\pm$ 0.42	40.42 $\pm$ 0.97	0.54			10.40 $\pm$ 0.52	10.46 $\pm$ 0.66	0.59	
GF-NF-5	40.00 $\pm$ 1.56	40.25 $\pm$ 0.97	0.63	1.69 $\pm$ 0.98	PL65-10-5	16.44 $\pm$ 0.88	16.62 $\pm$ 1.33	1.04	1.10 $\pm$ 1.14
	31.40 $\pm$ 0.97	32.00 $\pm$ 1.21	1.91			14.50 $\pm$ 0.71	14.50 $\pm$ 0.89	0.00	
	22.50 $\pm$ 0.53	23.07 $\pm$ 0.83	2.54			8.00 $\pm$ 0.00	8.18 $\pm$ 0.40	2.27	

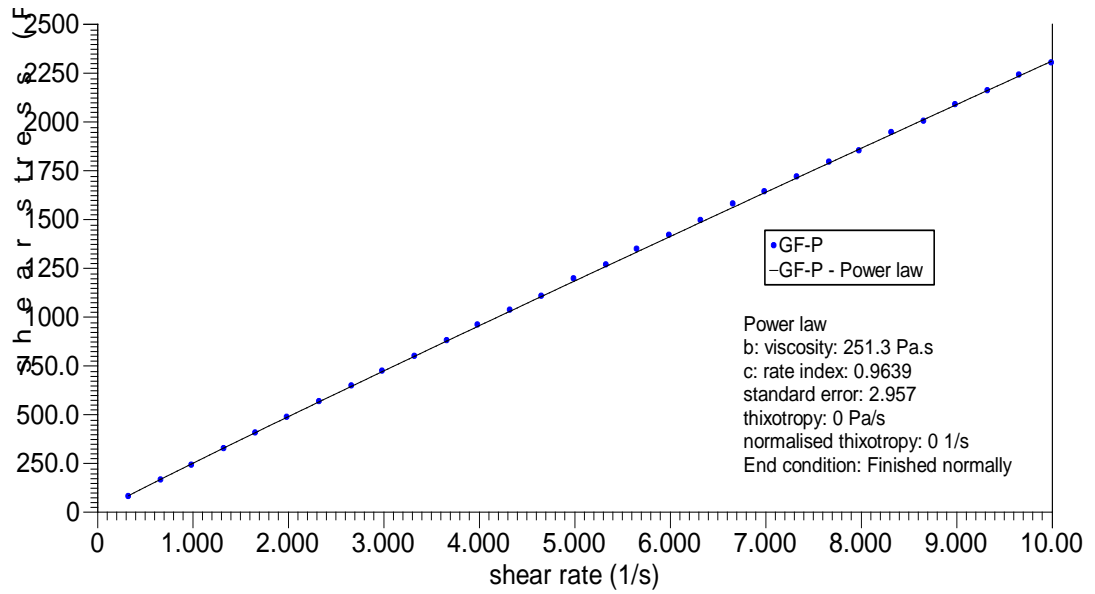


Figure A.10. Power model fits of GF-P

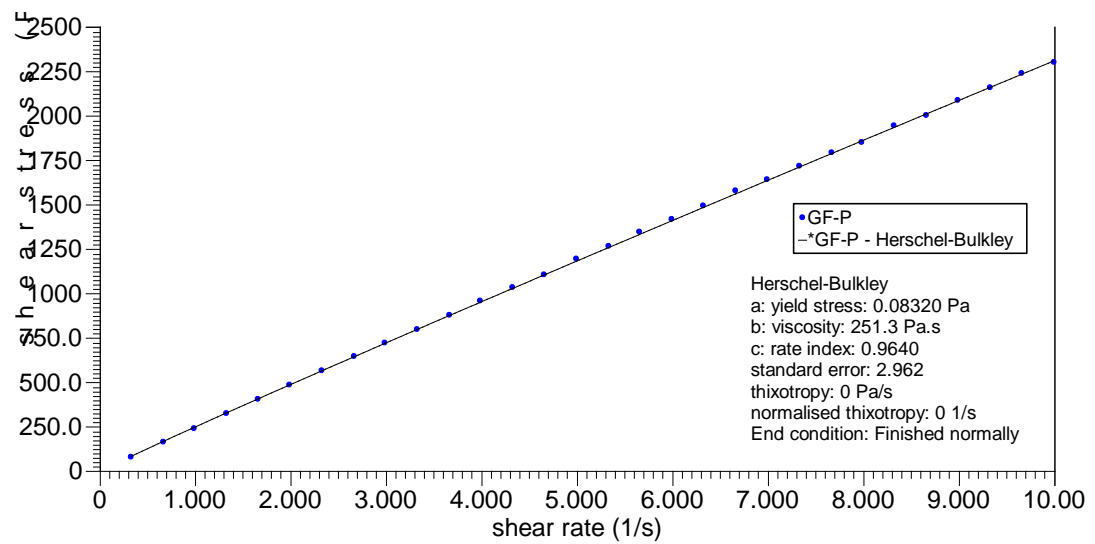


Figure A.11. Herschel-Bulkley fits of GF-P

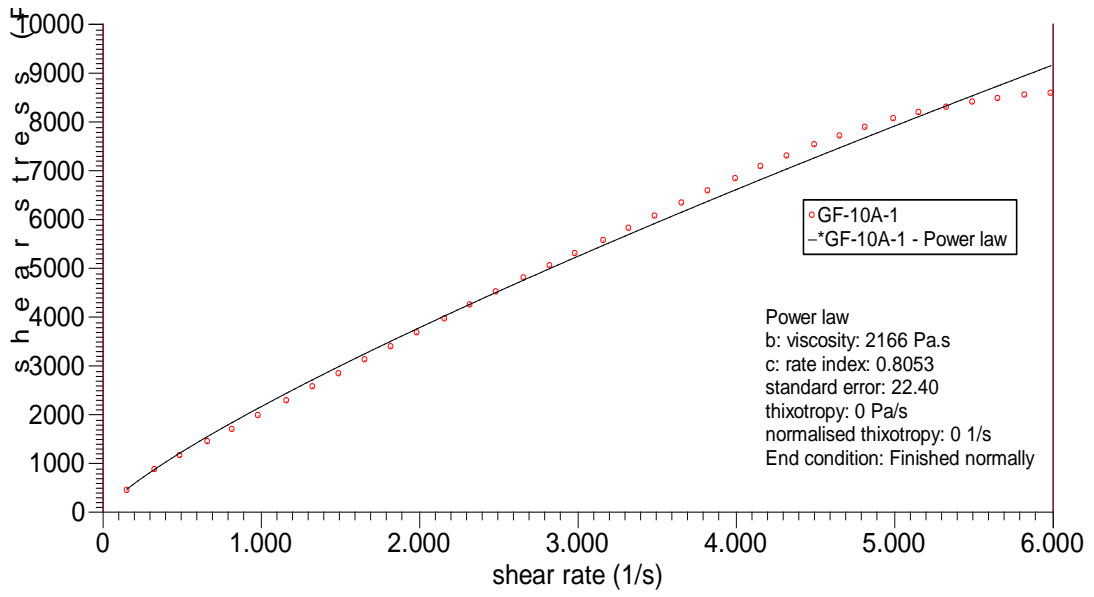


Figure A.12. Power model fits of GF-P

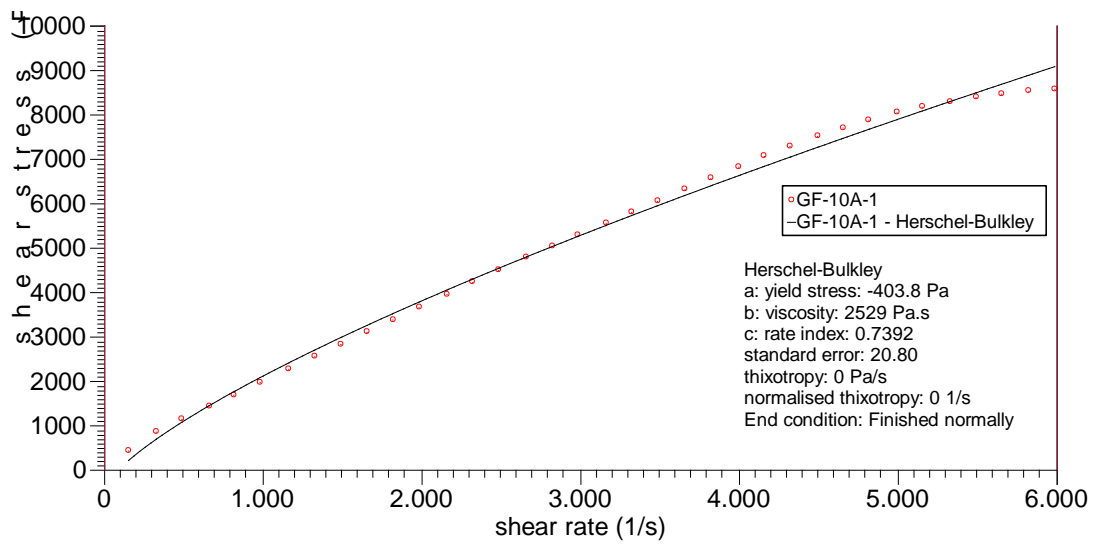


Figure A.13. Herschel-Bulkley fits of GF-10-1

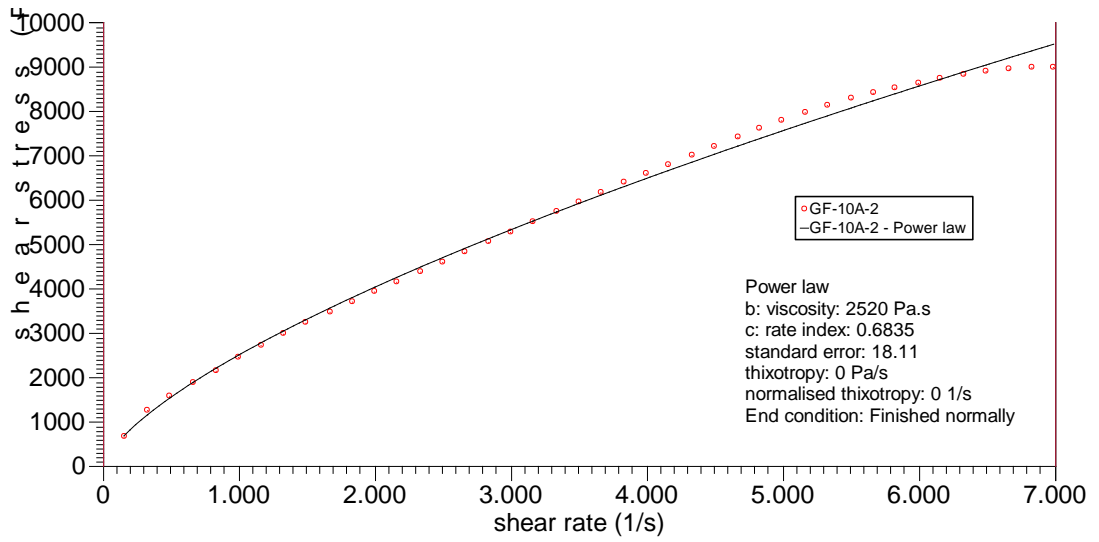


Figure A.14. Power model fits of GF-10A-2

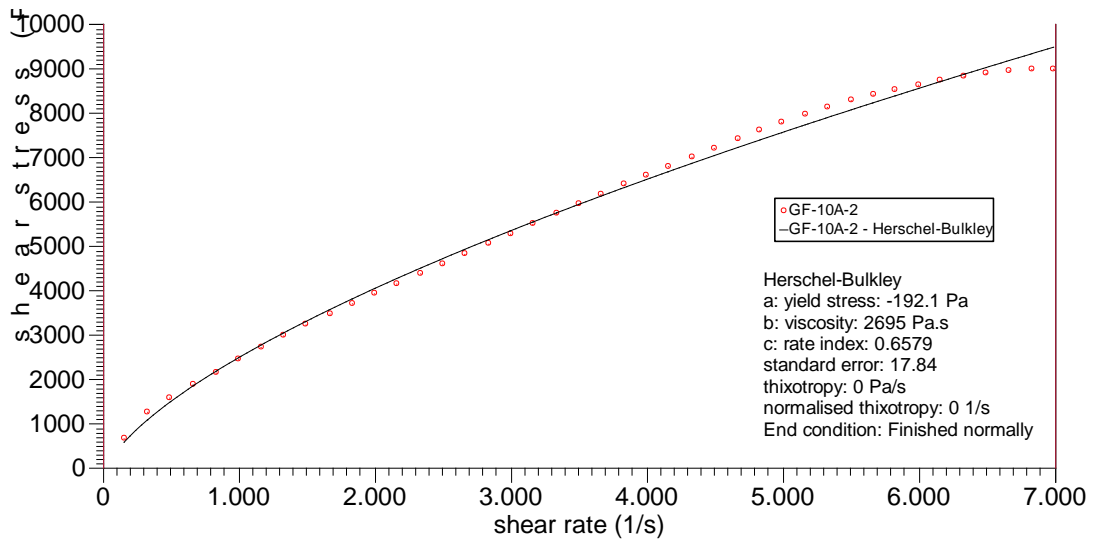


Figure A.15. Herschel-Bulkley fits of GF-10A-2

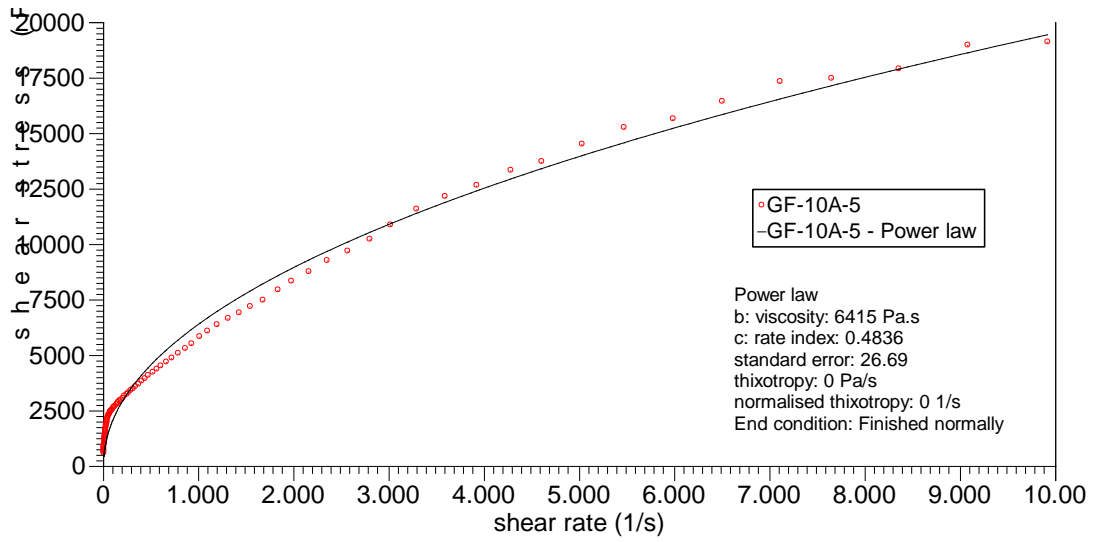


Figure A.16. Power model fits of GF-10A-5

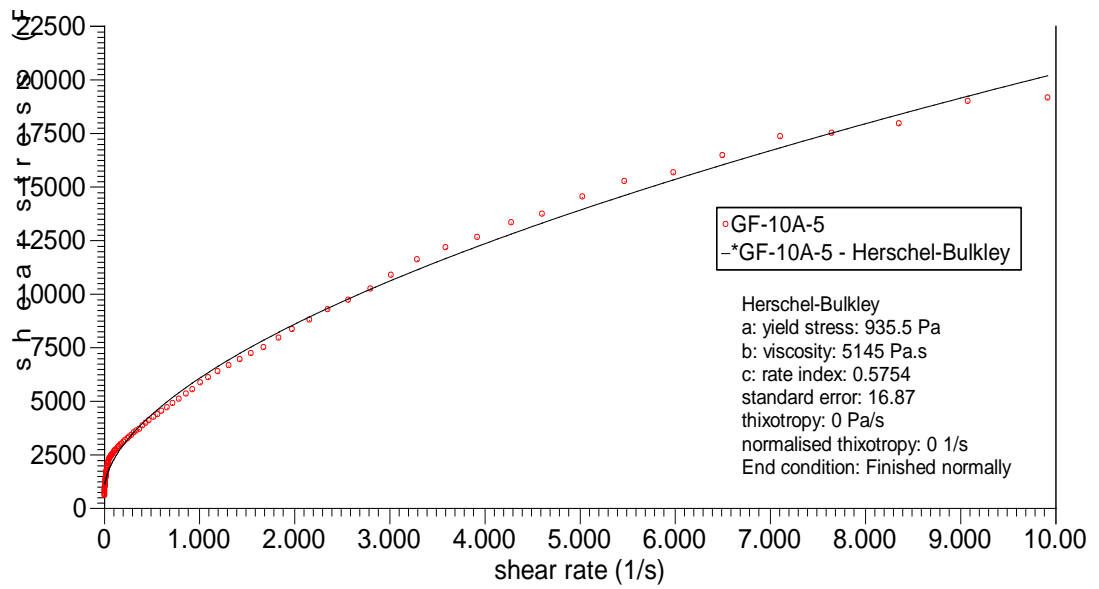


Figure A.17. Herschel-Bulkley fits of GF-10A-5

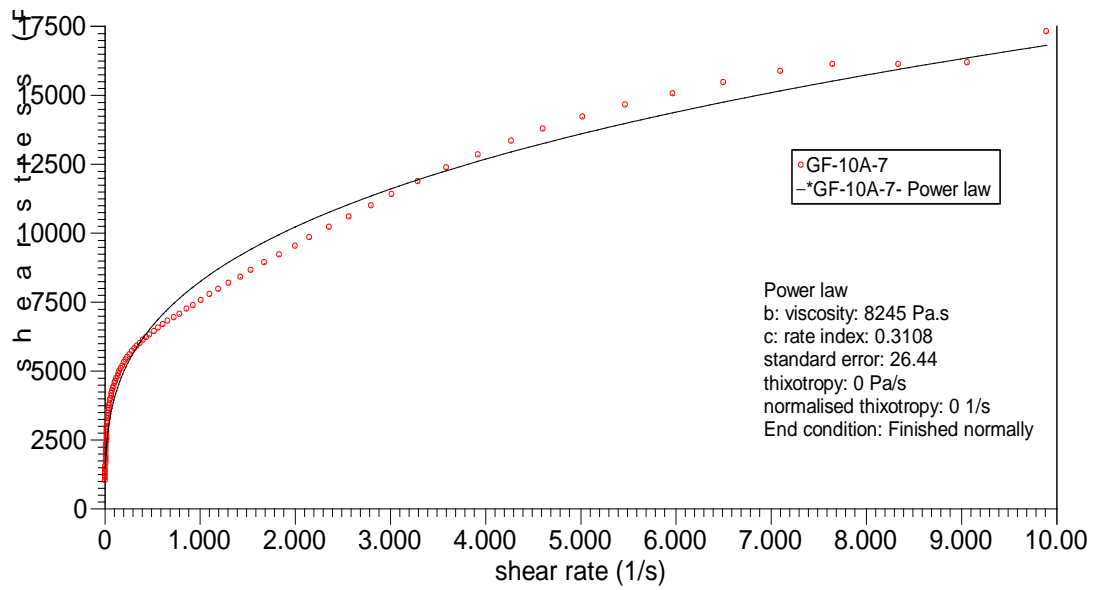


Figure A.18. Power model fits of GF-10A-7

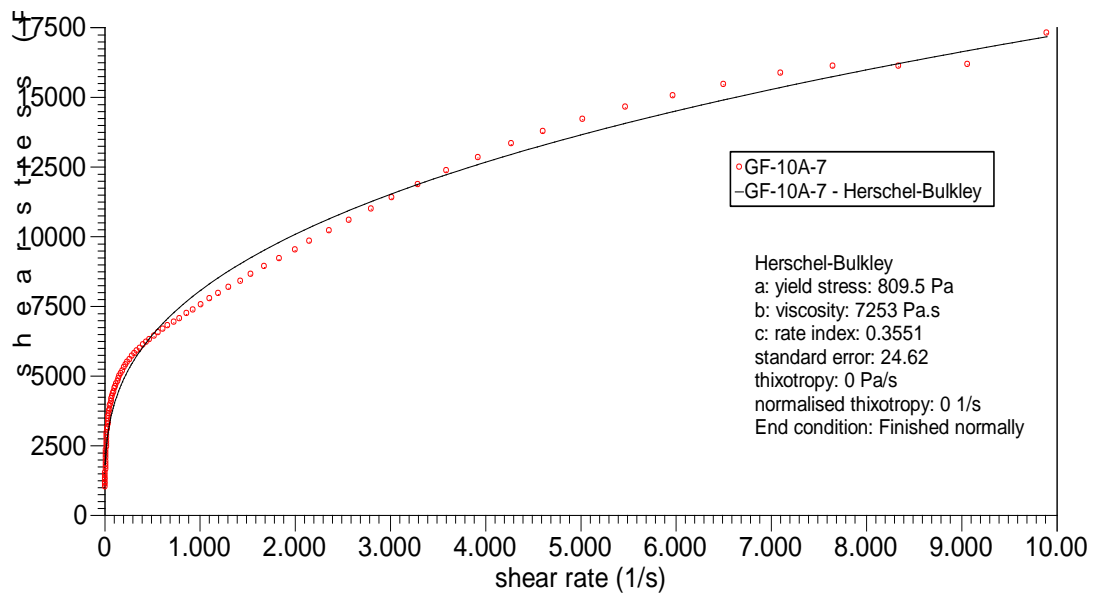


Figure A.19. Herschel-Bulkley fits of GF-10A-7

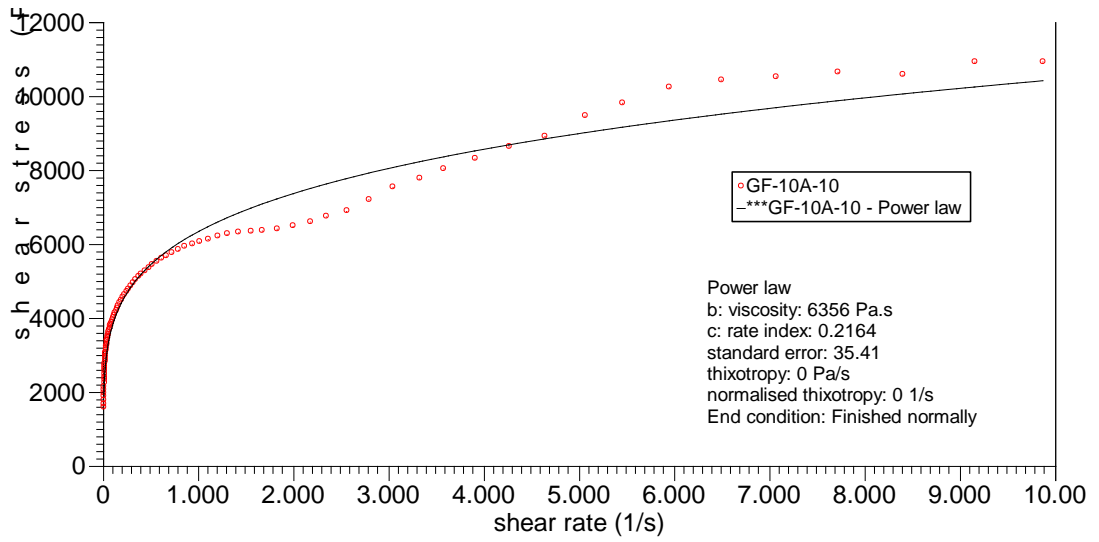


Figure A.20. Power model fits of GF-10A-10

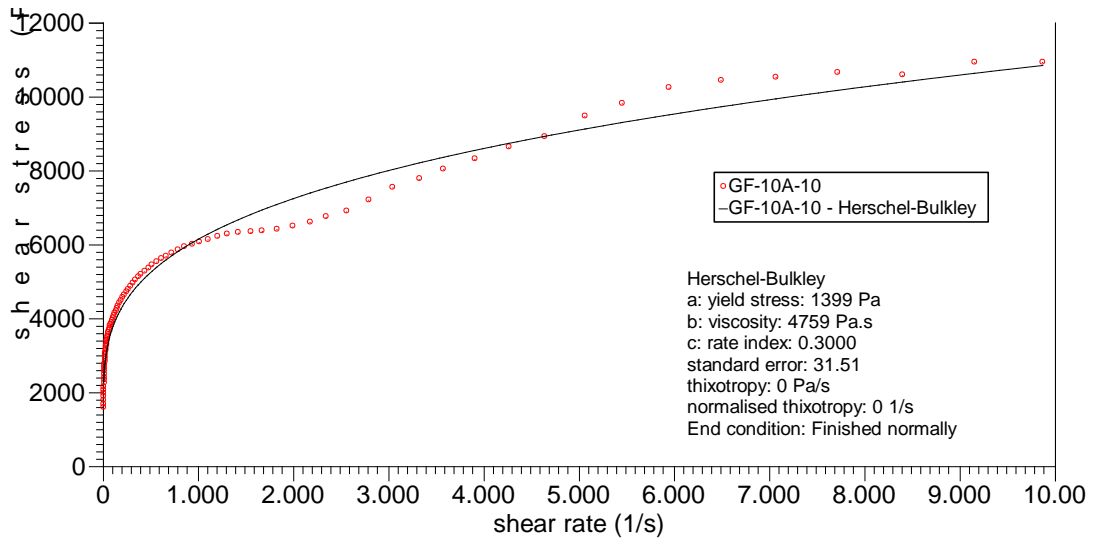


Figure A.21. Herschel-Bulkley fits of GF-10A-10